NRC Research and/or Technical Assistance Rept PDR

EGG-SEMI-6079
November 1982

QUICK LOOK REPORT FOR SEMISCALE MOD-2A MAIN STEAM LINE BREAK TESTS S-SF-4 AND S-SF-5

G. R. Berglund
D. J. Shimeck

Idaho National Engineering Laboratory
Operated by the U.S. Department of Energy

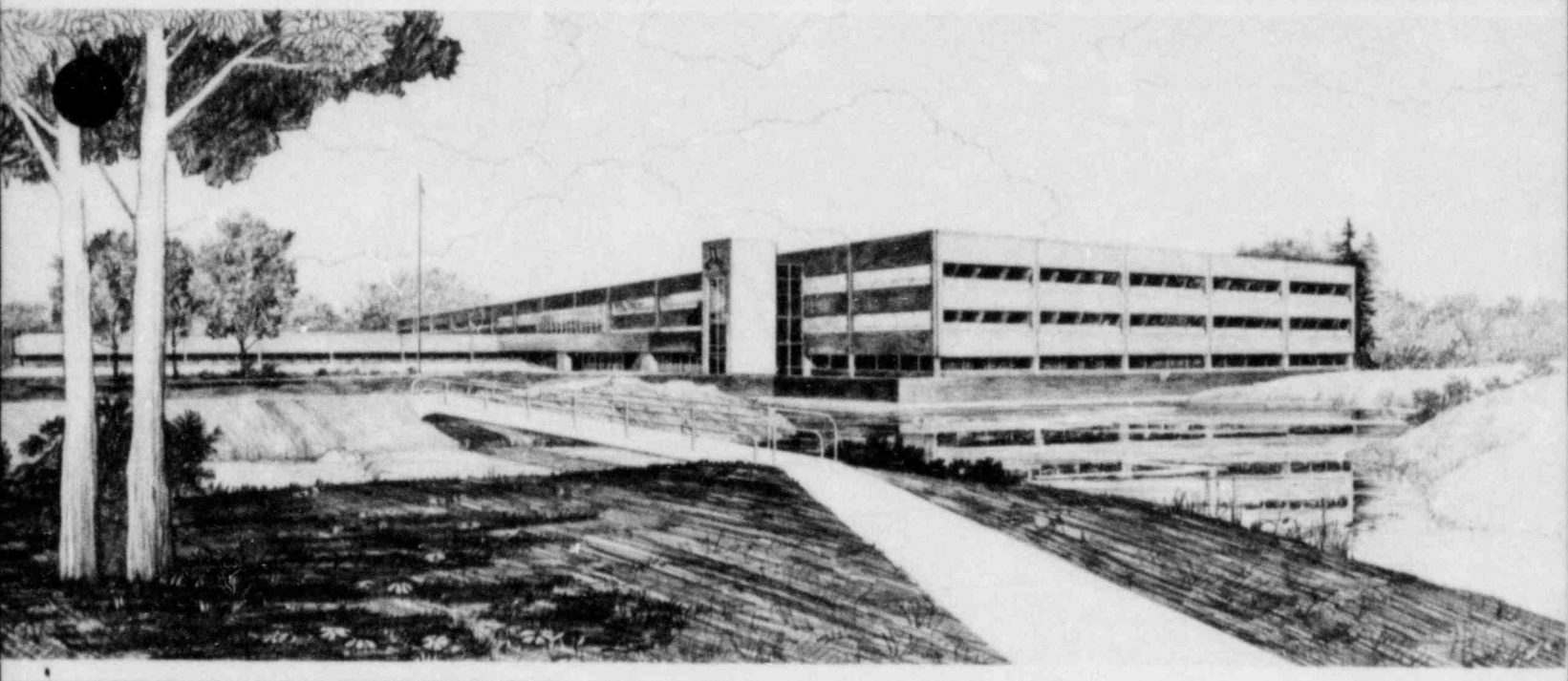

This is an informal report intended for use as a preliminary or working document

Prepared for the
U.S. NUCLEAR REGULATORY COMMISSION
under DOE Contract No. DE-AC07-76ID01570

EG&G Idaho

QUICK LOOK REPORT FOR SEMISCALE MOD-2A MAIN STEAM LINE BREAK TESTS S-SF-4 AND S-SF-5

Approved: Gary W Johnsen

P. North, Manager
Water Reactor Research Test Facilities Division

Approved: J L Martinell for

G. M. Johnsen, Manager
WRRTF Experiment Planning and Analysis Branch

EG&G Idaho, Inc.

FORM EG&G-396
(Rev. 11-79)

INTERIM REPORT

Accession No. _____

Report No. EGG-SEMI-6079

Contract Program or Project Title:

Semiscale

Subject of this Document:

Quick Look Report for Semiscale MOD-2A Main Steam Line Break Tests S-SF-4 and S-SF-5

Type of Document:

Quick Look Report

Author(s):

G. R. Berglund
D. J. Shimeck

Date of Document:

November 1982

Responsible NRC Individual and NRC Office or Division:

R. R. Landry, Reactor Safety Research

EG&G Idaho, Inc.
Idaho Falls, Idaho 83415

Prepared for the
U.S. Nuclear Regulatory Commission
Washington, D.C.
Under DOE Contract No. DE-AC07-76ID01570
NRC FIN No. A6038

INTERIM REPORT

ABSTRACT

Results are presented from a preliminary analysis of Semiscale Mod-2A Tests S-SF-4 and 5. These experiments simulated two break sizes in a steam generator secondary main steam line of a pressurized water reactor system. The experiments were initiated from a nominal hot standby condition. The primary objective of the tests was to evaluate the primary-to-secondary heat transfer response induced by a steam line break.

SUMMARY

This report presents the results of a preliminary analysis of data from Semiscale Mod-2A Tests S-SF-4 and 5. These experiments simulated breaks of two sizes in the secondary main steam lines of a pressurized water reactor (PWR) system. The steam line break was postulated to occur between the flow restrictor and main steam isolation valve of one steam generator. A break at this location precludes isolation of the affected steam generator. Communication was simulated between the generators by blowing down both secondaries. The intact loop steam generator was isolated upon receipt of a low broken loop steam generator secondary pressure signal. In general, main steam line breaks result in enhanced primary-to-secondary heat transfer which acts to depressurize the primary system. The scenario simulated in the experiments included auxiliary feedwater injection into the secondaries and high pressure emergency core coolant (ECC) injection into the primary. For both tests, the primary recirculation pumps were used to enhance primary-to-secondary heat transfer.

The primary objective of the experiments was to evaluate the primary-to-secondary heat transfer behavior that accompanies a steam generator secondary main steam line break. These two tests sought to provide a data base useful for evaluating the capabilities of water reactor safety computer codes to predict integral system response to secondary coolant system induced transients. Specific quantitative behavior of the primary system was considered to be of secondary importance in analyzing the experiments.

The transients were initiated from a hot standby condition by opening a blowdown valve on the broken loop steam generator. Prior to the transients the feedwater flow was terminated and the pressurizer heaters deactivated. Test S-SF-4 incorporated the use of a computerized core power controller to simulate the effects of moderator and fuel temperature reactivity feedback. The resultant core power excursion due to the negative temperature coefficient of reactivity acted in a manner so as to minimize depressurization of the primary. Test S-SF-5 was performed with a constant core power to enhance primary system depressurization.

Two other parameters were varied between the experiments which served to make them rather dissimilar. The break size for Test S-SF-5 was half the size of that for Test S-SF-4. Additionally, Test S-SF-4 was conducted with a significantly overscaled mass of water in the secondaries, while Test S-SF-5 was initiated with inventories closer to the correctly scaled values.

Prior to break initiation, most of the primary-to-secondary heat transfer occurred in the lower elevations of the steam generators. Following break initiation the decrease in secondary fluid temperature and two-phase level swell caused enhanced primary-to-secondary heat transfer which resulted in a primary system depressurization. When the intact loop steam generator secondary was isolated, heat transfer decreased rapidly because of a collapse in two-phase level swell and a repressurization of the secondary. The primary-to-secondary heat transfer occurring in the intact loop steam generator then was dependent on injection of ambient temperature auxiliary feedwater into the steam generator.

A similar phenomenon was observed in the broken loop steam generator. Following break initiation the level swell and decrease in secondary temperature resulted in enhanced primary-to-secondary heat transfer. This steam generator could not be isolated, however, and as the loss in secondary mass continued the secondary level decreased and uncovered the U-tubes. This resulted in a loss of heat transfer due to a change in heat transfer coefficient as the secondary side of the U-tubes dried out. Initiation of auxiliary feedwater flow into this generator, however, resulted in enhanced heat transfer at the lower elevations which increased the overall heat transfer.

In neither experiment was the primary cooldown and the associated coolant volume shrinkage great enough to empty the pressurizer. Consequently, the primary depressurization was not severe. Analysis of test data, and calculations performed with the RELAP5 computer code indicated that stored energy in the primary metal mass contributed to minimizing the depressurization by mitigating the cooldown induced by the

secondary blowdowns. The Mod-2A system has a large primary metal mass to fluid volume ratio relative to a full-scale PWR. The severity of the primary depressurization therefore, is expected to be distorted, and less severe than for a full-scale plant transient. However, the phenomenological information gathered is felt to be useful and valid for transient evaluation and code assessment.

ACKNOWLEDGEMENTS

The authors wish to extend their thanks to R. A. Shaw for his assistance in analyzing the Semiscale data, to J. S. Martinell for his direction and review and to J. Berrey, L. Theisen, and T. Demitropoulos for preparation of the report.

CONTENTS

FIGURES

TABLES

QUICK LOOK REPORT FOR
SEMISCALE STEAM LINE BREAK TESTS S-SF-4 and 5

1. INTRODUCTION

Testing performed in the Semiscale Mod-2A system is part of the water reactor safety research effort directed toward assessing and improving the analytical capability of computer codes used to predict the behavior of pressurized water reactors (PWRs) during postulated accident scenarios. For this purpose, the Mod-2A system was designed as a small-scale model of the primary system of a four-loop PWR nuclear generating plant. The system incorporates the major components of a PWR including steam generators, vessel, pumps, pressurizer, and loop piping. One loop (intact loop) is scaled to simulate three coolant loops in a PWR, while the other (broken loop) simulates a single loop. Geometric similarity has been maintained between a PWR and Mod-2A, most notably in the design of a 25 rod, full-length (3.66 m), electrically heated core; full-length upper head and upper plenum; component location; and relative elevations of various components. The scaling philosophy followed in the design of the Mod-2A system (modified volume scaling) preserves most of the first-order effects thought important in simulating transients which may occur in a PWR.

This report presents a preliminary analysis of the data taken during Tests S-SF-4 and 5. These tests simulated secondary side main steam line breaks of two sizes. The primary objective of these tests was to evaluate the primary-to-secondary heat transfer behavior that accompanies loss of secondary fluid via a steam line break. Secondary objectives were to evaluate the magnitude of primary cooldown due to enhanced primary-to-secondary heat transfer caused by the break, and the potential for repressurization of the primary once the secondary heat sink was lost. These phenomena are of concern with regard to the issue of pressurized thermal shock. As the primary coolant cools and shrinks, the level in the pressurizer is reduced. The primary fluid temperature decreases relatively slowly unless the shrinkage is sufficient to empty the pressurizer, at which time the primary pressure and temperature decrease rapidly. If the decrease in primary temperature is large enough it may reach a level where

pressurized thermal shock is of concern. Another phenomena that occurs during these transients, which is of interest, is the repressurization of the primary system once the secondary heat sink is lost due to isolation of intact generators from the break and from loss of secondary mass in the affected generator. In addition these tests will be used to provide information for possible future testing.

Figure 1 presents a simple flow schematic for the main steam lines in a typical PWR plant. For these tests the break is assumed to occur in the main steam line of one generator somewhere between the flow restrictor and the main steam line isolation valve. At the initialization of the break all generators have communication with, and loose secondary coolant inventory through the break. Once the appropriate automatic safety trip is reached the unaffected generators are isolated by closing the main steam line isolation valves. As can be seen in Figure 1, steam line break flow is limited by the size of the flow restrictors which have a 40.6 cm inside diameter (for a 3411 MW PWR). The broken loop steam line break sizes for Tests S-SF-4 and 5 were scaled to simulate 40.6 cm and 28.7 cm diameter steam line breaks in a PWR, respectively.[1] The communication of the unaffected generators with the break in a full-scale 4-loop plant is simulated in the Semiscale Mod-2A system with a single break orifice on the intact loop steam generator. The corresponding break area for each test was three times that of the broken loop.

The system configuration and test conduct are presented in Section 2. Section 3 presents the preliminary thermal-hydraulic response to the steam line breaks followed by a sensitivity study of the primary depressurization. Conclusions are presented in Section 4.

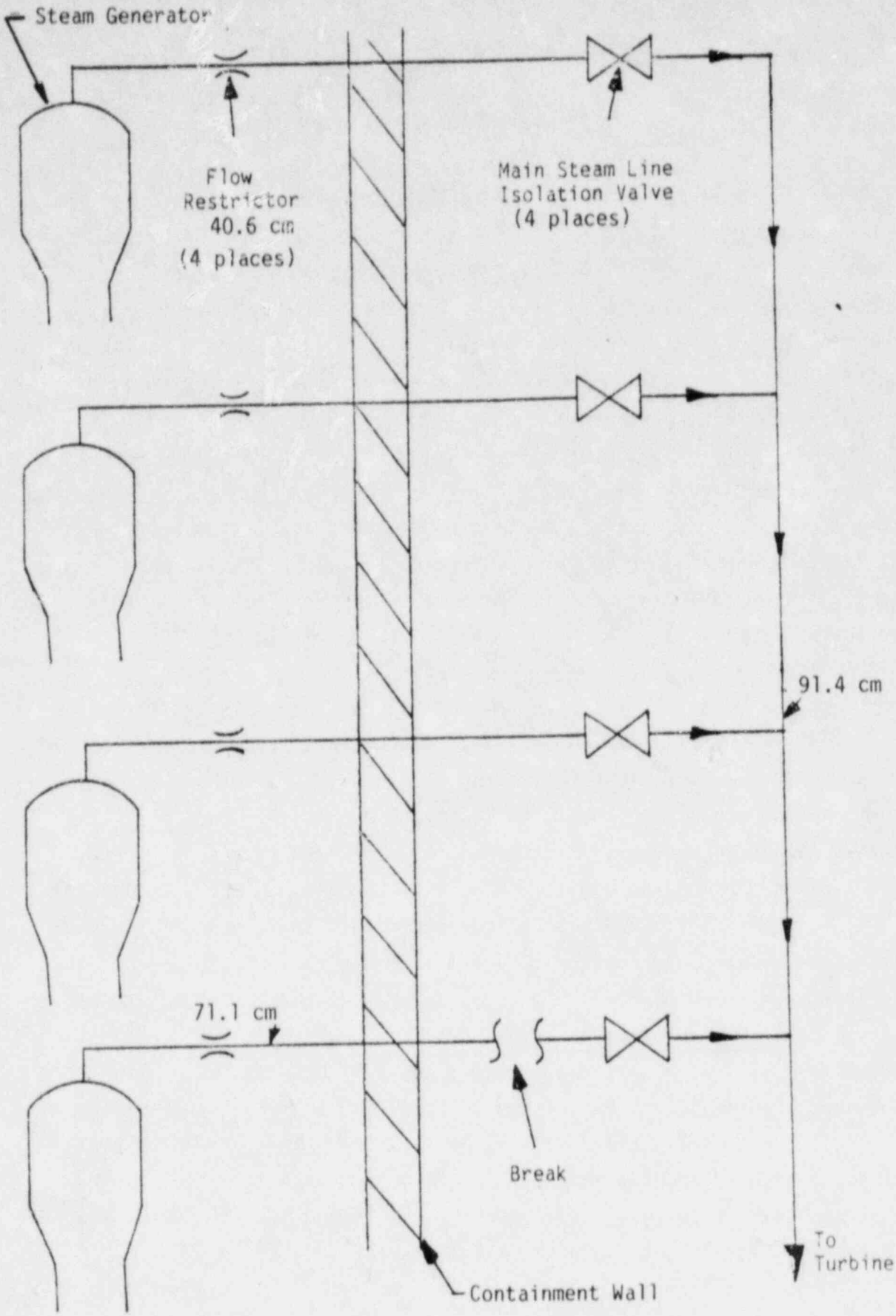

Figure 1. Assumed plant configuration for steam line breaks.

2. SYSTEM CONFIGURATION AND TEST CONDUCT

2.1 System Configuration

For Semiscale Mod-2A Tests S-SF-4, and 5 the Mod-2A system was configured as shown in Figure 2. The major components of the system were the vessel with electrically heated core and external downcomer, intact and broken loop steam generators, intact and broken loop recirculation pumps, and loop piping. The vessel core consists of a 5 x 5 array of internally heated electric rods, 23 of which were powered. The rods are geometrically similar to nuclear rods with a heated length of 3.66 m and an outside diameter of 2.072 cm. The primary system also incorporated the use of external heaters on loop piping and on the pressure vessel to mitigate the effects of heat loss to the environment. A more detailed description of the Mod-2A system may be found in Reference 2. The following paragraphs highlight important features of the steam generators that are of interest for these experiments.

Both the intact loop and broken loop steam generators are of a tube and shell design. Primary fluid flows through vertical, inverted, U-shaped tubes and secondary coolant passes through the shell side. The intact loop steam generator has two short, two medium, and two long tubes representative of bend elevations in a PWR steam generator. The broken loop steam generator has two tubes, a long tube and a short tube both of which are identical to the intact loop generator long and short tubes. Figure 3 shows a cross-sectional view of the broken loop steam generator. The same tube stock (2.22 cm O.D. x 0.124 cm wall thickness) and tube spacing (3.175 cm triangular pitch) used for PWR U-tubes are used in the Mod-2A design. Since the heat transfer area was based on the ratio of PWR to Semiscale core power, the number of tubes was therefore determined by the specified tube diameter and lengths. Filler pieces are installed in the shell side to provide a more properly scaled secondary fluid volume. Cross-sectional plan views of the intact and broken loop steam generator U-tubes and filler pieces are shown in Figure 4.

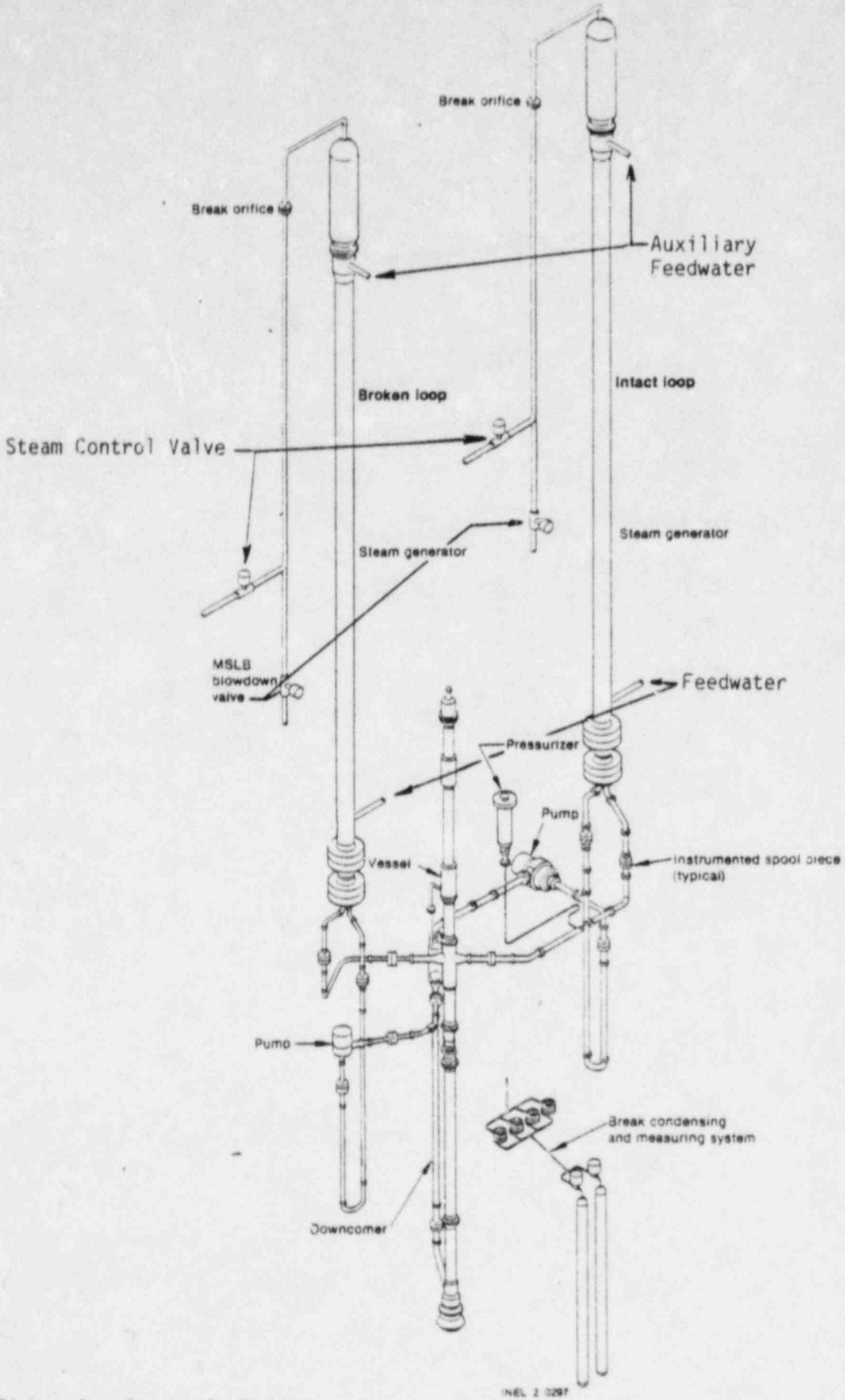

Figure 2. Semiscale Mod-2A configuration for main steam line break experiments, S-SF-4 and 5.

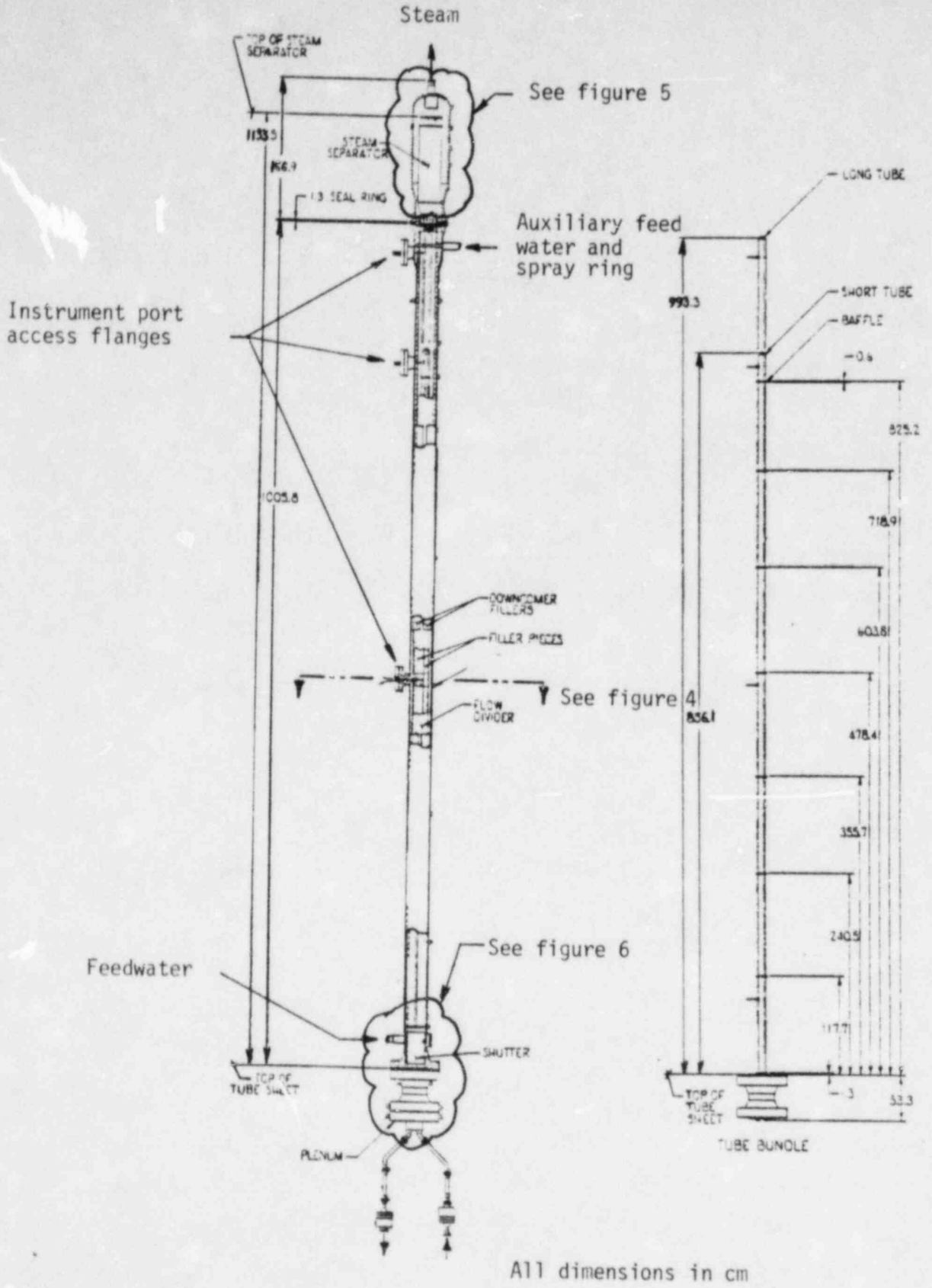

Figure 3. Broken loop steam generator cross section and tube bundle elevation.

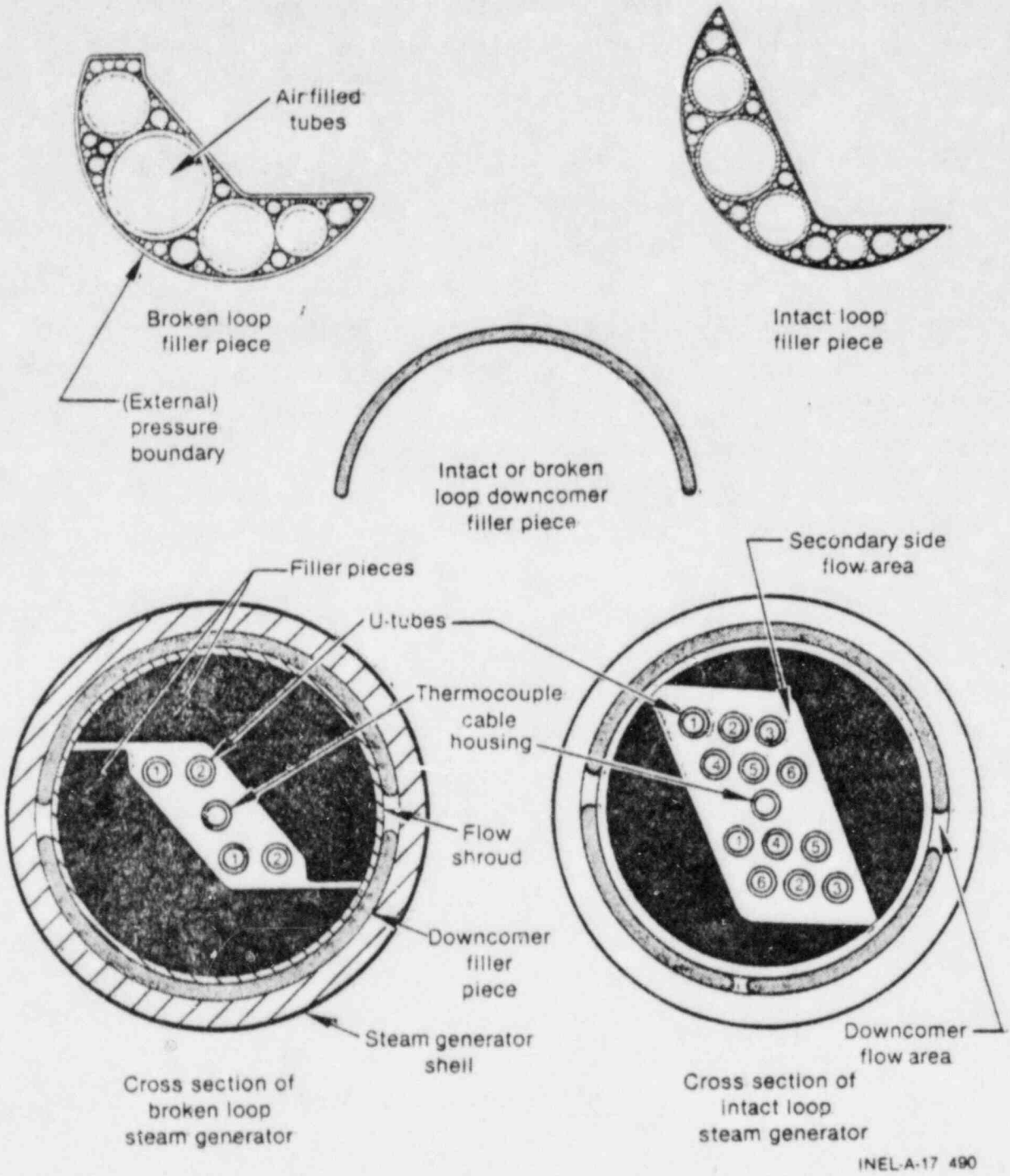

Figure 4. Cross-section of the Semiscale Mod-2A steam generators.

Elevations of the steam generator nozzles, plenums, and tubes are similar to those of a PWR. The steam dome, however, is shorter than the steam dome in a PWR and the steam drying equipment in the steam dome is of a simpler and less efficient design. Figure 5 is a detail of the steam dome region showing the centrifugal vane separator and the downcomer annulus configuration.

As seen in Figure 6 the lower portion (approximately one-half meter) of the steam generator downcomer is of an annular geometry. The majority of the downcomer length consists of two (broken loop) or three (intact loop) flow channels that connect the steam dome and lower downcomer annular regions (see Figure 4). This configuration is used to reduce the fluid volume of the downcomer region. Feedwater enters the steam generators at a point 36 cm above the tube sheet. The feedwater mixes with recirculated water from the downcomer and enters the riser section (where the tubes are located) through four slots in the flow divider. For these tests auxiliary feedwater was injected into a spray ring at the lower end of the steam dome annulus.

For the steam line breaks two different break nozzles were used as shown in Figure 7, and located as shown in Figure 2. The break flow area for the intact loop steam generator was 3 times that for the broken loop which is consistent with typical licensing calculation assumptions that the flow from each generator chokes across the individual flow restrictors or break, whichever is smaller. The breaks were initiated by opening the main steam line break (MSLB) blowdown valves on each generator while the steam control valve on the broken loop was closed. This provided choked flow across each break nozzle. The intact loop steam generator was eventually isolated by closing both the steam control valve and MSLB blowdown valve.

2.2 Test Procedures and Conditions

2.2.1 Preblowdown Activities

Prior to initiation of the transients the Semiscale system was stabilized to the initial conditions listed in Table 1. Priority was given

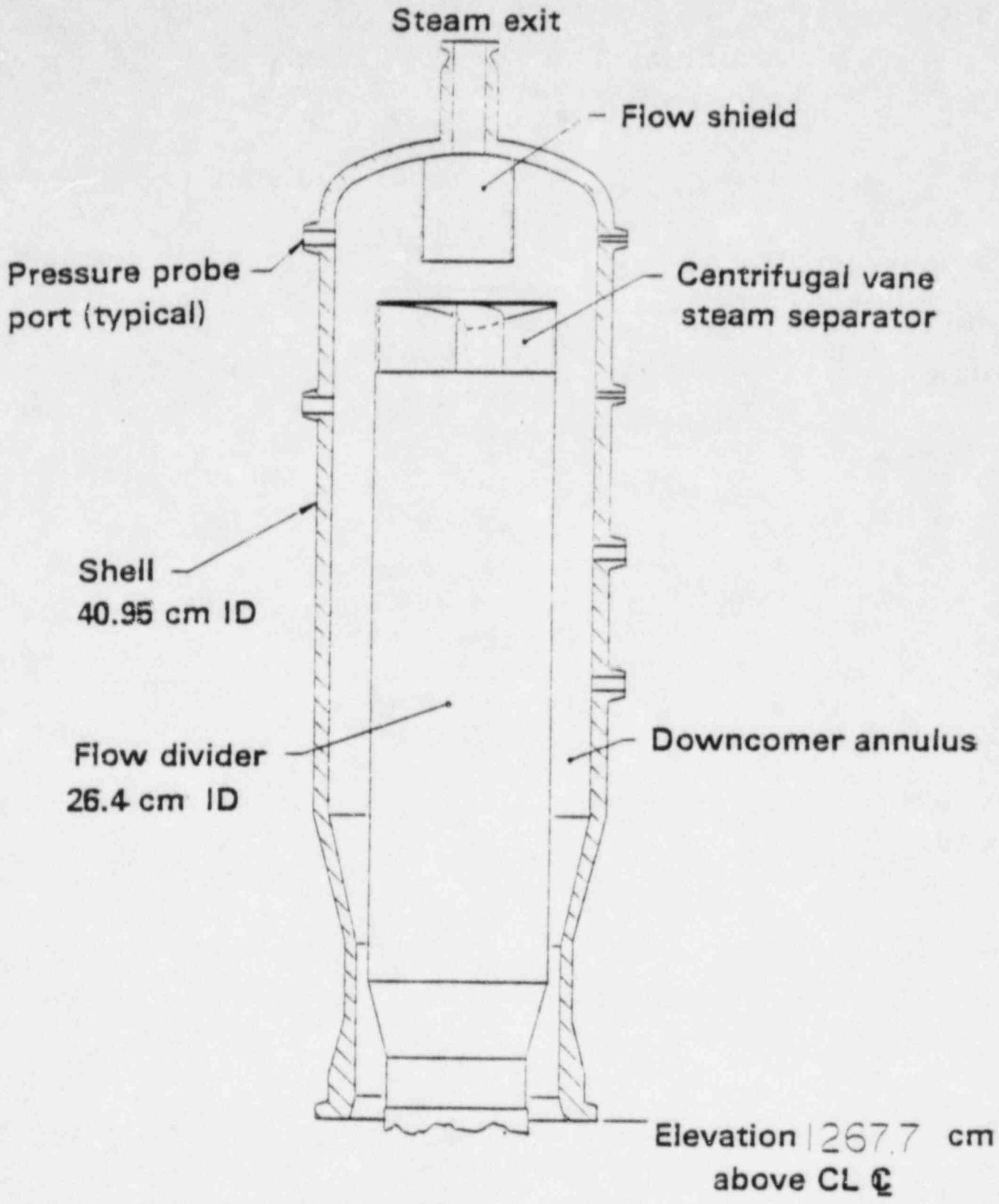

Figure 5. Steam generator steam dome cross-section.

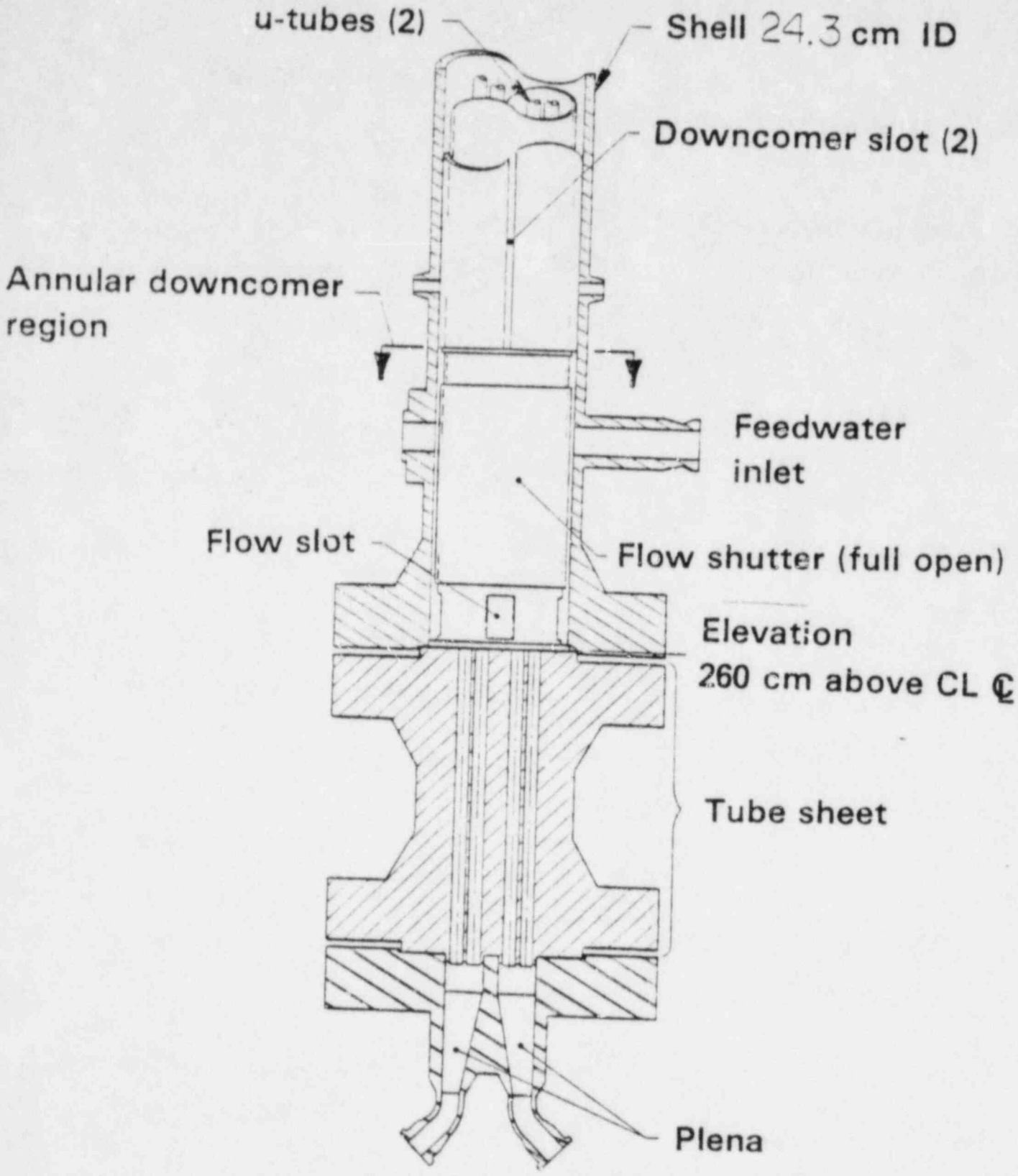

Figure 6. Broken loop steam generator; detail of tube sheet and lower secondary volume.

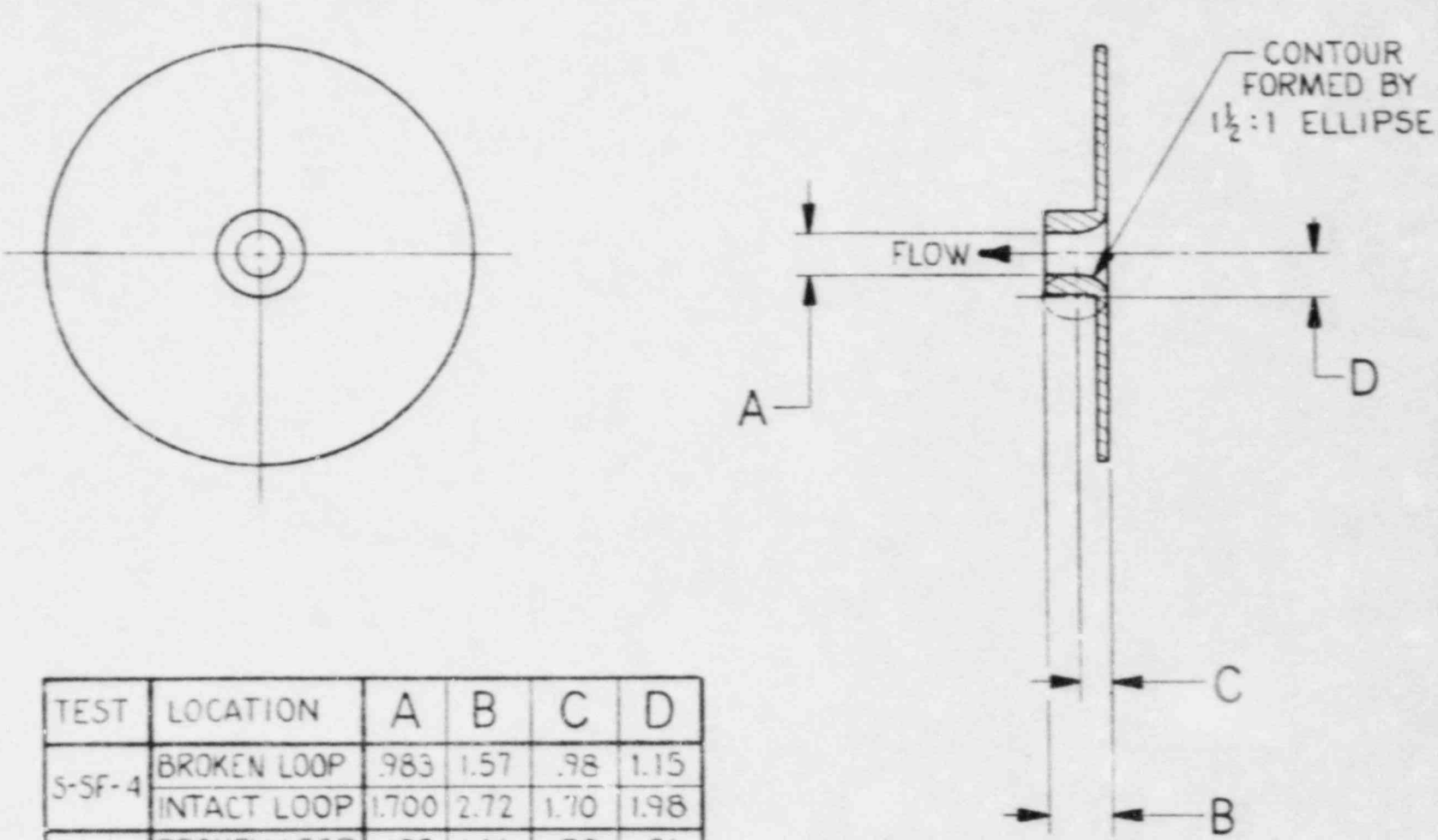

TEST	LOCATION	A	B	C	D
S-SF-4	BROKEN LOOP	.983	1.57	.98	1.15
	INTACT LOOP	1.700	2.72	1.70	1.98
S-SF-5	BROKEN LOOP	.695	1.11	.70	.81
	INTACT LOOP	1.202	1.92	1.20	1.40

DIMENSIONS IN cm

Figure 7. Break nozzle configuration for experiments S-SF-4 and 5.

TABLE 1. INITIAL CONDITIONS AND ECC PARAMETERS FOR TESTS S-SF-4 AND 5

Parameter	S-SF-4	S-SF-5
Pressurizer pressure	15.54 MPa	15.63 MPa
Core temperature differential	5 K	5 K
Cold leg fluid temperature		
Intact loop	555 K	556 K
Broken loop	555 K	555 K
Total core power	100 kW	107.8 kW
Band heaters	See Table 3	See Table 3
Pressurizer liquid mass	7.15 kg	7.1 kg
SG secondary pressure		
Intact loop	6.9 MPa	7.0 MPa
Broken loop	6.9 MPa	6.5 MPa
SG secondary water mass		
Intact loop	184.5 kg	118.1 kg
Broken loop	76.1 kg	42.8 kg
Configuration		
Break size		
Intact	1.70 cm ID	1.20 cm ID
Broken	.983 cm ID	.695 cm ID
Break type	Noncommunicative	Noncommunicative
Break location	Secondary steamline	Secondary steamline
Pressurizer location	Intact loop	Intact loop
Pressurizer surge line resistance	3.36×10^9 m^{-4}	3.36×10^9 m^{-4}
ECC injection		
IL HPIS		
Actuation pressure	14.41 MPa	14.41 MPa
Injection rate	See Figure 12	See Figure 15
Temperature	301 K	298 K

to establishing the correct secondary mass inventory, primary pressure, and cold leg temperature. The loop flow rates and secondary side pressures were adjusted as necessary. The core power was adjusted to maintain steady conditions. The initial value therefore compensated for primary and secondary heat losses in excess of that made up by the external heaters. It also compensated for nonsteady conditions within the secondaries. The indicated secondary mass inventories were kept within a selected band by throttling the feedwater as necessary.[a] Once conditions had been established within allowable tolerances the feedwater flow was stopped, pressurizer heaters deactivated, and the transient initiated by opening the blowdown valves in the main steam lines. The sequence of events for Tests S-SF-4 and 5 are given in Table 2.

2.2.2 Component Controls

S-SF-4. Core power for Test S-SF-4 was computer controlled on-line to simulate the reactivity effects to primary coolant and fuel rod temperature changes. The following equation shows the parameters used for determining the reactivity used in the point kinetics calculation:

$$R_T = R\ (T_F) + R\ (T_M) + R\ (\text{control rods})$$

where

R_T	=	total reactivity. Initially -1.75 dollars. This is based on a typical shutdown reactivity with the control rod bundle with the largest worth stuck out of the core.
$R\ (T_F)$	=	reactivity as a function of fuel rod temperature.
$R\ (T_M)$	=	reactivity as a function of moderator temperature.
R(control rod)	=	reactivity due to control rods in core. Does not change during test.

a. Initial conditions are generally insensitive to secondary inventory.

TABLE 2. SEQUENCE OF EVENTS FOR TESTS S-SF-4 AND 5

Event	Time (s)	
	S-SF-4	S-SF-5
Begin closing intact and broken loop feedwater valves	-2.0	-2.0
Open intact and broken loop MSLB blowdown valves	0.0	0.0
Close broken loop steam control valve	65	90
Safety injection signal reached (4.31 MPa in broken loop secondary)	65	90
Initiate auxilary feedwater injection	65	90
Termination of test	555	400

TABLE 3. EXTERNAL HEATER POWER CONTROL

Location	Power (kW)
Vessel	20
Hot legs	7.1
Cold legs	3.3
IL pump suction	8.5
BL pump suction	4.2

For this experiment the coefficients of reactivity simulated for the moderator (primary coolant) and fuel rod were negative, i.e. as temperature decreases reactivity increases. Figure 8 shows the reactivity as a function of temperature for the moderator and fuel. The coefficients were adopted from representative values found in Reference 9. As can be seen the coefficient of reactivity for the fuel is much less than that for the moderator. For Test S-SF-4 a representative core heater rod clad temperature and a representative core coolant temperature were used as inputs to the core power controller. The representative temperatures and the core power are shown in Figure 9. It should be noted that the clad temperature was used as input to an inverse heat conduction model to calculate fuel rod average temperature. This temperature was then used as input to determine reactivity changes due to fuel rod temperature. For further information on computerized core power control see References 3 & 4.

The primary coolant pumps were left running during each test. The flow rates in the primary loops for Test S-SF-4 are shown in Figure 10. Secondary side auxiliary feedwater injection began when the broken loop steam generator low secondary pressure safety injection signal was reached. The auxiliary feedwater flow rates as a function of time are shown in Figure 11. High Pressure Injection System (HPIS) flow began when primary pressure reached 14.1 MPa. HPIS flow is shown in Figure 12.

S-SF-5. Core power for test S-SF-5 remained constant at 107 kW during the test. The core power was held constant to enhance primary cooldown (increase severity of transient). Primary coolant pumps were also running during the test and the loop flow rates are shown in Figure 13. Auxiliary feedwater injection began after the low broken loop secondary pressure safety injection signal was received and these flow rates are shown in Figure 14. HPIS flow for Test S-SF-5 is shown in Figure 15.

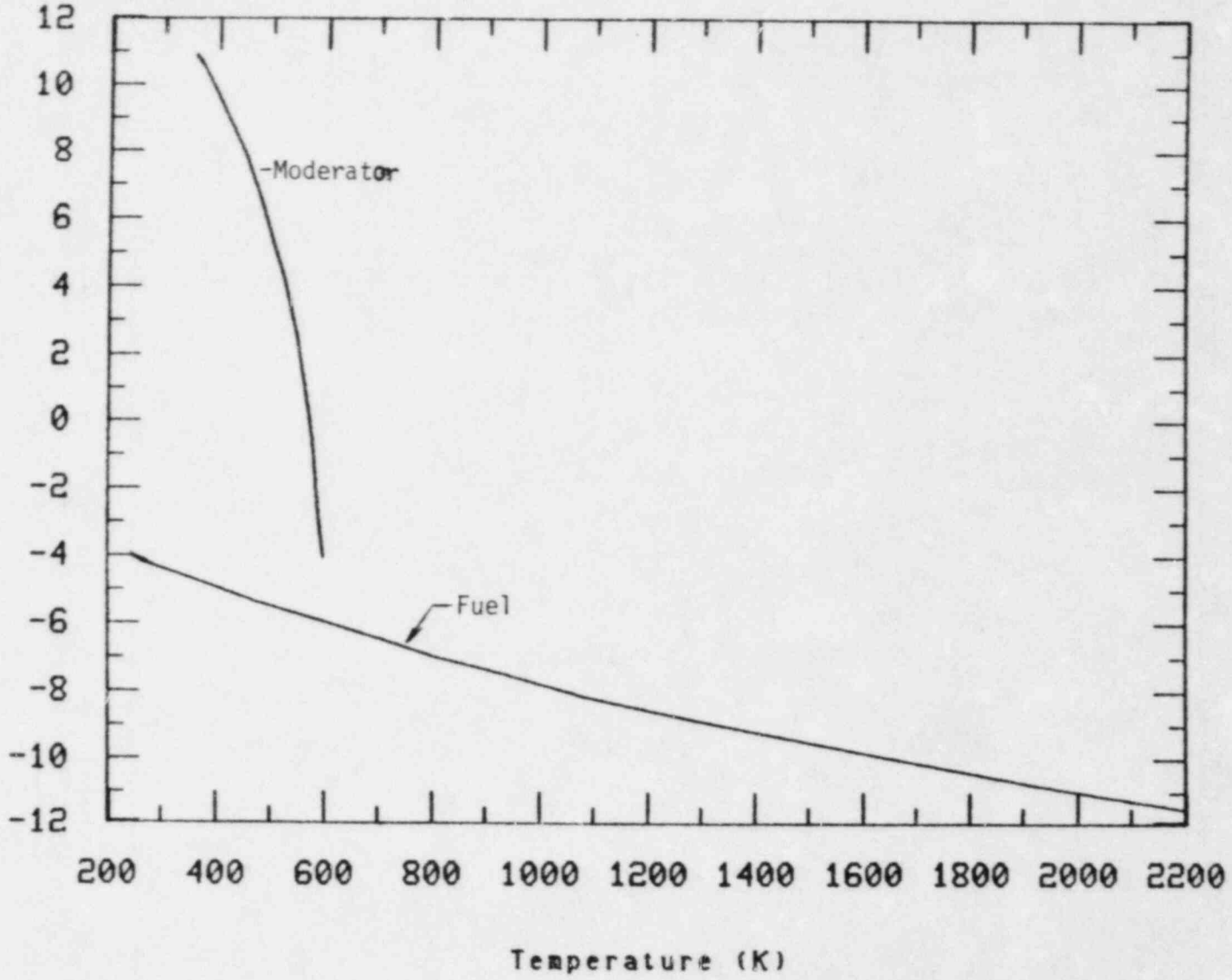

Figure 8. Reactivity vs. temperature for moderator and fuel. Test S-SF-4.

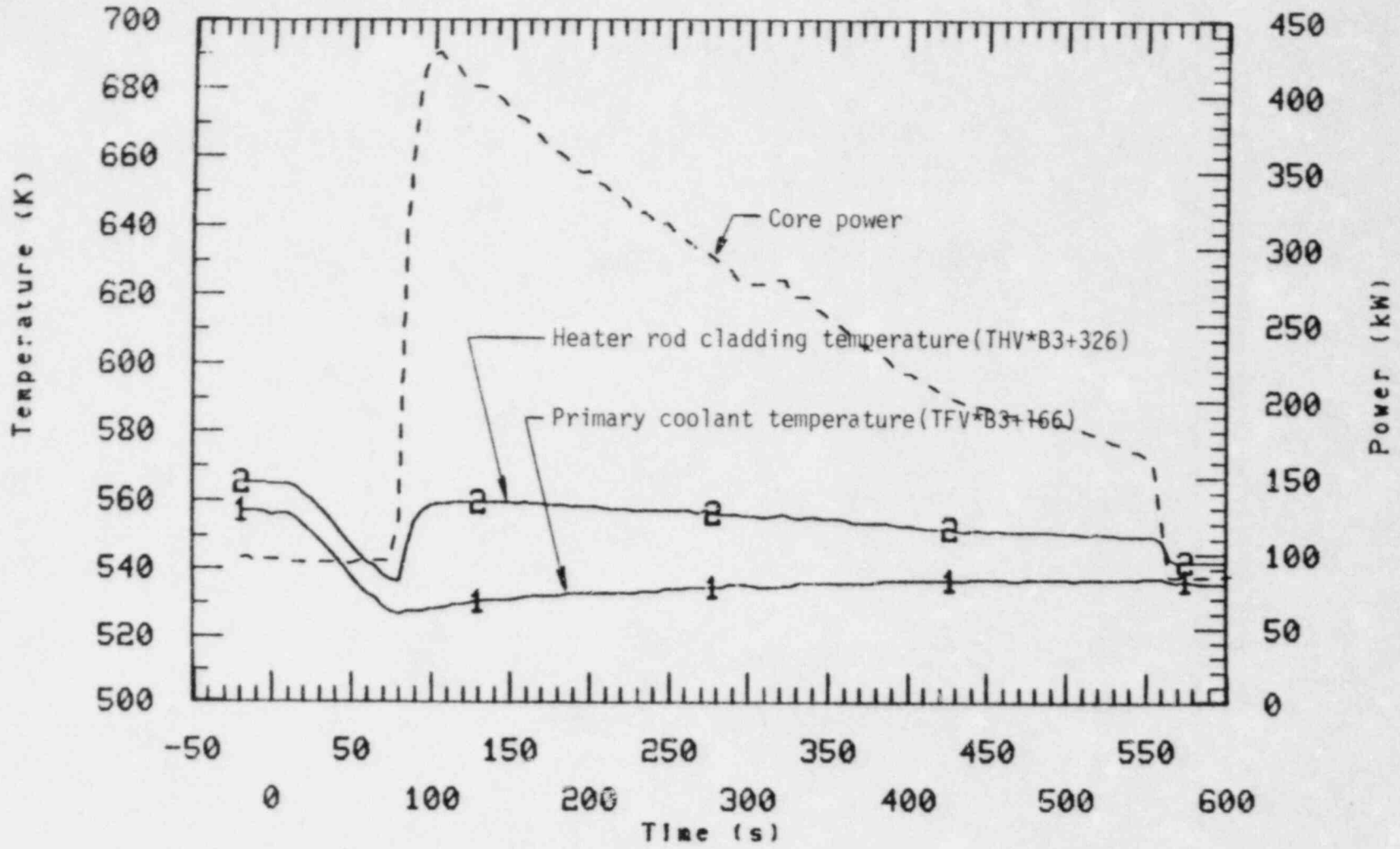

Figure 9. Core control heater rod cladding and primary coolant temperature and core power. Test S-SF-4.

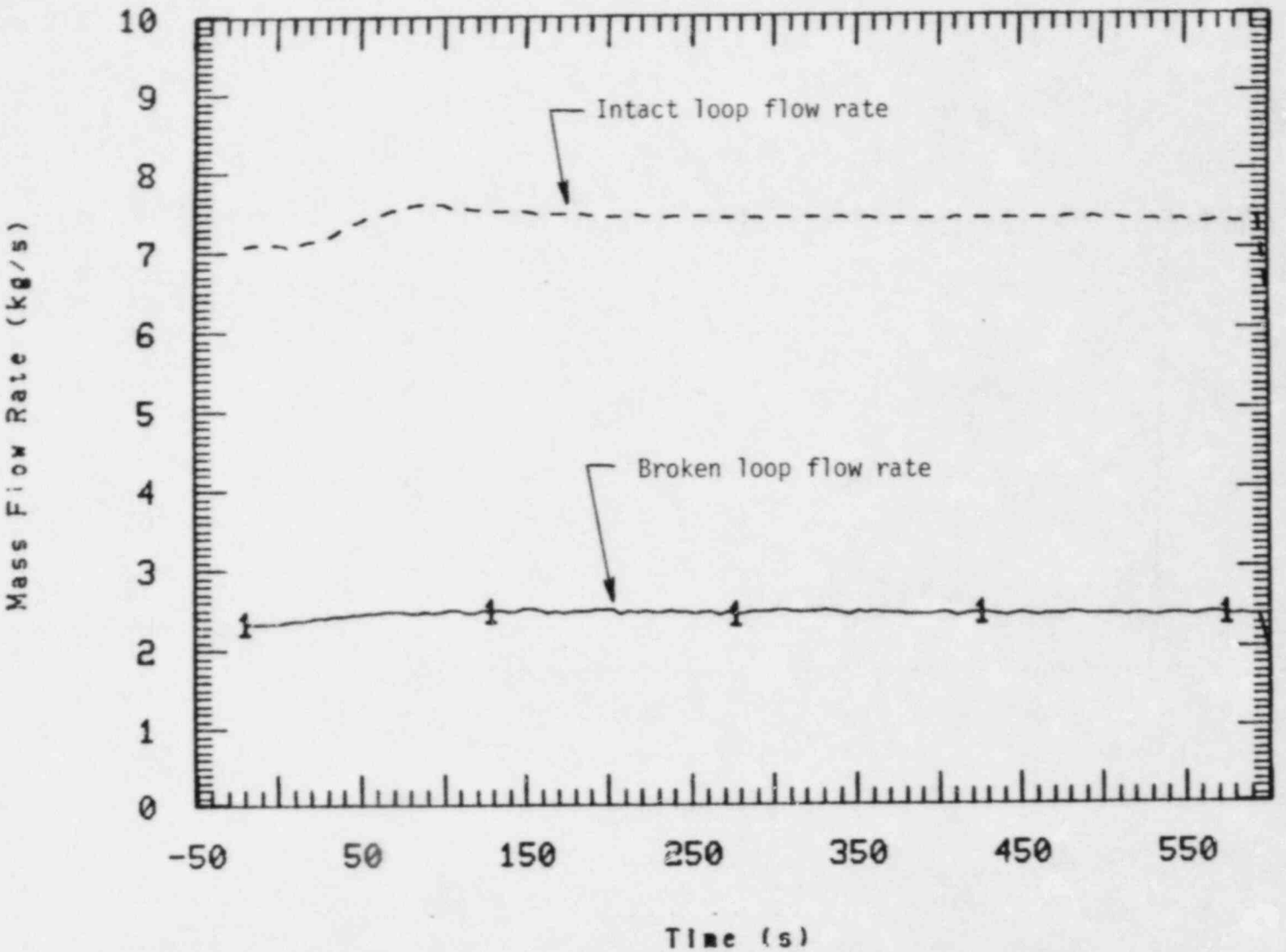

Figure 10. Primary loop recirculation flow rates for test S-SF-4.

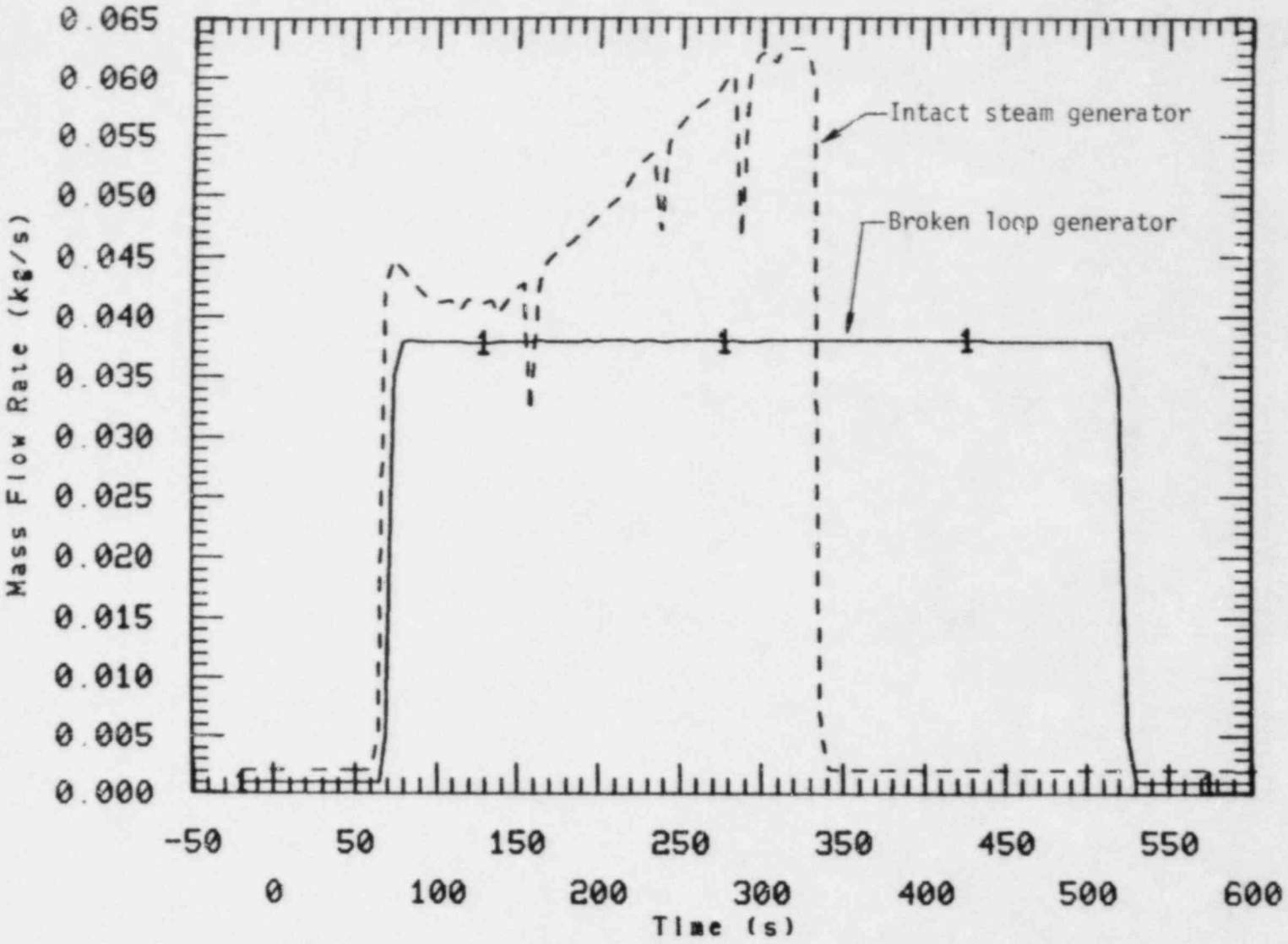

Figure 11. Auxiliary feedwater flow rates for Test S-SF-4.

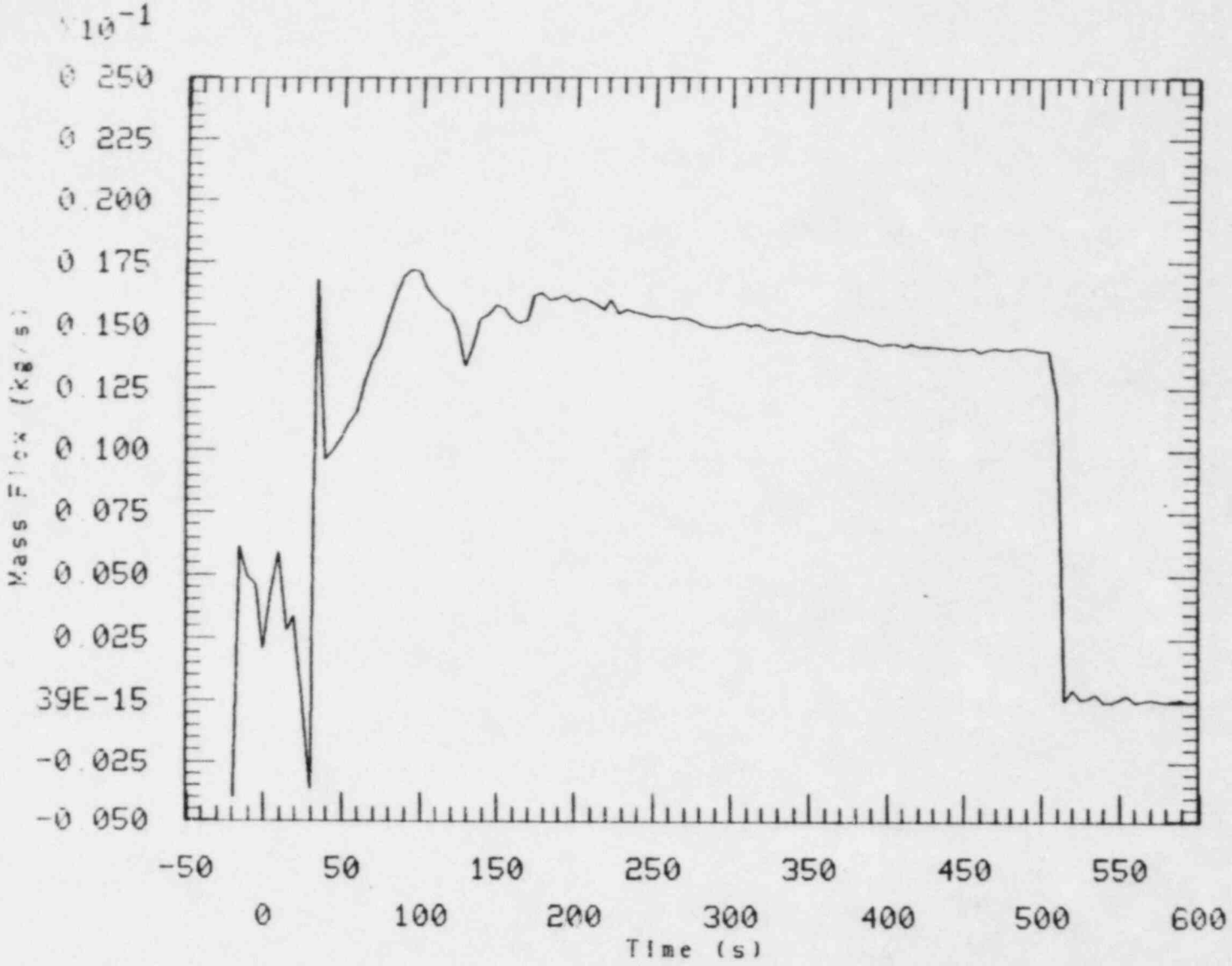

Figure 12. HPIS Injection flow rate for Test S-SF-4.

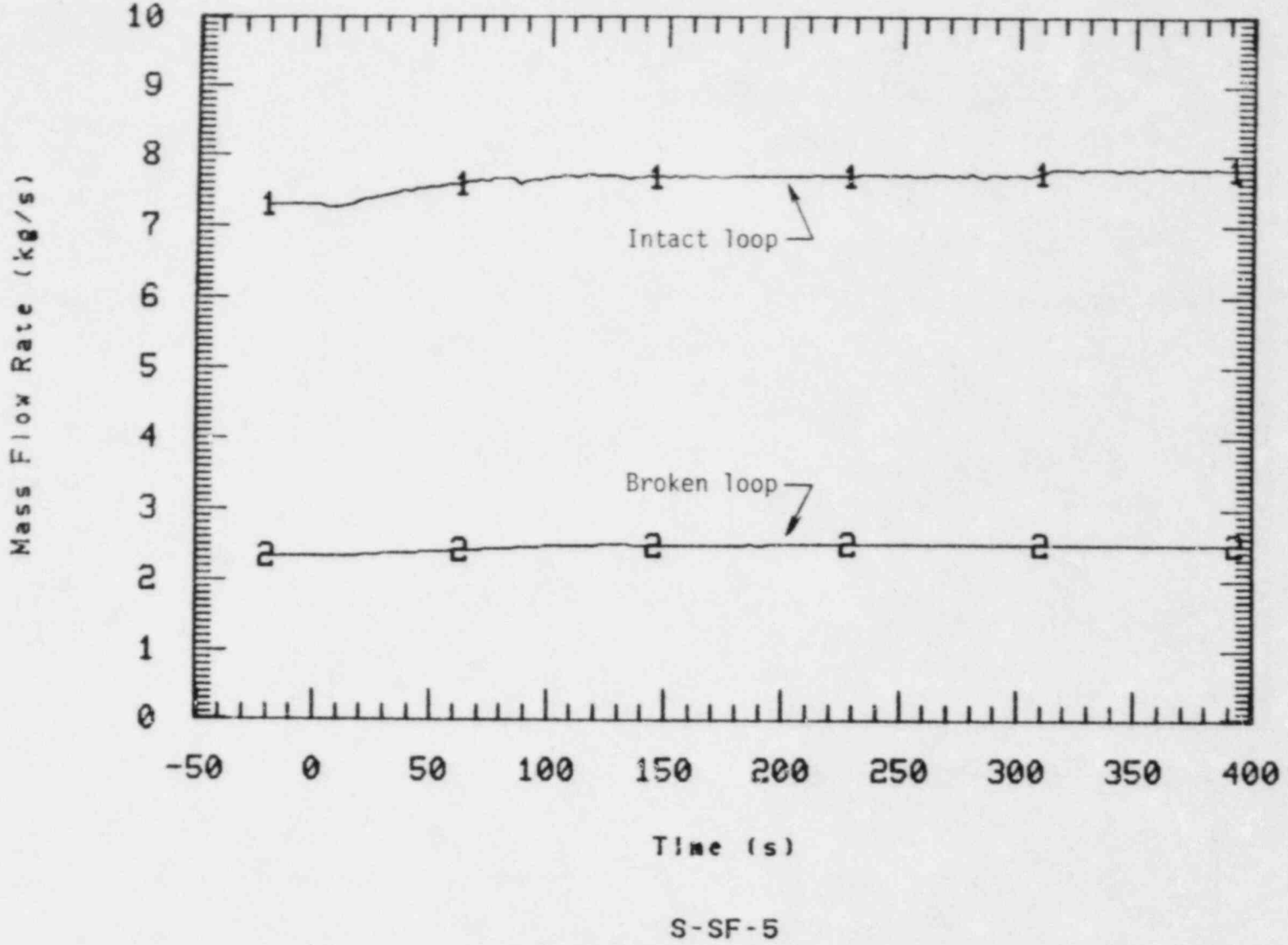

Figure 13. Primary loops recirculation flow rates for test S-SF-5.

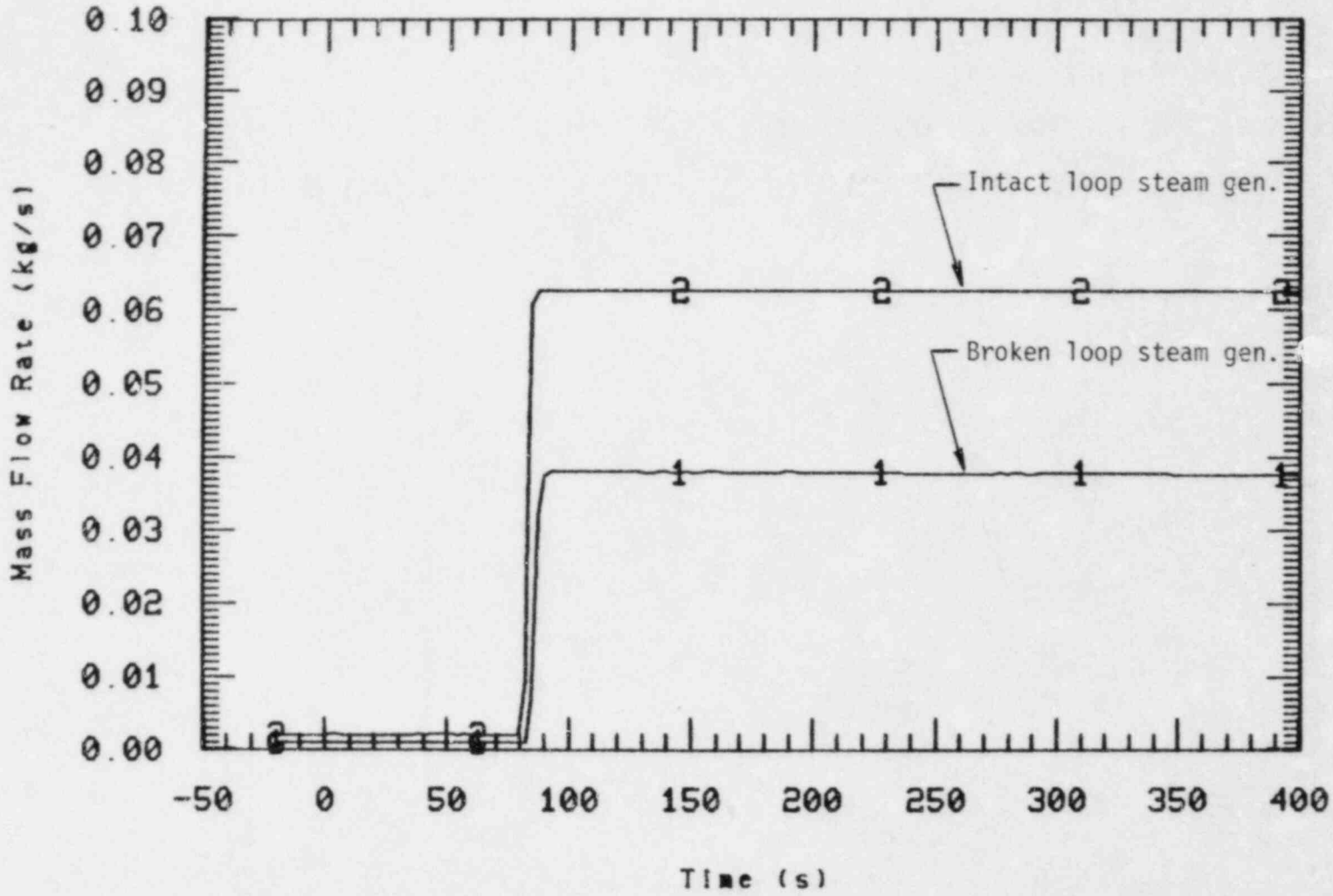

Figure 14. Auxiliary feedwater flowrates for test S-SF-5.

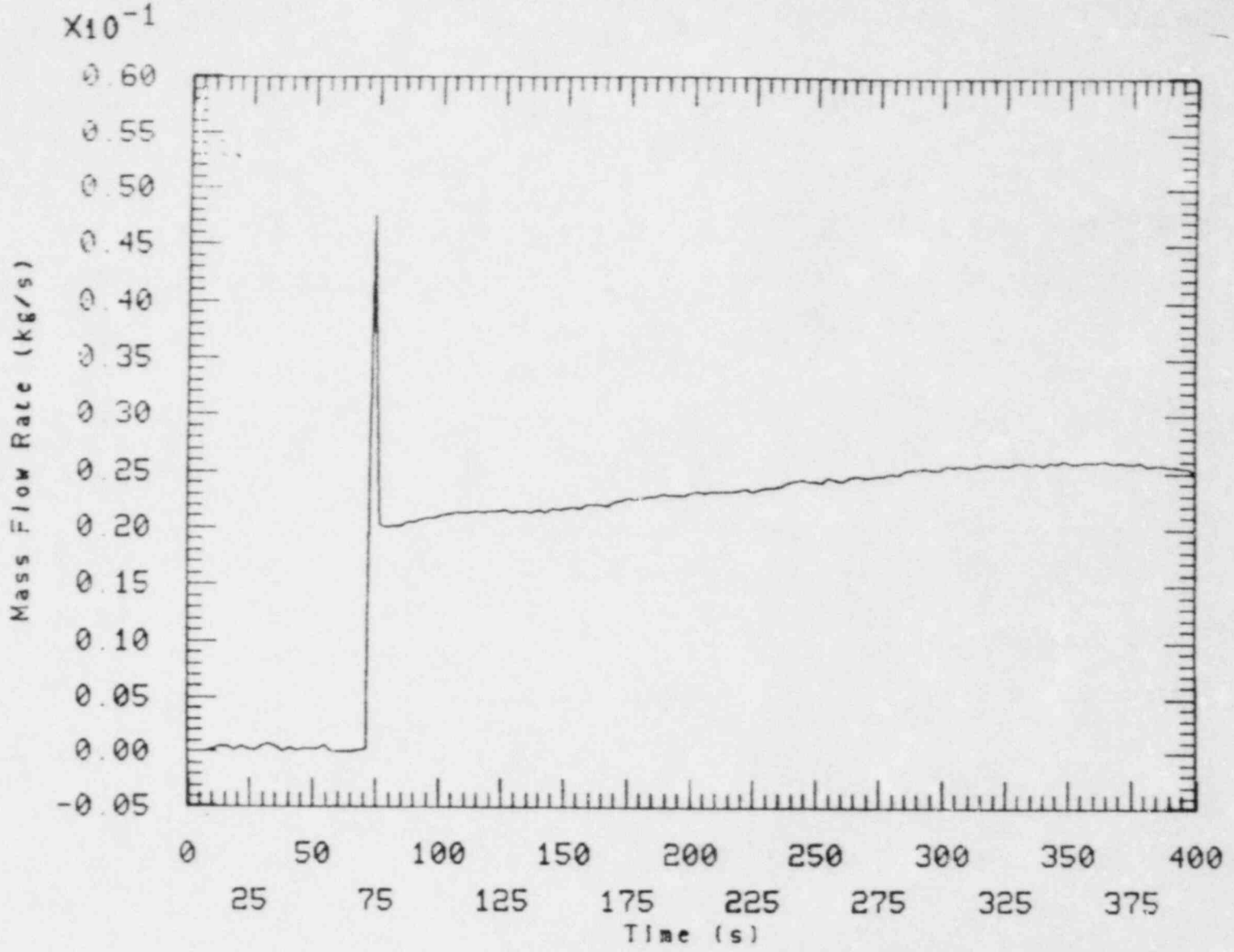

Figure 15. HPIS injection flow rate for Test S-SF-5.

3. TEST RESULTS

Preliminary results of the two steam line break tests are presented in this section. First, three major parameters that served to differentiate the boundary conditions between the tests are reviewed. Since the tests were significantly dissimilar the results for each are then presented separately. Comparisons between the two tests are made where appropriate. General primary and secondary behavior are first examined, followed by a more detailed thermal-hydraulic analysis including a discussion on primary-to-secondary heat transfer.

The three major differences between the two tests were:

1. In Test S-SF-4 the core power was controlled on-line to simulate the effects of reactivity feedback. This had the effect of increasing reactivity (power) in the core as the primary coolant temperature decreased which acted to minimize cooldown of the primary coolant. For Test S-SF-5 the core power was held constant to enhance the primary coolant cooldown.

2. The secondary coolant inventories were different for each test. The initial secondary levels in the steam generators as originally specified in the experimental operating specification[5] for these tests was 1020 cm. This was to have given a secondary volume in the intact loop steam generator (ILSG) three times that of the broken loop steam generator (BLSG) secondary. An error was found in the reported secondary volume information after performing Test S-SF-4. The initial levels in the secondaries for Test S-SF-5 were then changed to obtain the properly scaled mass inventories. The ratio of intact to broken loop steam generator secondary mass inventories for Tests S-SF-4 and 5 were 2.45 and 2.9, respectively. The collapsed secondary liquid levels were 1080 cm and 810 cm in the ILSG and BLSG, respectively, for Test S-SF-4. The respective secondary liquid levels were 952 cm and 452 cm for the ILSG and BLSG for Test S-SF-5.

3. The break sizes were different for each test. In Test S-SF-4 the break sizes of .983 cm and 1.70 cm diameter on the broken and intact loop steam generators, respectively, simulated the behavior of a break the size of the flow restrictor nozzles (see Figure 1). For Test S-SF-5 the break orifice areas on the respective steam generators were reduced by 50%.

3.1 Test S-SF-4

3.1.1 General Response

Test S-SF-4 was initiated from a hot standby condition. Core power, augmented by band heaters, was high enough to compensate for environmental heat losses and to maintain initial conditions. In addition, the core power was computer controlled to simulate the effects of moderator and fuel (Doppler) temperature reactivity feedback.

At t = 0 the break was initiated. Figure 16 shows the response of the primary system pressure and pressurizer liquid level during the test. The primary pressure rapidly decreased at break initiation, then at 85 s the pressure began to recover slightly. The primary pressure drop was a result of primary fluid shrinkage due to increased primary-to-secondary heat transfer during the secondary side blowdowns. Primary fluid shrinkage also resulted in liquid draining from the pressurizer to the hot leg (see Figure 16). Figure 17 shows the core power and primary system pressure responses during the test. At 75 seconds the core power increased substantially from a standby power level as a result of the net core reactivity increasing above 0 dollars. This large increase in heat addition to the primary resulted in stopping the depressurization and cooldown of the primary caused from large primary to secondary heat transfer. When the primary heated up again (as evidenced by an increase in primary pressure) the corresponding expansion of the primary fluid resulted in a liquid level increase in the pressurizer.

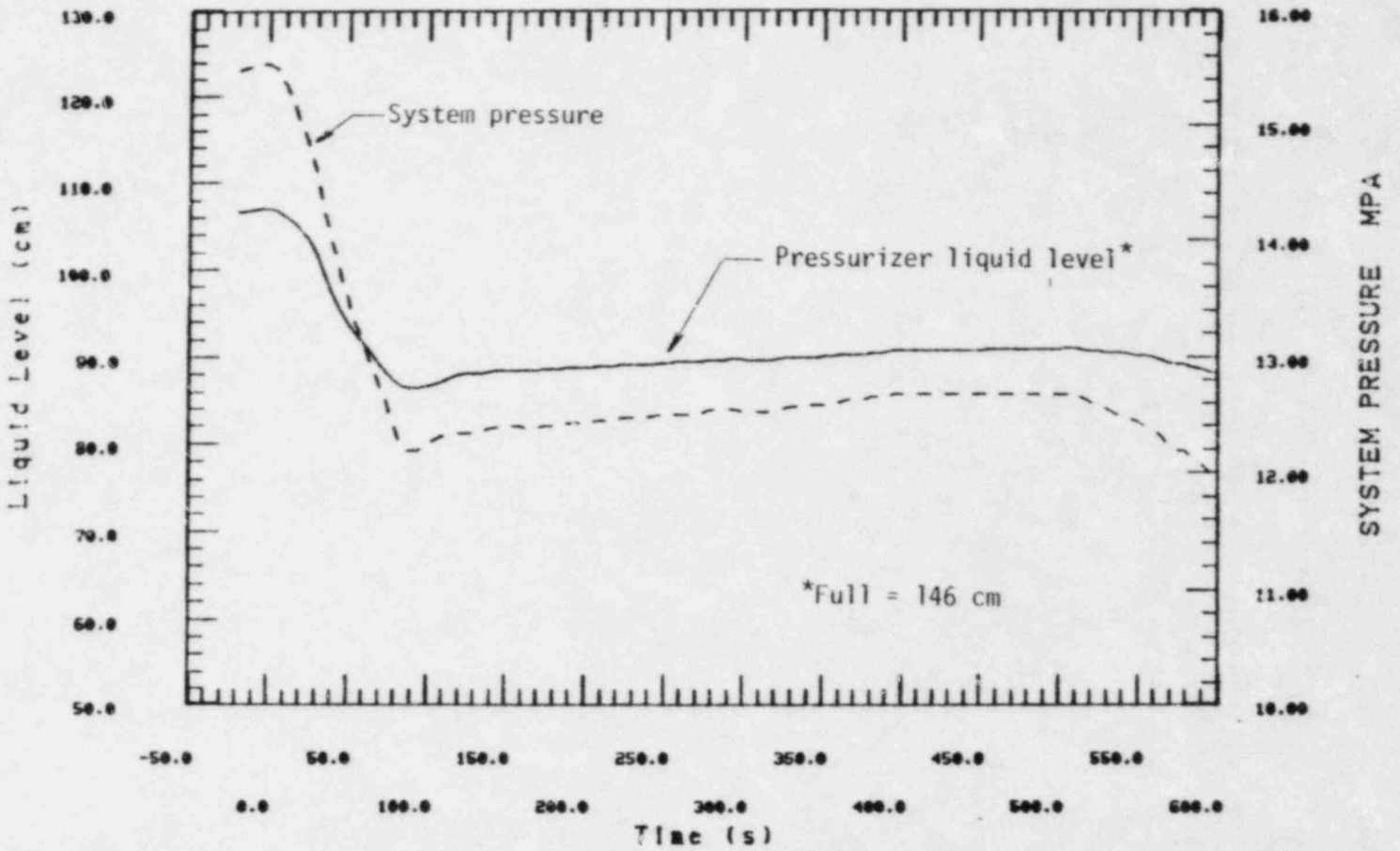

Figure 16. Pressurizer liquid level and system pressure for test S-SF-4.

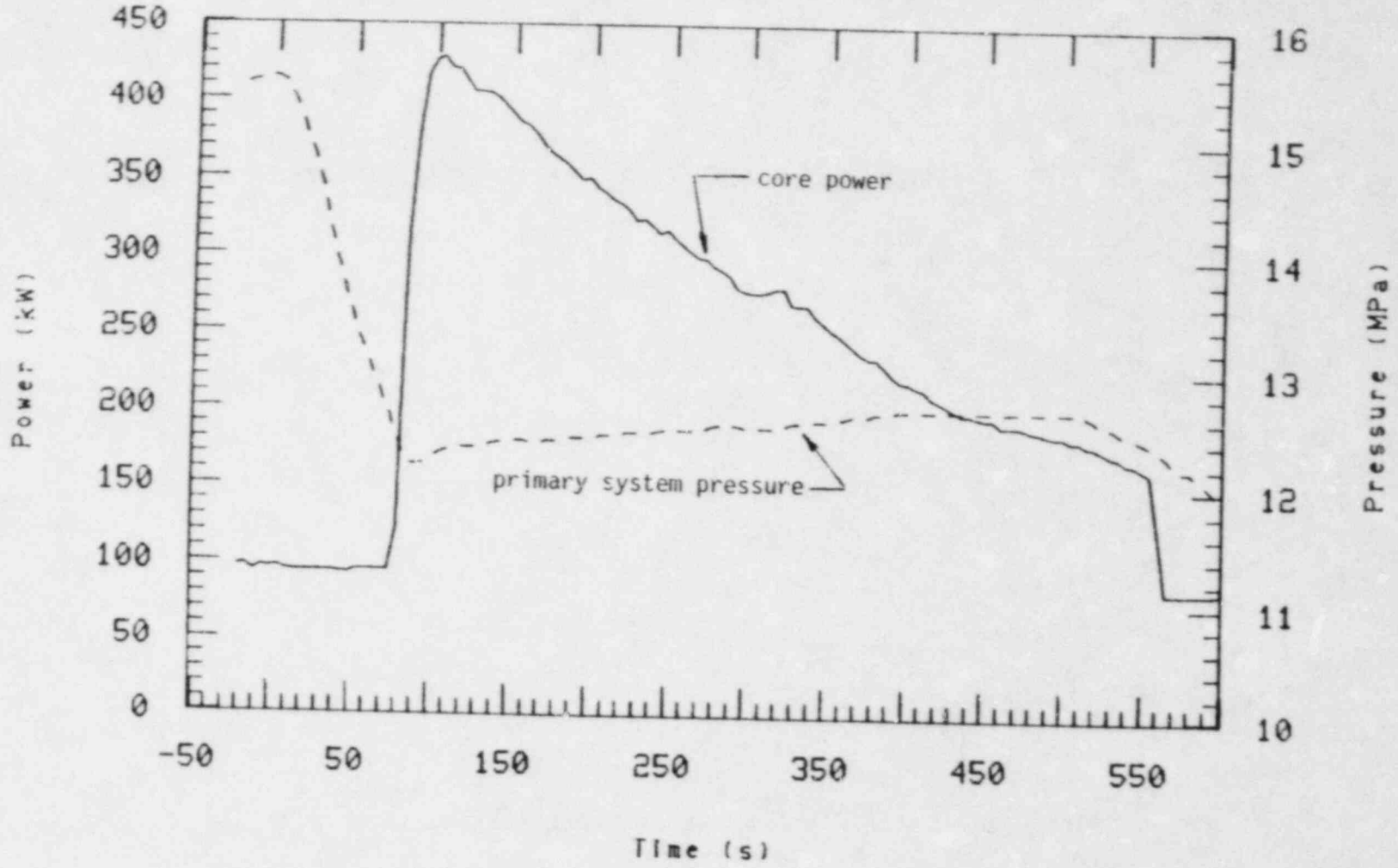

Figure 17. Core power and system pressure for Test S-SF-4.

Figure 18 compares the secondary pressures to primary system pressure. The BLSG secondary pressure decreased over the length of the test to ambient pressure. At 65 seconds the pressure in the BLSG reached the safety injection signal pressure of 4.13 MPa. At that pressure the steam valves on the ILSG closed resulting in an increase ILSG secondary pressure. At the same time auxiliary feedwater began to flow to both steam generators (see Figure 9) and the HPIS was enabled but did not start flowing until the primary pressure reached 14.4 MPa. It can be seen in Figure 18 that the BLSG pressure did not decrease as fast as the ILSG. This was due to the relatively large BLSG secondary volume compared to that in the ILSG and the relatively large metal volume (heat storage) in the BLSG compared to that in the ILSG.

3.1.2 Break Flow

At t = 0 the steam line breaks were initiated for both steam generators. Figure 19 shows the break mass flow rate for the intact and broken loop steam generators. As expected, the break flows choked and then decreased as the secondary pressures decreased in each steam generator. The ILSG break flow, after reaching choked conditions, decreased faster than the BLSG break flow because the ILSG secondary pressure decreased faster (see Figure 18).

3.1.3 General Secondary Heat Transfer

At 65 s the safety injection signal due to low BLSG secondary pressure (4.13 MPa) was reached (see Figure 18) and the ILSG steam valves closed thus, isolating the ILSG break flow. The break flow from the BLSG slowly decreased as the secondary pressure decreased to ambient pressure. As the pressures in the steam generators decreased the secondary fluid temperatures also decreased, maintaining saturation temperatures throughout the bulk secondary fluid. Figures 20 and 21 show selected secondary temperatures and corresponding saturation temperatures in the BLSG and ILSG, respectively. It should be noted that as the thermocouples become uncovered due to secondary mass depletion the temperature indication remains higher than the saturation temperature. This is due to conduction

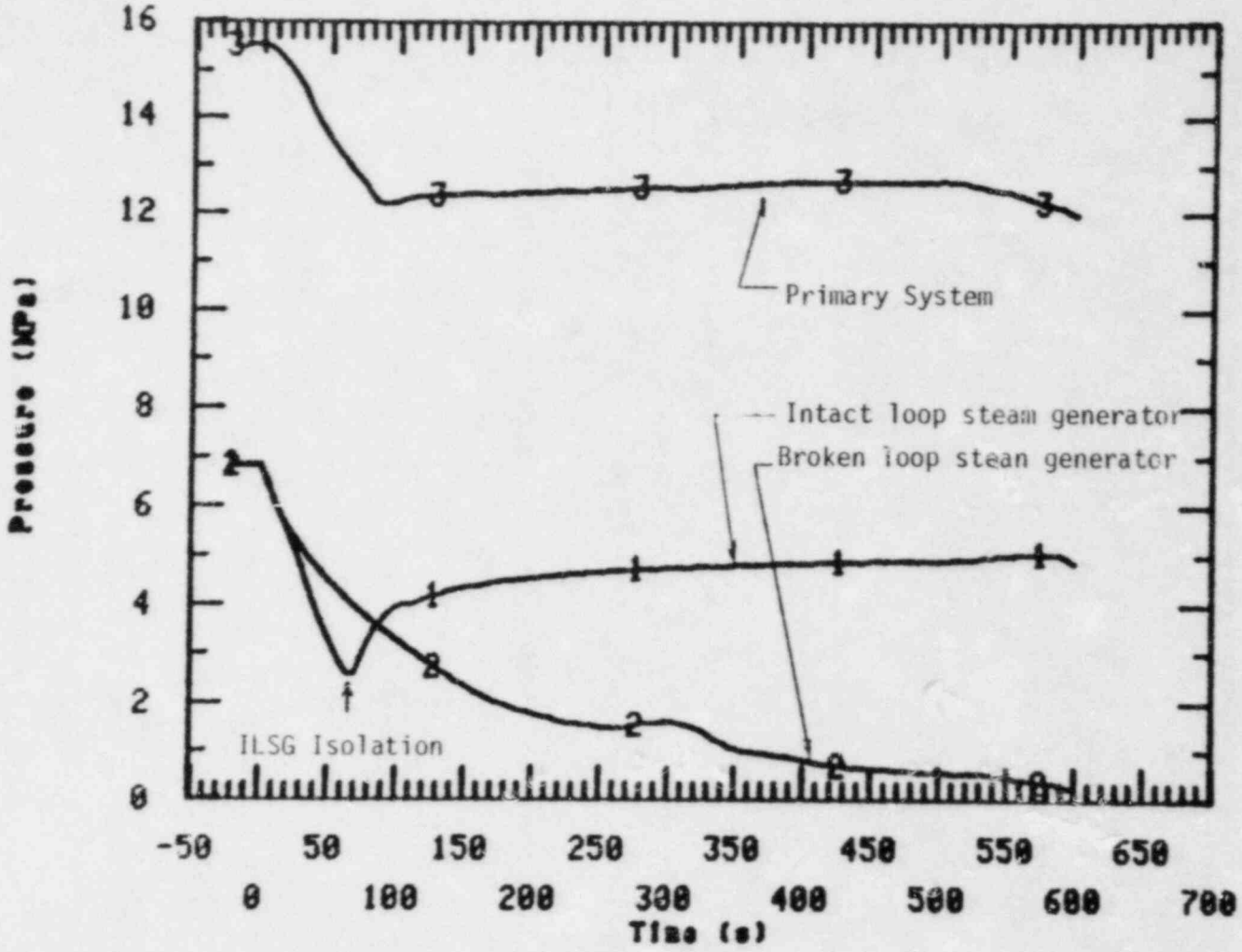

Figure 18. Secondary steam generator pressure for Test S-SF-4.

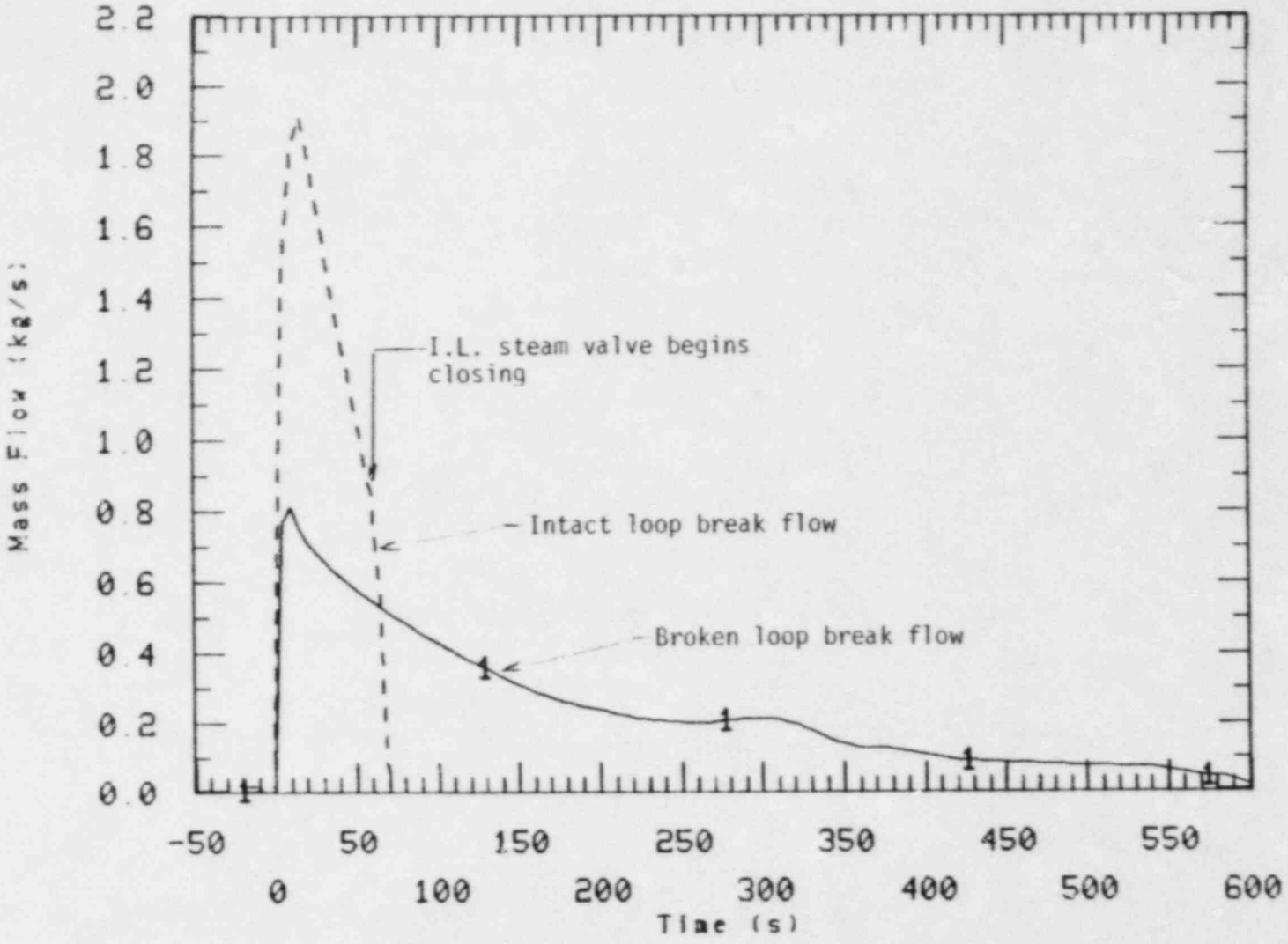

Figure 19. Break flows for S-SF-4.

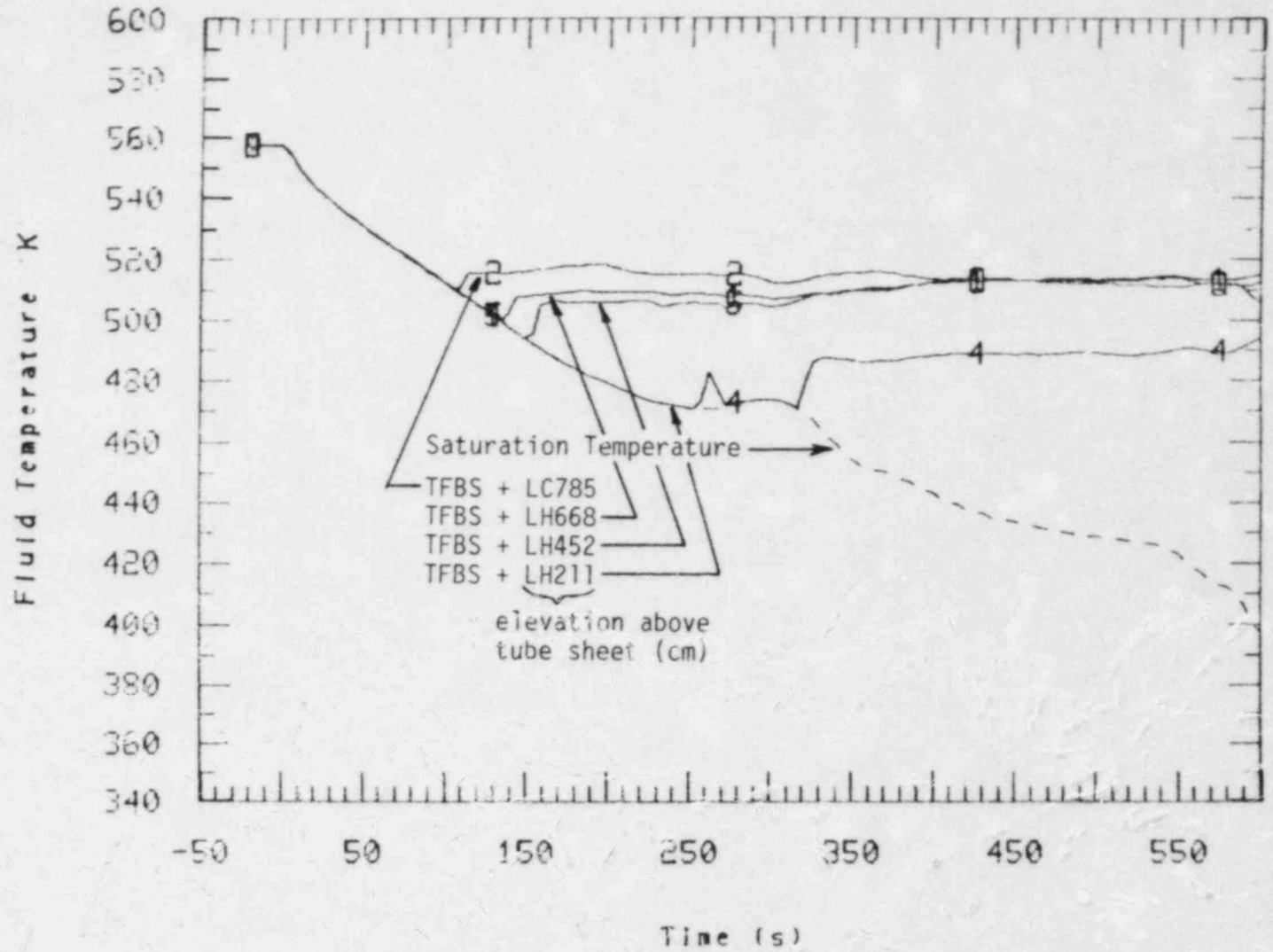

Figure 20. Selected broken loop secondary and saturation temperatures for Test S-SF-4.

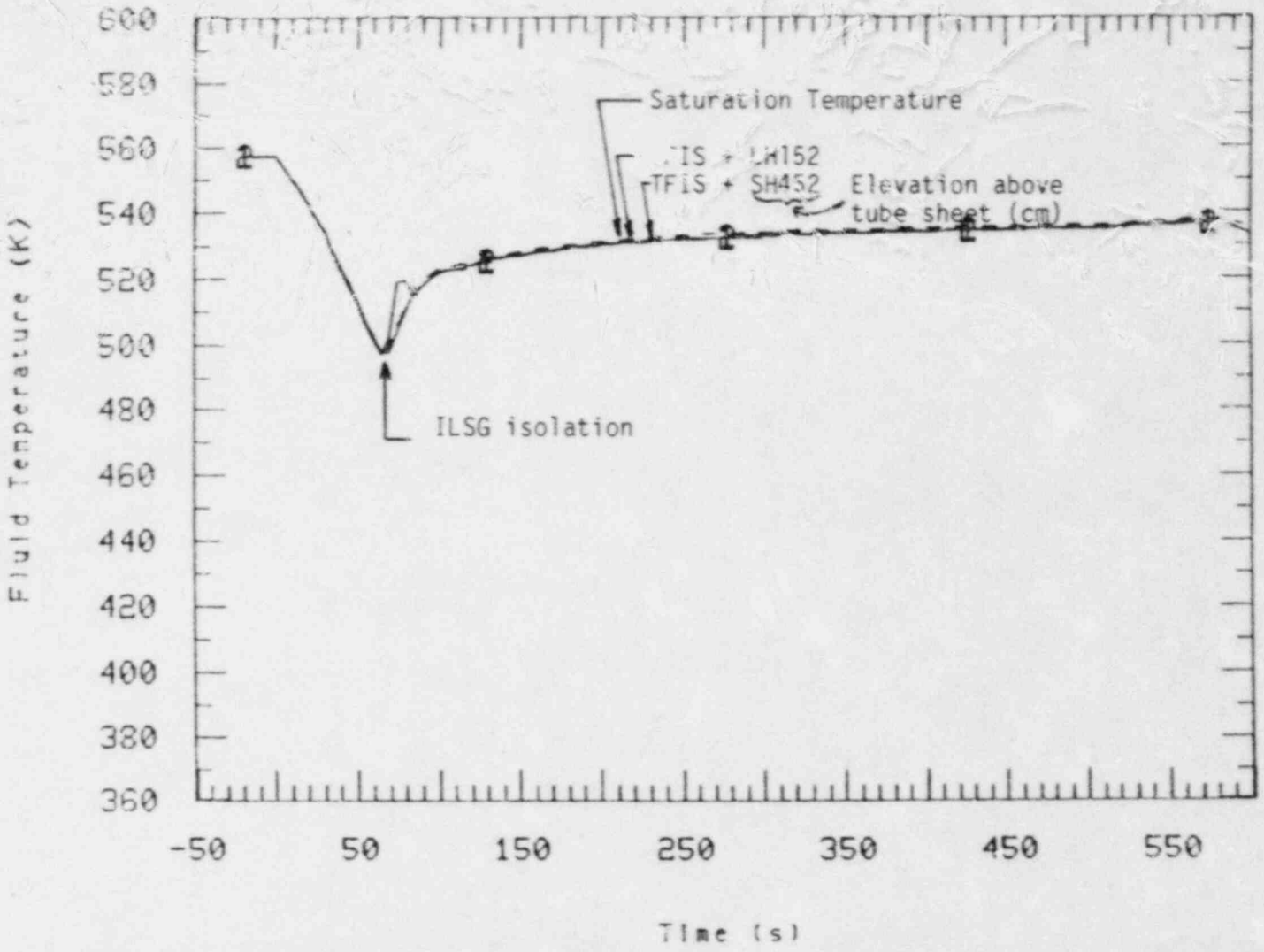

Figure 21. Selected intact loop secondary and saturation temperatures for Test S-SF-4.

and radiation from the U-tubes which are at primary temperature. Figure 22 compares saturation temperatures in the secondary of the two steam generators.

3.1.3.1 Broken Loop Primary-to-Secondary Heat Transfer. As the secondary fluid temperatures decreased the heat transfer from the primary to the secondary increased. The intact and broken loop overall primary-to-secondary heat transfer rates are shown in Figure 23. The heat transfer for the ILSG was divided by a factor of three so that it could be compared easily to the BLSG heat transfer rate. (The ILSG has three times the heat transfer area as the BLSG). The ILSG heat transfer peaked then decreased to a lower quasi-steady state level, then decreased again when the ILSG was isolated from the break at 65 seconds. Heat transfer into the secondary then became primarily a function of injection of ambient temperature auxiliary feedwater.

Figure 23 also indicates that the BLSG primary-to-secondary heat transfer initially increased at break initiation, then after about 35 seconds decreased to a relatively stable level. The heat transfer rate then stayed at this level until the core power increased at which time the BLSG heat transfer rate increased substantially. The heat transfer then slowly decreased as core power decreased and BLSG secondary mass inventory was lost.

Figures 24 and 25 show local heat transfer rates in the BLSG at selected elevations for the upflow side and downflow side of the U-tubes, respectively. These heat transfer rates were determined by considering the decrease in primary fluid temperature as it flowed through the U-tubes. The following relationship was used:

$$Q = \frac{\dot{M}\, Cp \quad (Tp_2 - Tp_1)}{Lp_2 - Lp_1}$$

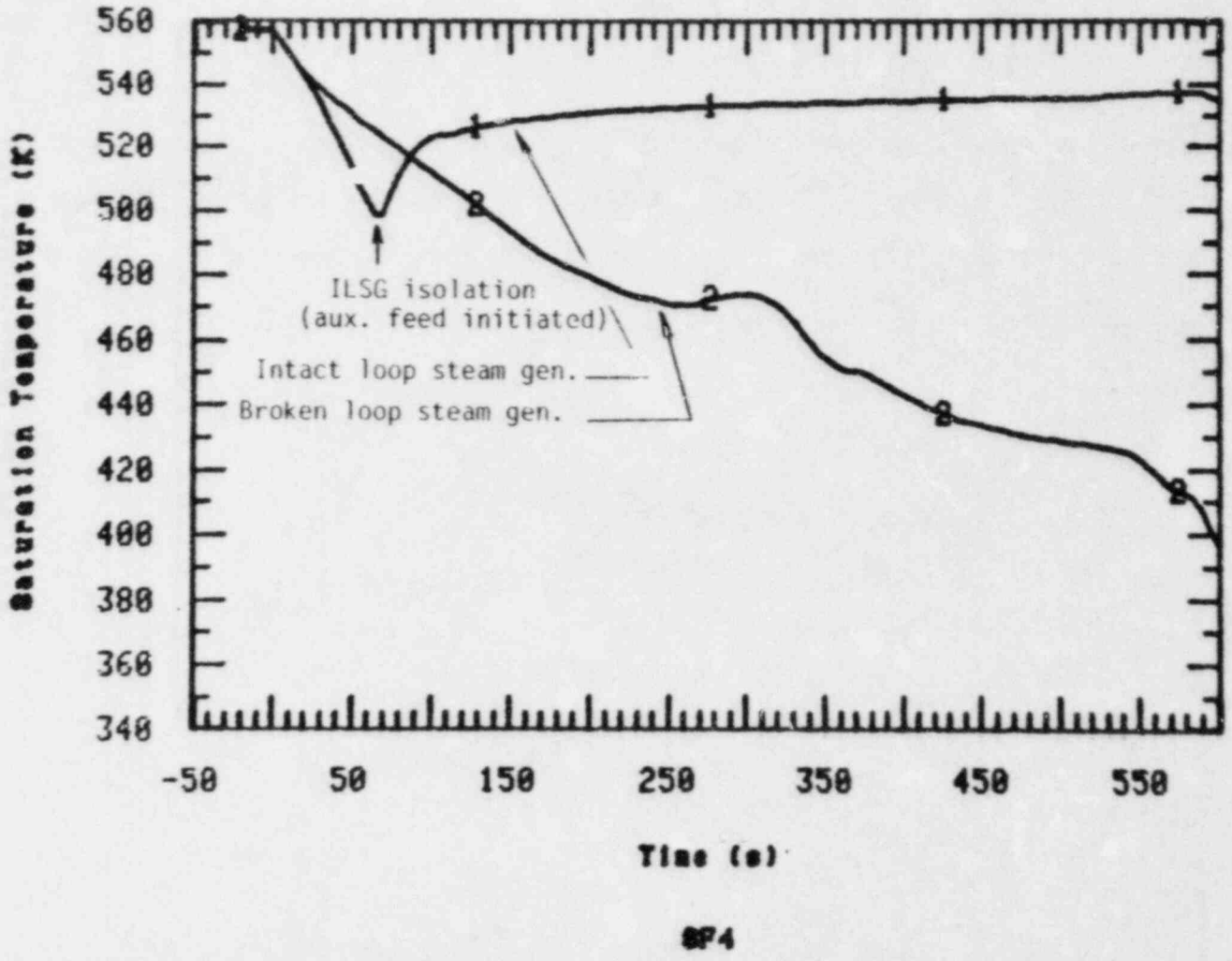

Figure 22. Secondary fluid saturation temperature in intact and broken loop steam generator for Test S-SF-4.

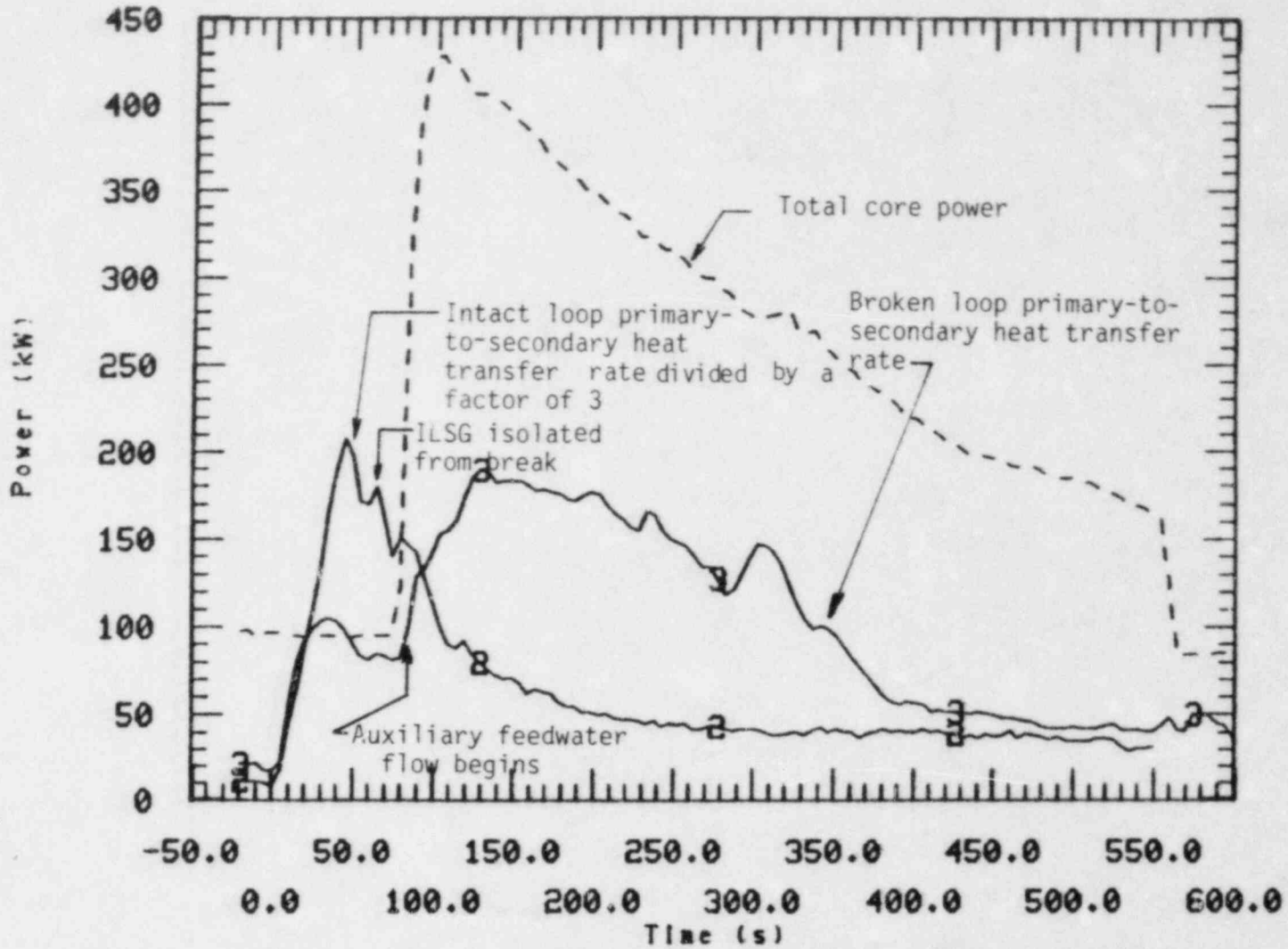

Figure 23. Core power and primary-to-secondary heat transfer rates for Test S-SF-4.

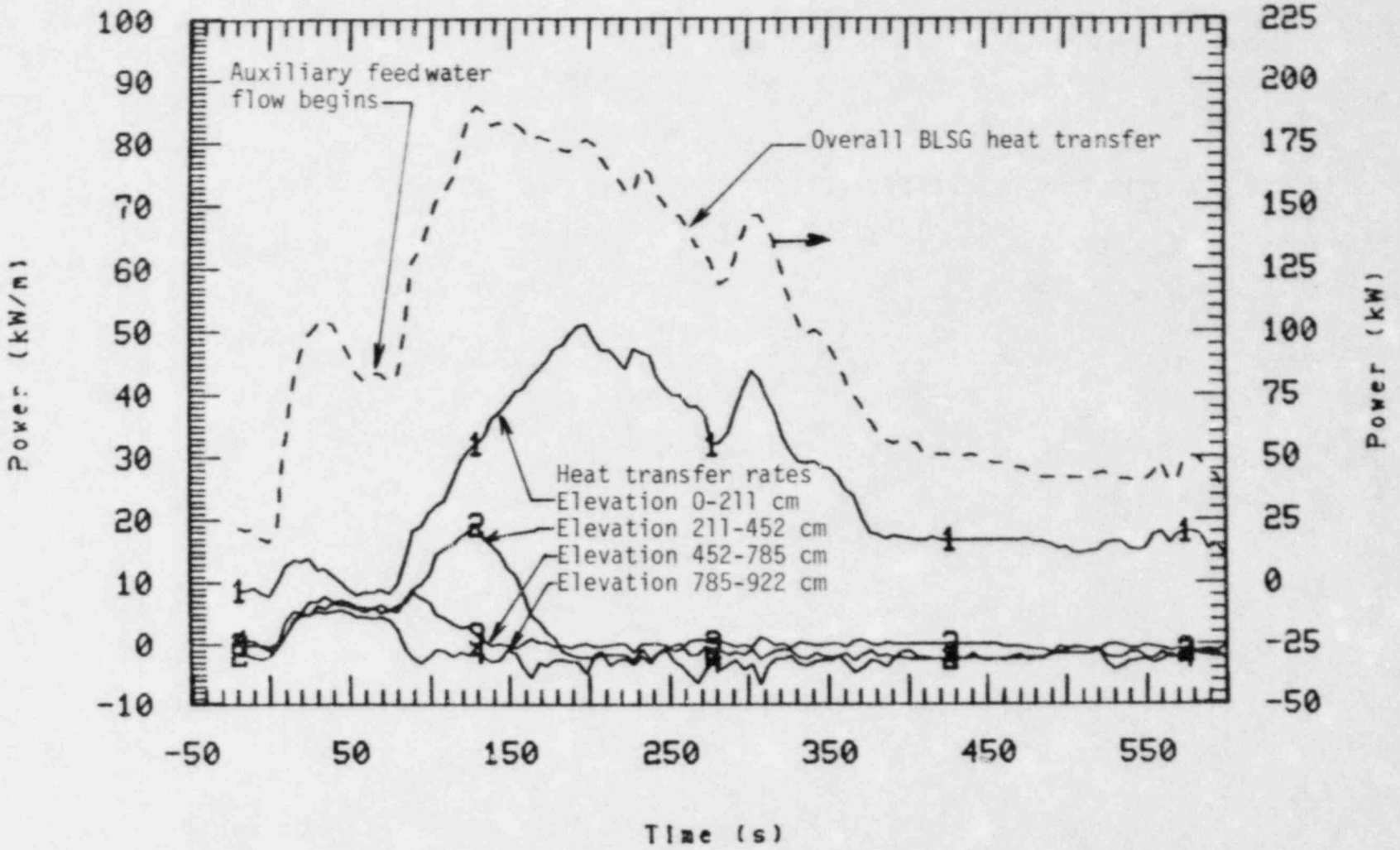

Figure 24. Local primary-to-secondary heat transfer rates for the upflow side of U-tubes and overall heat transfer rate for BLSG. Test S-SF-4.

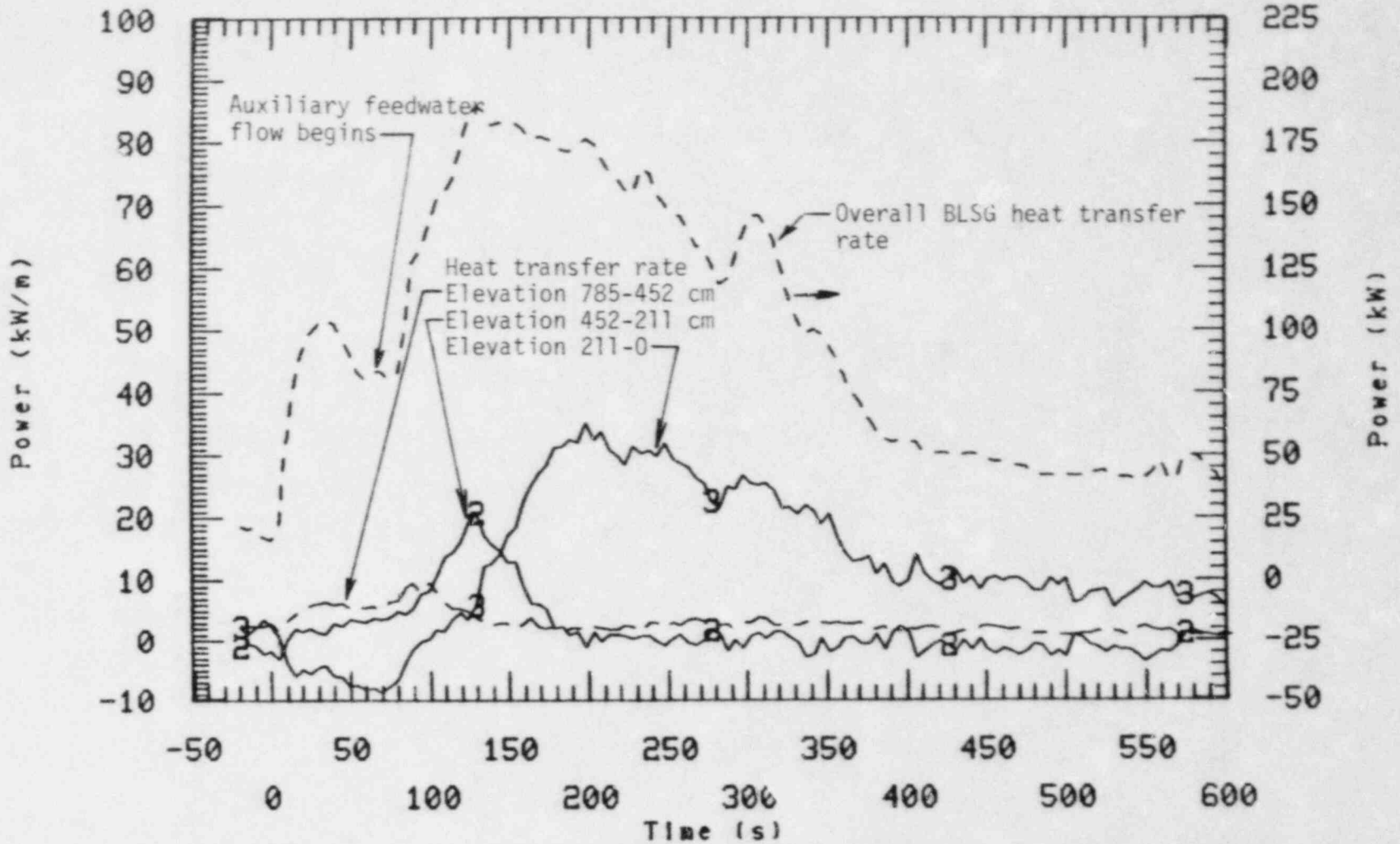

Figure 25. Local primary-to-secondary heat transfer rates for the downflow side of U-tubes and overall BLSG heat transfer. Test S-SF-4

where

Q is the heat transfer rate per unit of length

$\dot{M}$ is the primary mass flow rate through the generator

Cp is the specific heat of the primary fluid

Tp_2 is the temperature of the primary fluid at elevation L_{p2}

Tp_1 is the temperature of the primary fluid at elevation L_{p1}.

Lp_2 is the elevation of Tp_2

Lp_1 is the elevation of Tp_1.

These figures also show the overall BLSG primary-to-secondary heat transfer rate. (The initial negative heat transfer rate observed at the bottom of the downflow side (Figure 25) is due to the location of the temperature measurement used to determine the heat transfer rate. The downstream T.C. was located in the primary loop piping external to the steam generator. At break initiation the primary fluid flowing through the steam generator decreased substantially in temperature, but the large metal mass in the plenum and loop piping was still hot, which contributed to heating the primary fluid flowing from the steam generator. This is the reason that the indicated heat transfer at this location is negative until the primary metal decreases in temperature.) Inspection of these two figures shows that the reduction in overall BLSG heat transfer between 35 and 75 seconds was due to a decrease in local heat transfer rates near the bottom of the U-tubes. Initially the heat transfer in the bottom of the steam generator riser was enhanced, but then decreased. This decrease was attributed to a change in heat transfer coefficient, since the primary-to-secondary temperature differences (Figure 26) were relatively

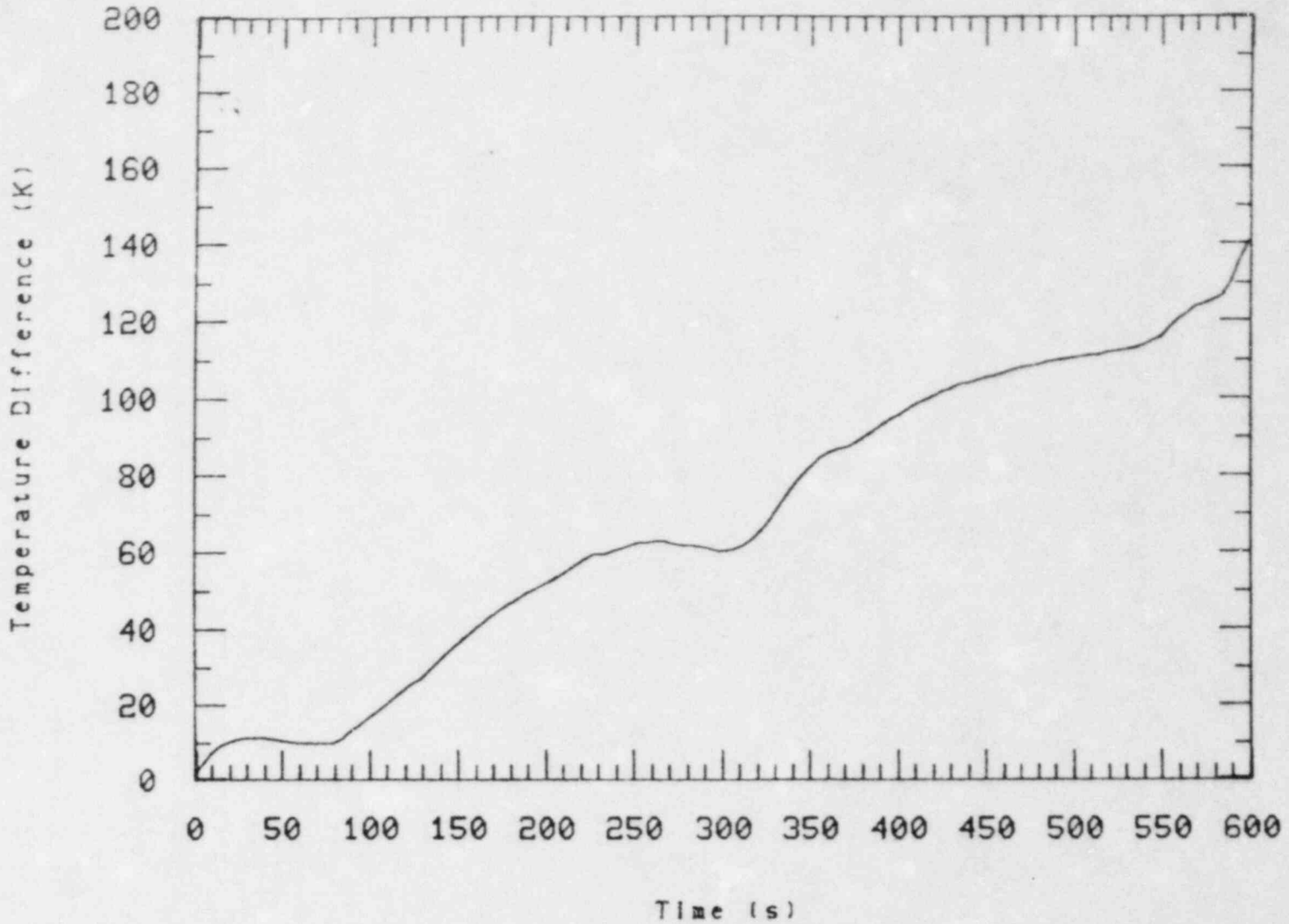

Figure 26. BLSG primary-to-secondary temperature difference for Test S-SF-4.

constant from 35 to 75 seconds. The temperature difference presented here is much greater than the primary temperature difference from inlet to outlet of the BLSG.

Figures 24 and 25 also show that local heat transfer above 211 cm increased to a relatively stable level during this same time period indicating that fluid was either swelled or advected into the upper regions of the secondary.

When the core power increased, the local heat transfer rates throughout the entire BLSG rose except for the heat transfer between 785 and 922 cm at the top of the tubes (see Figure 24). The local increases in heat transfer rates are attributed to the increased primary-to-secondary temperature difference which is readily seen in Figure 26. The loss of heat transfer at the top of the steam generator is attributed to a loss in secondary inventory which results in a convective heat transfer coefficient change as the outside of tubes go from a wetted condition to a dry condition. This loss in heat transfer was also apparent at other elevations (Figures 24 and 25) as the local heat transfer rate decreased as a function of elevation (top to bottom). After 65 seconds the heat transfer on both the upflow and downflow sides at the bottom of the riser section increased much more than at higher elevations. This was due to the ambient temperature feedwater which entered near the bottom of the steam generator riser. The local heat transfer rate at the bottom then decreased as a result of decreasing secondary mass. The heat transfer rate increase at the bottom of the generator was much larger than the decrease at the top.

To more clearly understand the effects of secondary mass inventory, the local heat transfer rates for the upflow side of the U-tubes are shown along with BLSG secondary mass inventory in Figure 27. On this figure 100% mass inventory is the mass required to fill the secondary to the top of the U-tubes at initial conditions. Due to the low initial power levels and resultant minimal level swell, an 81% initial mass inventory was not sufficient to cover the top portion of the U-tubes. At the initiation of break, however, a two-phase level swell occurred covering the upper portion

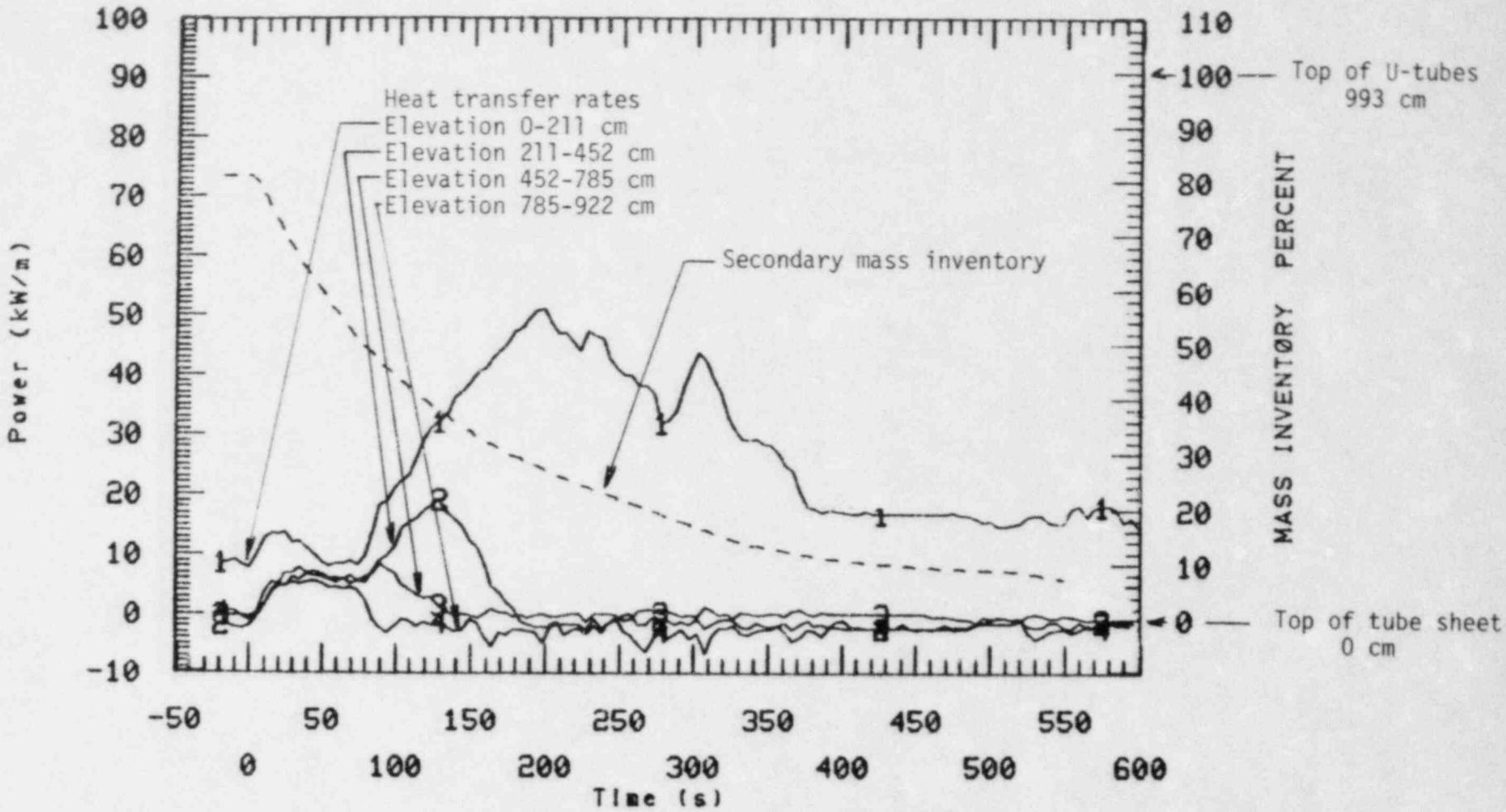

Figure 27. Local primary-to-secondary heat transfer rates for up-flow side of U-tubes in Broken Loop Steam Generator and secondary mass. Test S-SF-4.

of the U-tubes. As inventory was lost this two-phase level swell shrank and once again the U-tubes uncovered. This phenomenon can be seen in Figure 27. At the initiation of the steam line break, local heat transfer was enhanced by a two-phase level swell and by a decrease in secondary temperature. The break also caused a loss of inventory resulting in a drop of the two-phase level which can be seen as a reduction in local heat transfer rates at the higher U-tube elevations. The local heat transfer rates decreased in order from top to bottom as secondary inventory was lost. At 65 seconds the auxiliary feedwater flow injection began which reduced the loss of secondary inventory. The secondary mass exponentially approached an equilibrium value as did the local heat transfer rate at the bottom of the BLSG.

Figure 28 shows overall BLSG heat transfer as a function of BLSG secondary mass. In this figure the BLSG primary-to-secondary heat transfer has been normalized to the instantaneous core power. This was done in an attempt to remove some of the heat transfer effects due to changing core power. 100% heat transfer in this figure indicates that the BLSG primary-to-secondary heat transfer rate was equal to the total core power. When the break was initiated (@ 81% inventory) the overall heat transfer rate in the BLSG increased to 110% of the power produced by the core. The overall heat transfer then decreased due to a reduction in the heat transfer coefficients on the U-tube surfaces (as already discussed) at the lower elevations of the BLSG. At approximately 53% inventory the normalized heat transfer began to decrease significantly to about 30%. This was due to the rapid increase in core power at this time. The BLSG then started to respond to the increase in core power by increasing heat transfer rates. This increase in heat transfer was primarily due to increasing primary-to-secondary temperature differences (see Figure 26). Also during this time the two-phase level swell was covering most of the tube length. The heat transfer then began to level off. The heat transfer at the upper elevations of the steam generator then started to decrease due to loss of secondary inventory but the heat transfer at the bottom of the steam generator increased during this same period. On this curve it is difficult to see the effects of mass inventory on overall heat transfer due to the large increases in local heat transfer occurring at the bottom of the

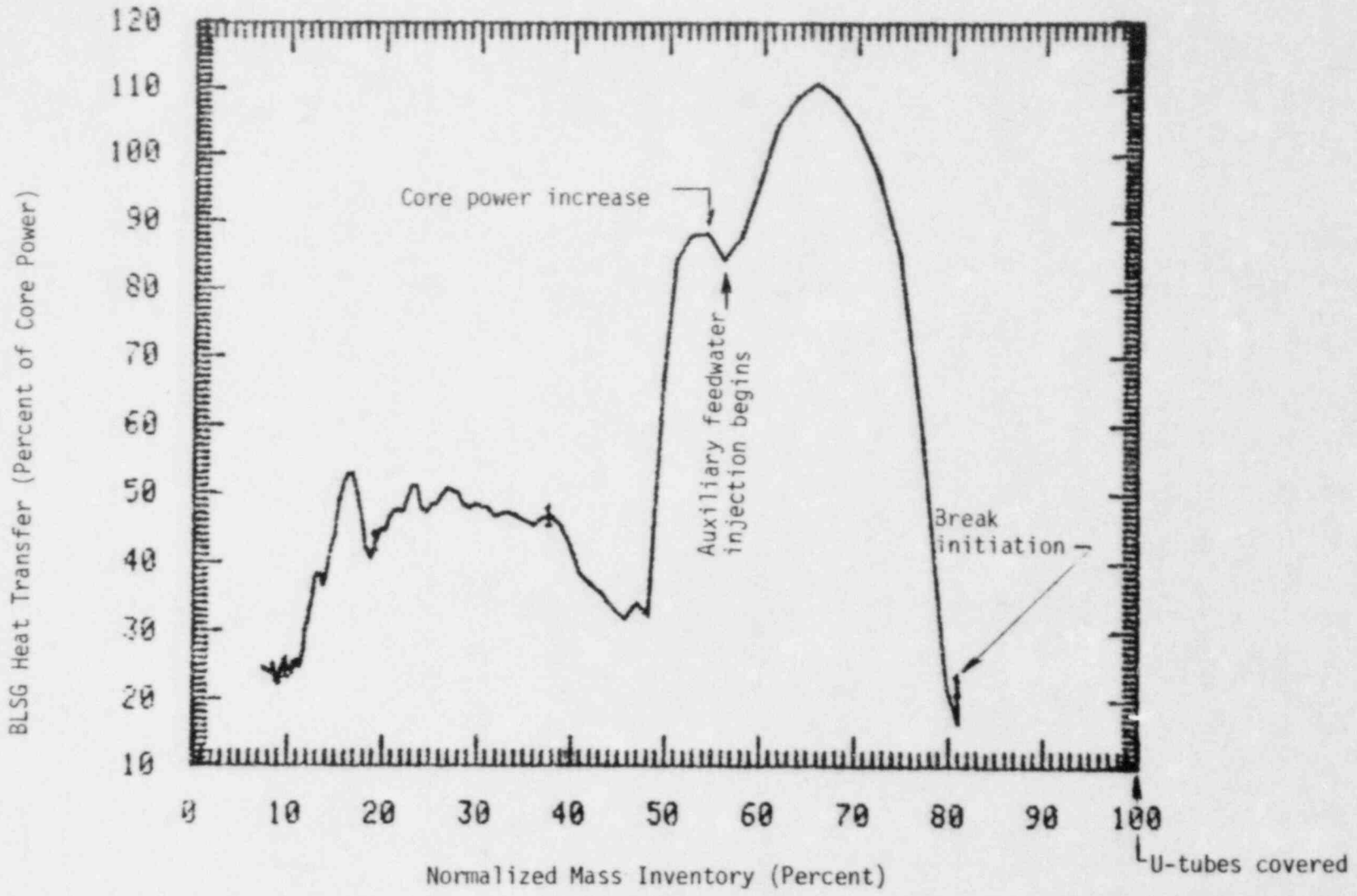

Figure 28. Normalized BLSG heat transfer vs. normalized BLSG secondary inventory. Test S-SF-4.

U-tubes at the same time small decreases in local heat transfer rates are occurring at the top of steam generator (see Figures 24 and 25). At low core power levels most of the overall heat transfer occurred near the primary inlet to the steam generator. The heat transfer at higher elevations in the U-tubes is insignificant compared to heat transfer at the bottom.

3.1.3.2 Intact Loop Primary-to-Secondary Heat Transfer. The primary-to-secondary heat transfer rate behavior in the ILSG was somewhat different than that in the BLSG. Figures 29 and 30 show representative local heat transfer rates at selected elevations in the upflow and downflow side of the U-tubes, respectively. The local heat transfer rates were determined in the same manner as those for the BLSG. Also shown in the figures is the overall ILSG primary-to-secondary heat transfer rate. Unlike the BLSG, the local heat transfer increased significantly in the upflow side of the U-tubes only, resulting in an overall heat transfer increase at break initiation. The ILSG local heat transfer is similar to the BLSG in that the local heat transfer decreases after the initial peaking. Again this was a result of an increase in heat transfer coefficient on the shell-side of the U-tubes. Figure 31 indicates that the primary-to-secondary temperature differential changed smoothly and, before ILSG isolation, (0-65 seconds) rapidly increased. This indicates that it was a change in heat transfer coefficient which caused the local heat transfer rate to decrease in the upflow side of the U-tubes rather than a decrease in the temperature difference. The temperature difference presented in Figure 31 is representative of local primary-to-secondary temperature differences.

An interesting difference in the heat transfer behavior between the two steam generators was that the local heat transfer in the upper elevations of the ILSG peaked, then decreased; whereas at corresponding levels in the BLSG local heat transfer reached a maximum level and stayed there until the core power changed. Again, this change in heat transfer rate was due to a change in the heat transfer coefficient since primary-to-secondary temperature differential was relatively constant. It should also be noted that there was enough secondary mass to keep the

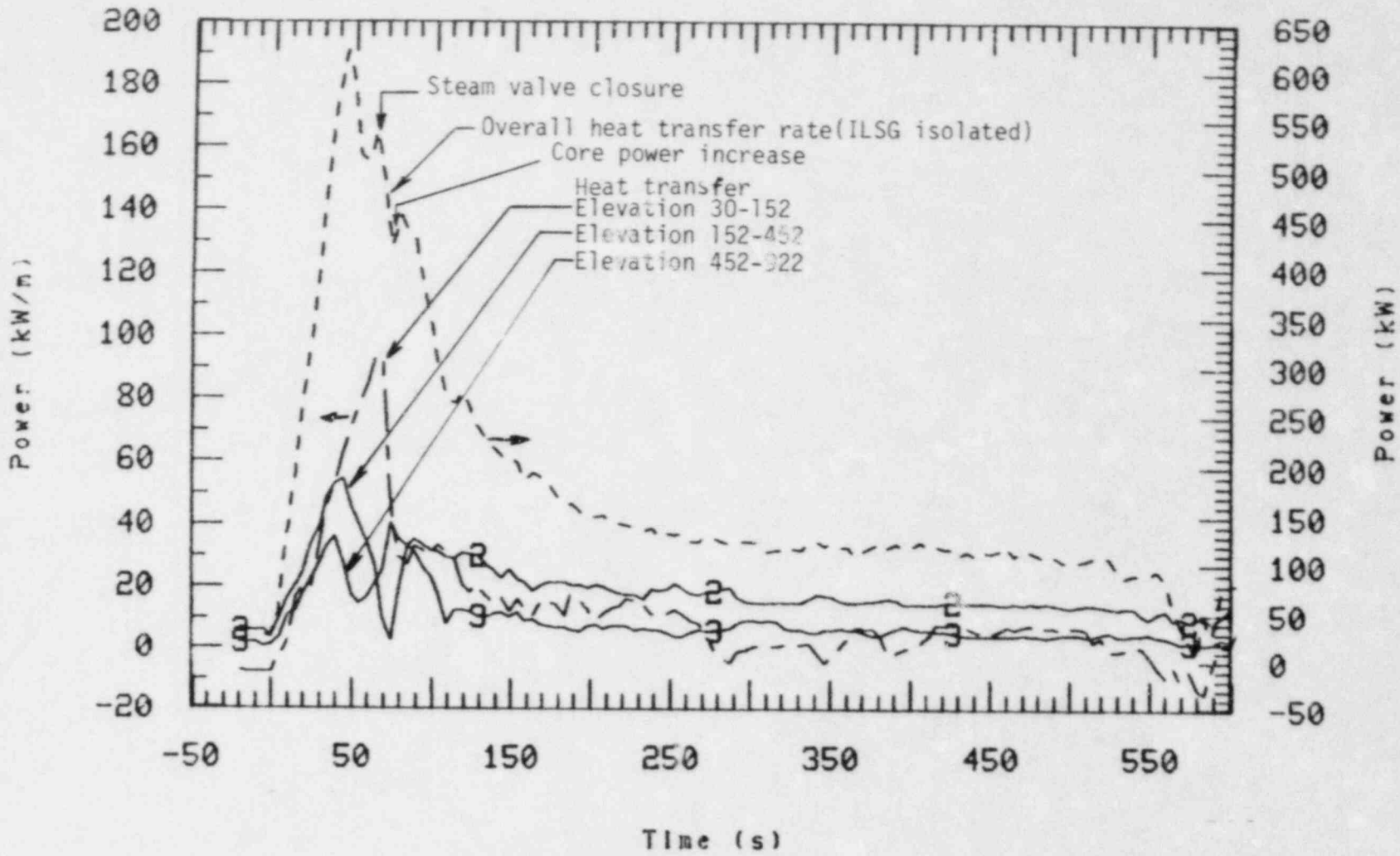

Figure 29. ILSG local heat transfer rate in upflow side of U-tube and overall heat transfer for Test S-SF-4.

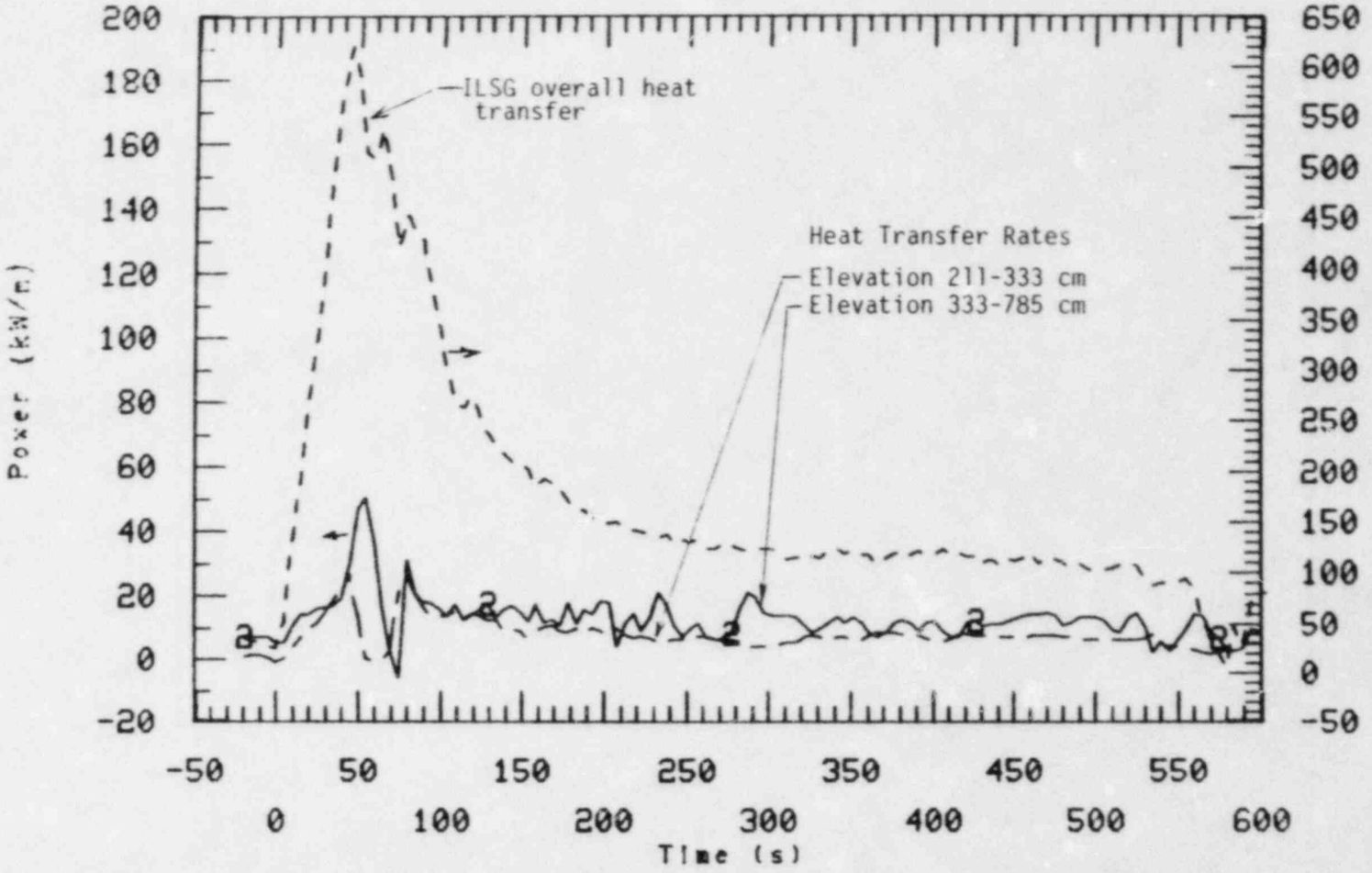

Figure 30. ILSG local heat transfer rate in downflow side of U-tube and overall heat transfer rate. Test S-SF-4.

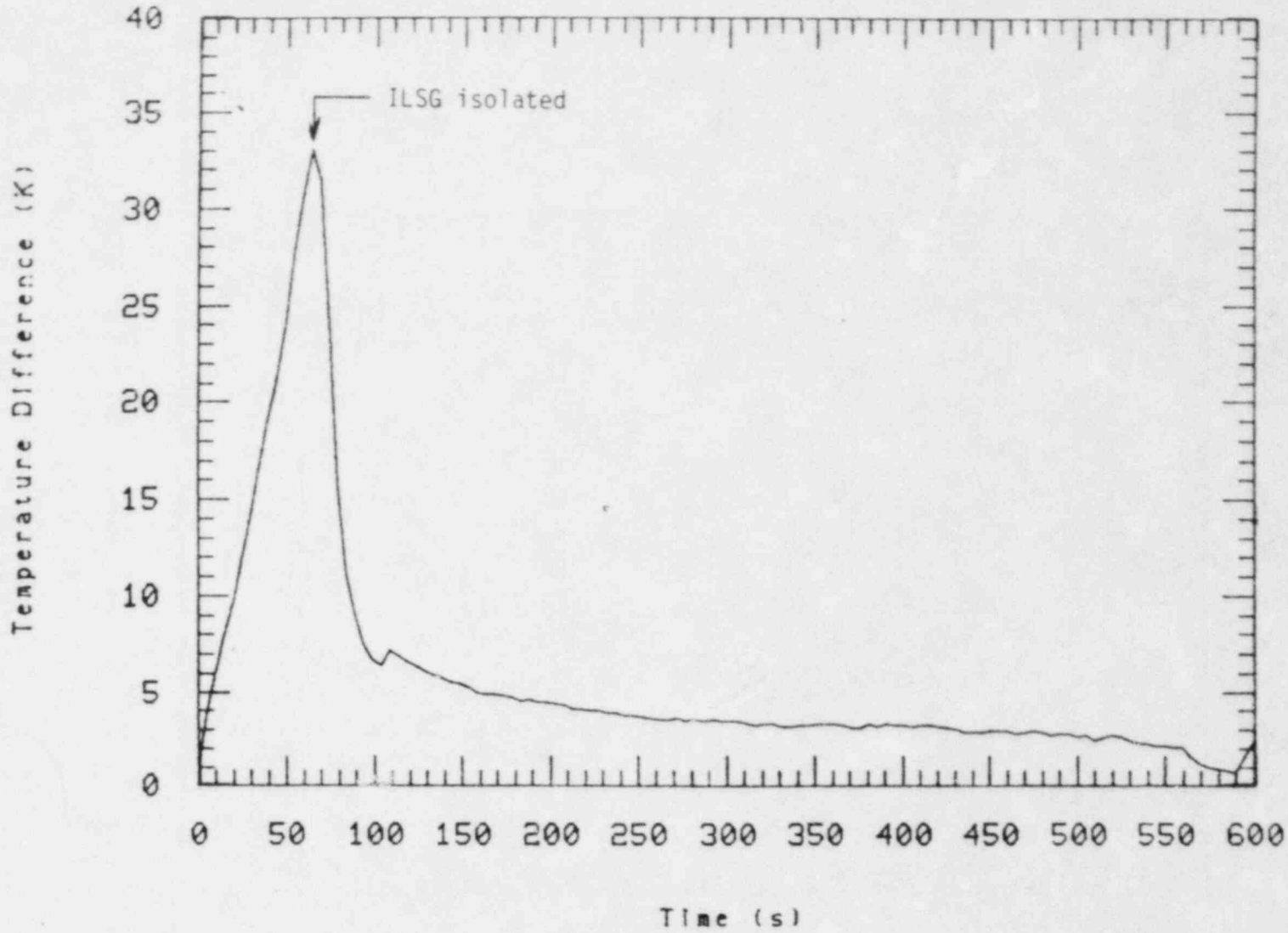

FIgure 31. Intact loop primary-to-secondary temperature difference for Test S-SF-4.

U-tubes covered with liquid. Another behavior difference between the two steam generators was the local heat transfer at the bottom of the U-tubes. The heat transfer in the BLSG peaked then decreased but in the ILSG it was still on the increase until the ILSG was isolated. The reason for this heat transfer behavior difference is not fully understood because of limited instrumentation available to measure local phenomena in the steam generators. One difference between the conditions in the two generators, however, is the initial mass. Figure 32 shows local heat transfer from the upflow side of the U-tubes and the secondary mass inventory for the ILSG. (Again 100% on the mass inventory curve represents the mass required to cover the top of the U-tubes.) Note that the ILSG inventory begins at about 150% compared to 81% for the BLSG. Differences in the initial mass inventories (level difference) may be one reason that the localized heat transfer behavior is different in the two steam generators.

Figure 32 also indicates that the initial overall heat transfer peaking and subsequent decrease was not a result of inventory depletion since inventory was still in the 90 to 80% range. The two-phase level swell associated with the depressurization would keep the U-tubes covered at this inventory. The local heat transfer in the upflow side of the U-tubes then decreased due to a change in heat transfer coefficient since abrupt changes in primary-to-secondary temperature differential were not observed. The heat transfer then decreased at 65 seconds as a result of the two-phase level swell collapsing as the ILSG was isolated from the steam line break.

Figure 33 shows the normalized ILSG primary-to-secondary heat transfer rate as a function of ILSG secondary inventory. Again, to minimize the effects of changing core power the ILSG heat transfer rate was normalized to the heat generated (power) produced by the core. 100% heat transfer indicates the heat transfer rate of the ILSG was equivalent to the core power. Due to the large initial mass inventory the loss of inventory prior to ILSG isolation had no effect on the heat transfer rates. The two phase level swell kept the tubes covered up until time of isolation. Figure 33 shows the mass inventory beginning at 150%. Following break initiation the heat transfer rate in the ILSG rises to 6.5 times that produced by the

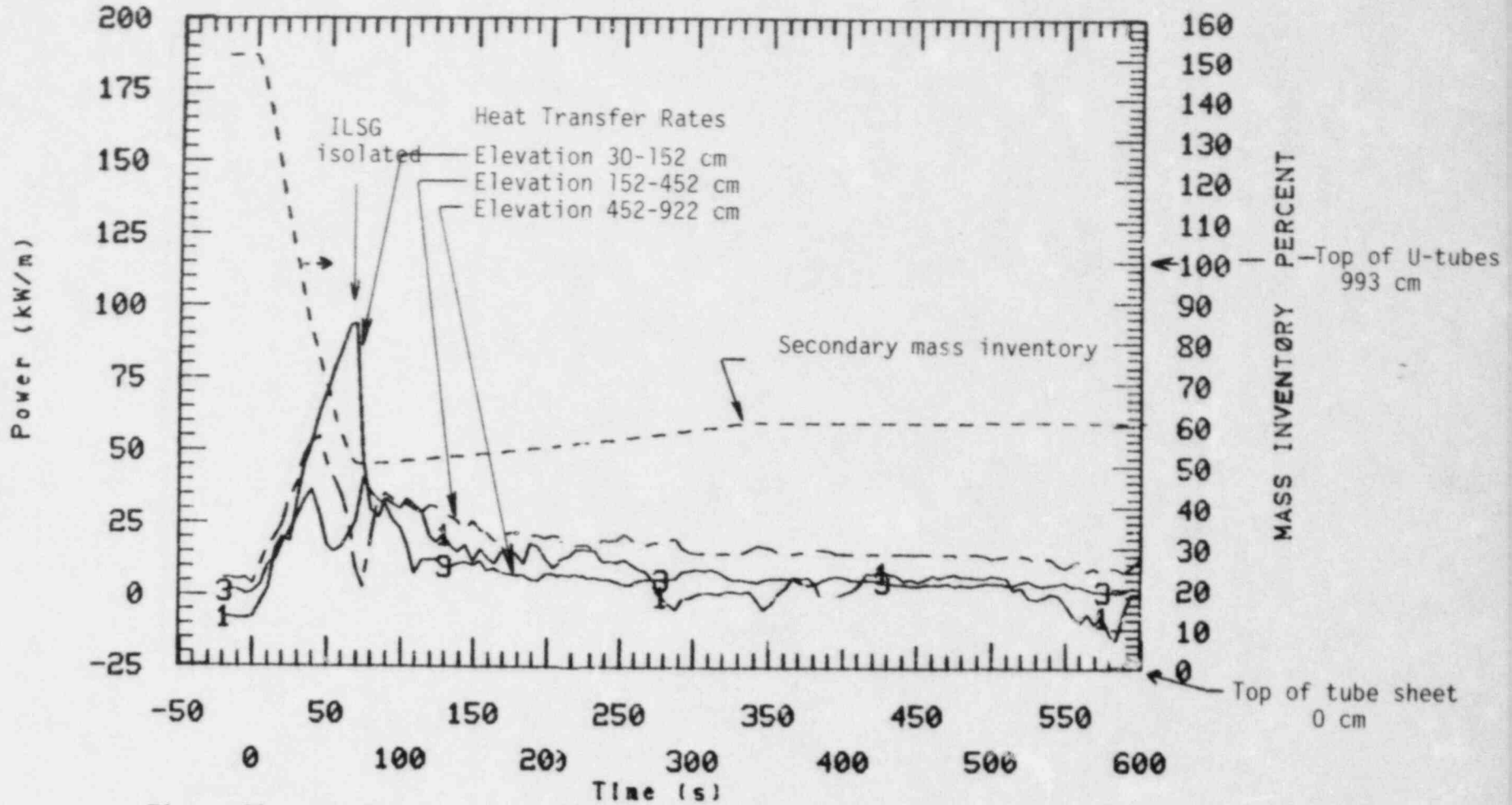

Figure 32. Local primary-to-secondary heat transfer rates for the intact loop steam generator upflow side of the U-tubes and secondary mass inventory. Test S-SF-4.

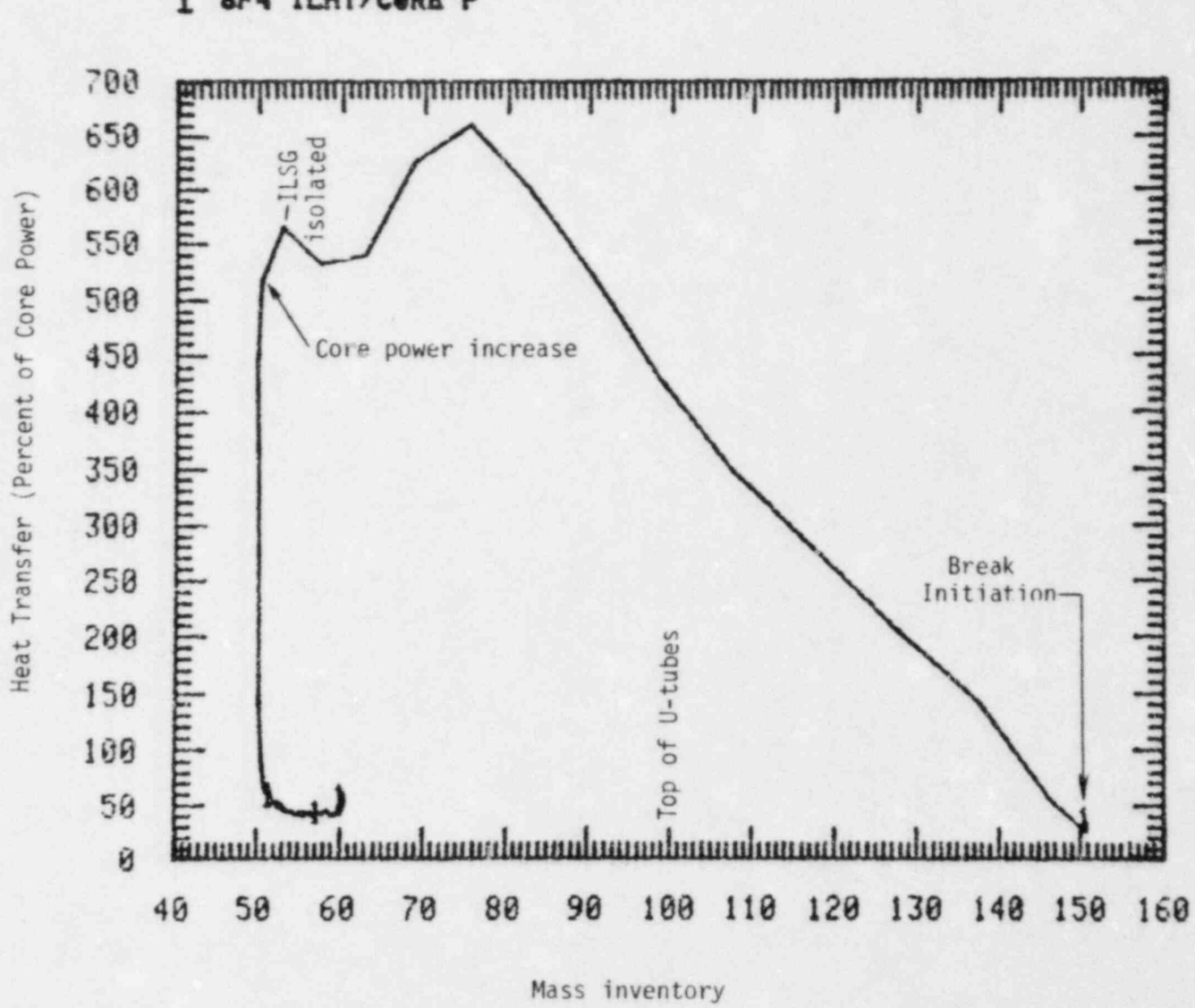

Figure 33. Normalized ILSG primary-to-secondary heat transfer vs.normalized mass inventory. Test S-SF-4.

core. The heat transfer then decreased due to changes in heat transfer coefficients as already discussed. At approximately 55% inventory the ILSG is isolated from the break which resulted in loss of heat transfer. At approximately 52% inventory the core power rapidly rises which decreased the normalized ILSG heat transfer rapidly. Due to isolation of the break, two-phase level swell was suppressed preventing total tube coverage. In addition the secondary pressure increased which reduced heat transfer by phase change. The ILSG heat transfer rate then decreased to approximately 50% of the core power.

3.2 Test S-SF-5

3.2.1 General Response

Test S-SF-5 was also initiated from a hot standby condition. Core power, augmented by guard heaters, was sufficient to compensate for environmental heat losses and to maintain initial conditions. For Test S-SF-5 the core power was held constant in an attempt to increase the primary depressurization and cooldown. In addition the break nozzles were scaled to represent a steam line break 50% of the size of one flow restrictor in a full-scale plant (see Figure 1). Another important change was that the secondary coolant volumes (ILSG and BLSG) were significantly less than in S-SF-4.

At t = 0 the break was initiated. Figure 34 shows the response of the primary system pressure and pressurizer liquid level. The primary pressure decreased throughout the duration of the test. This was a result of primary fluid shrinkage caused from enhanced primary-to-secondary heat transfer. The liquid level in the pressurizer also decreased as a result of primary volume shrinkage.

Figure 35 shows secondary pressures in the steam generators and the primary system pressure. The BLSG secondary pressure decreased continually during the test approaching ambient conditions. When the BLSG secondary pressure reached 4.13 MPa (at 90 seconds) the ILSG secondary was isolated and repressurized slightly to a constant level. This resulted in the

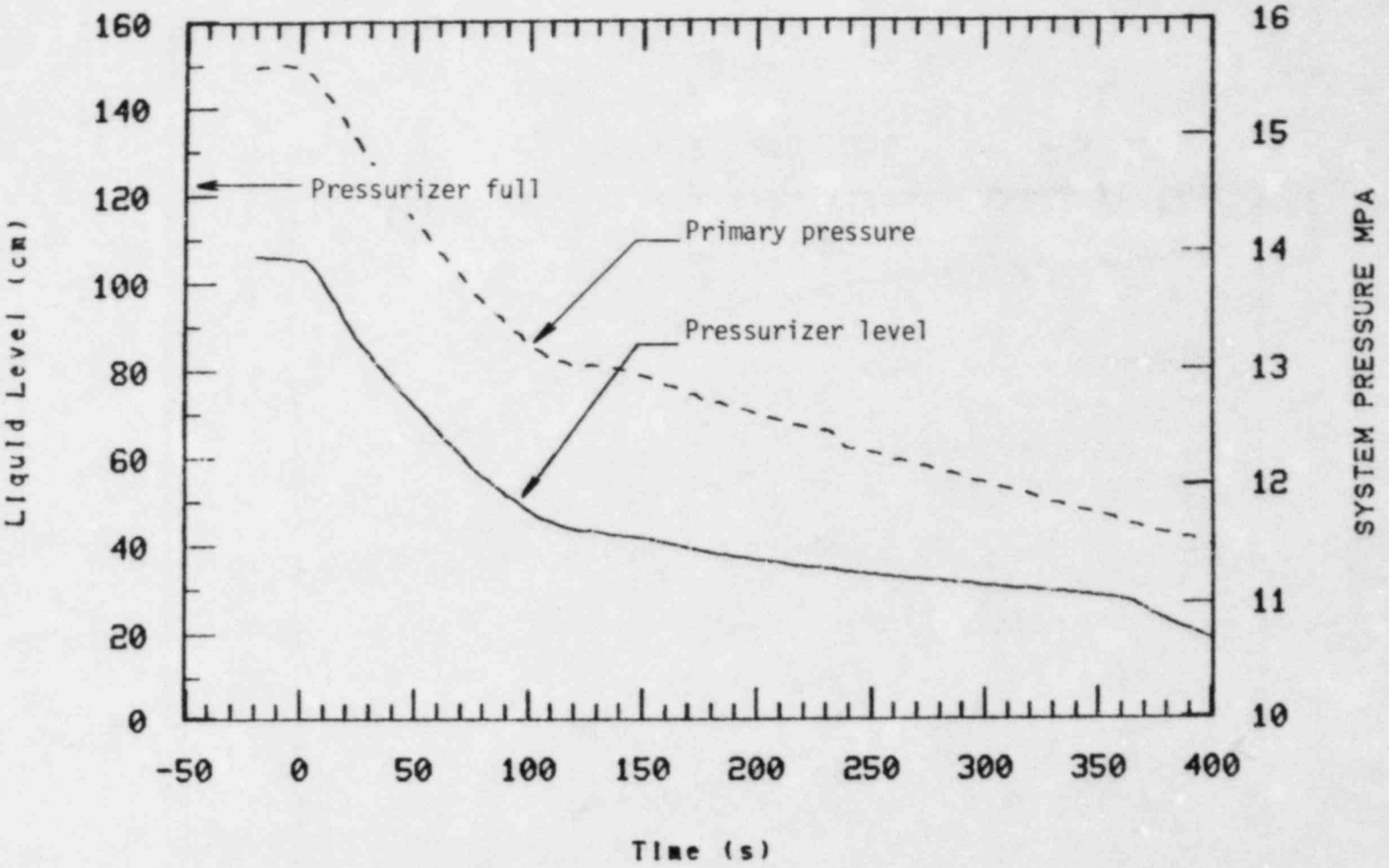

Figure 34. Pressurizer level and primary pressure for test S-SF-5.

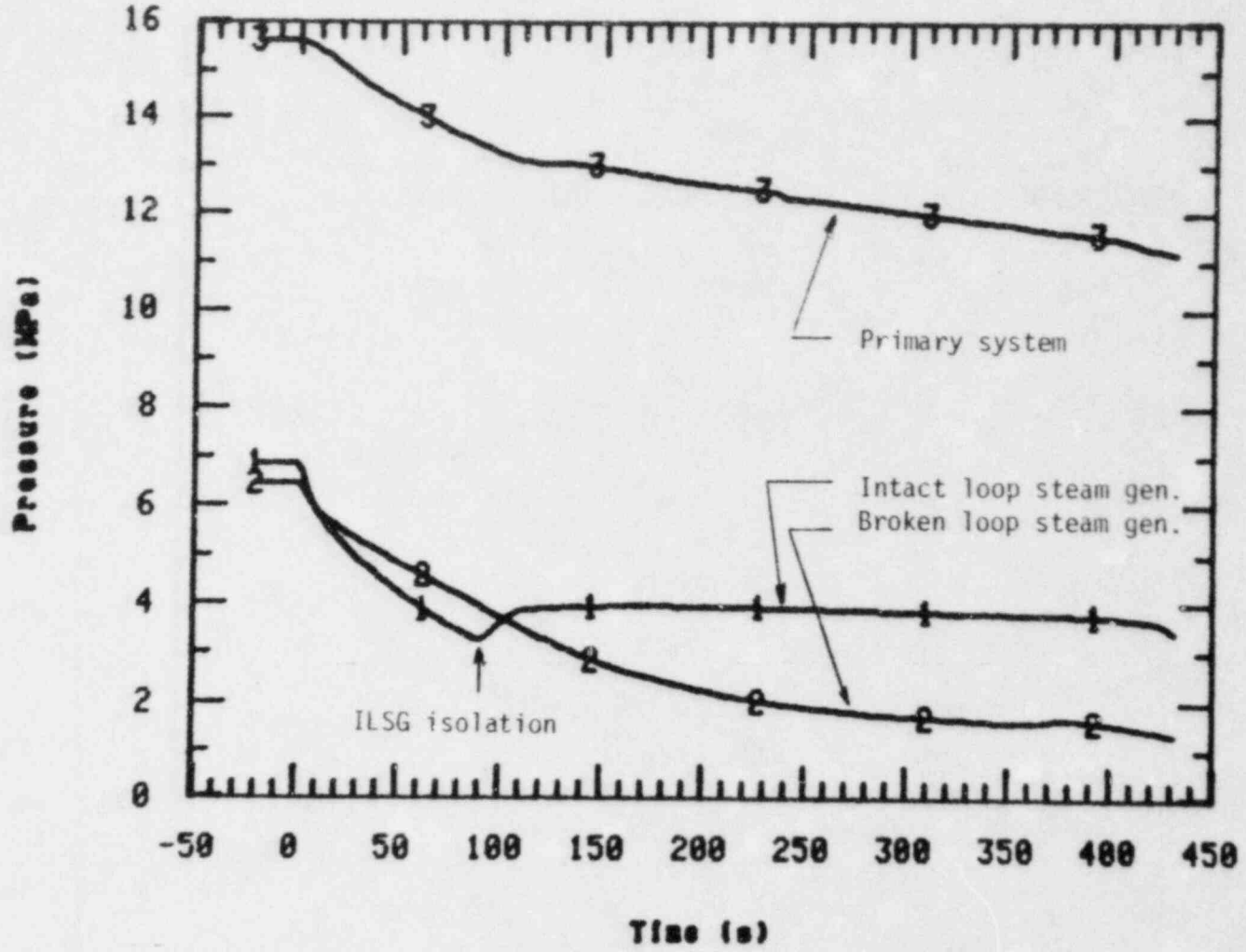

Figure 35. Primary system and steam generator secondary pressures for Test S-SF-5.

reduction of primary-to-secondary heat transfer in the ILSG. This loss in heat transfer can be seen in the slope change in the primary system depressurization at 100 seconds.

Figure 36 shows the core power and system pressure during the test. As can be seen, the core power remained constant during the test and as a consequence it did not affect the primary system depressurization as it did in Test S-SF-4.

3.2.2 Break Flow

Figure 37 shows the break flow for each steam generator. As expected the flows were choked and then decreased as secondary pressure decreased. Again the ILSG break flow decreased faster because its secondary pressure dropped faster than the BLSG secondary pressure (see Figure 35). When the safety injection signal was reached at 90 seconds the ILSG steam valves closed and the ILSG break flow dropped to 0. The break flow from the BLSG decreased slowly to a constant flow following the BLSG secondary pressure decrease.

3.2.3 General Secondary Heat Transfer

As the pressures in the secondaries decreased, so too did the bulk secondary fluid temperatures. Figure 38 shows the saturation temperatures corresponding to secondary system pressures. These saturation temperatures are representative of bulk secondary fluid temperatures and as a result of this secondary temperature drop the primary-to-secondary heat transfer increased. Figures 39 and 40 show selected secondary fluid temperatures and saturation temperatures in the BLSG and ILSG, respectively. The fluid temperatures follow the saturation temperatures. The thermocouples indicate higher than saturation temperature, however, when the liquid level drops below these locations. The higher temperatures are due to heat conduction from the U-tubes (which the thermocouples are mounted to) down the thermocouple sheath. Figure 41 shows the overall heat transfer rates in the steam generators and core power. Again, the total heat transfer in the ILSG has been decreased by a factor of three so that it can be readily

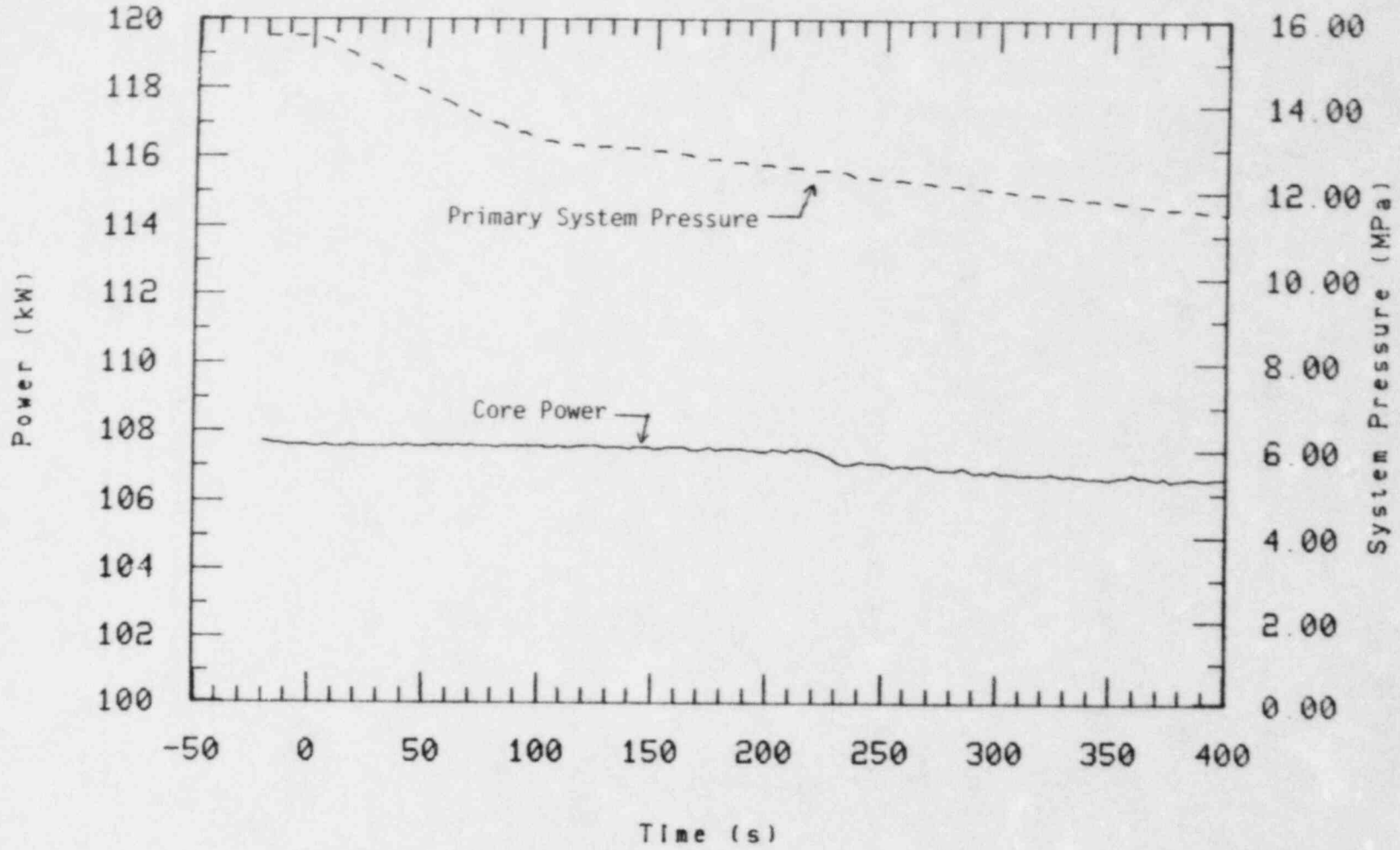

Figure 36. Core power and primary system pressure Test S-SF-5.

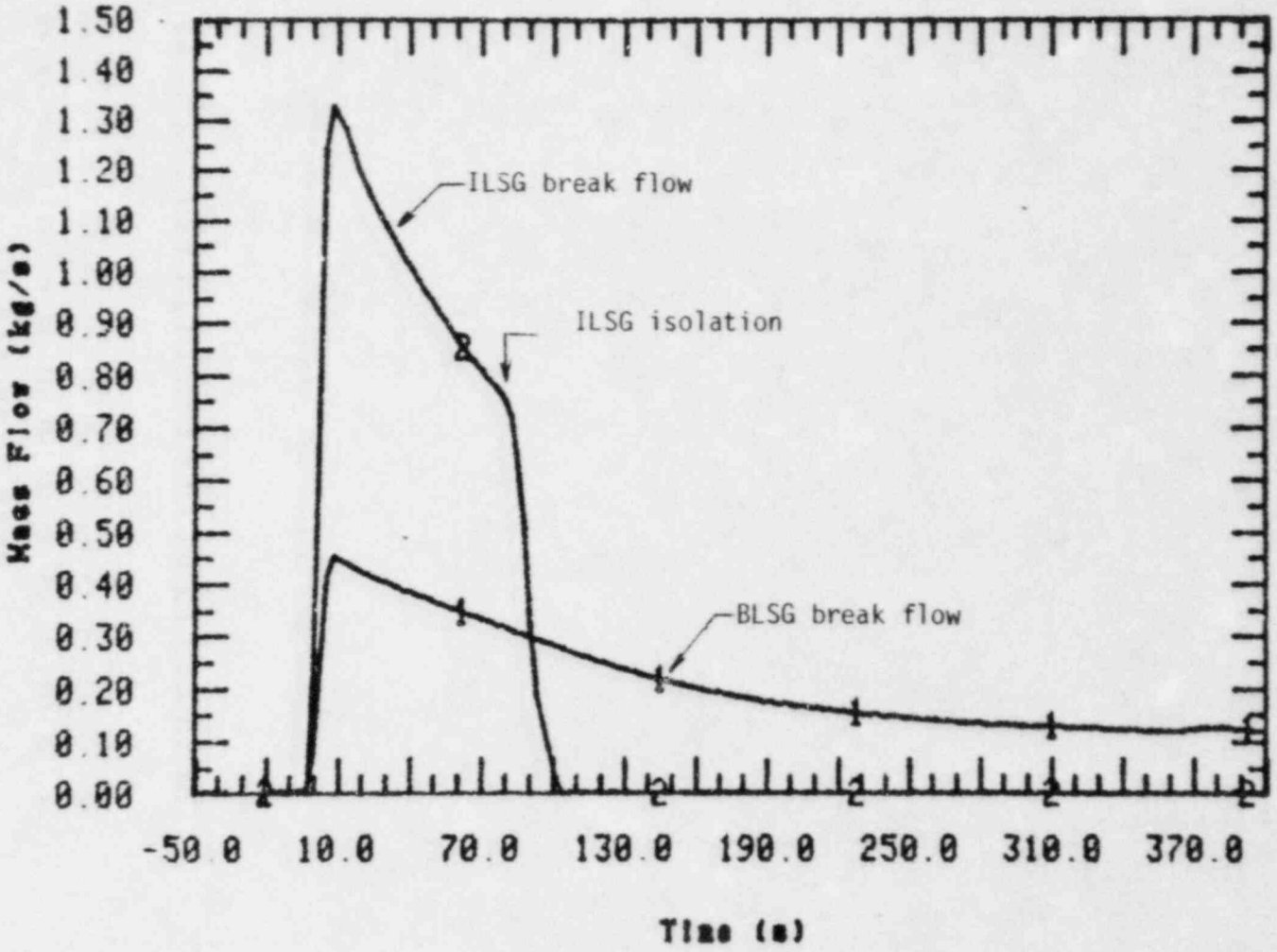

Figure 37. Break flow rates for Test S-SF-5

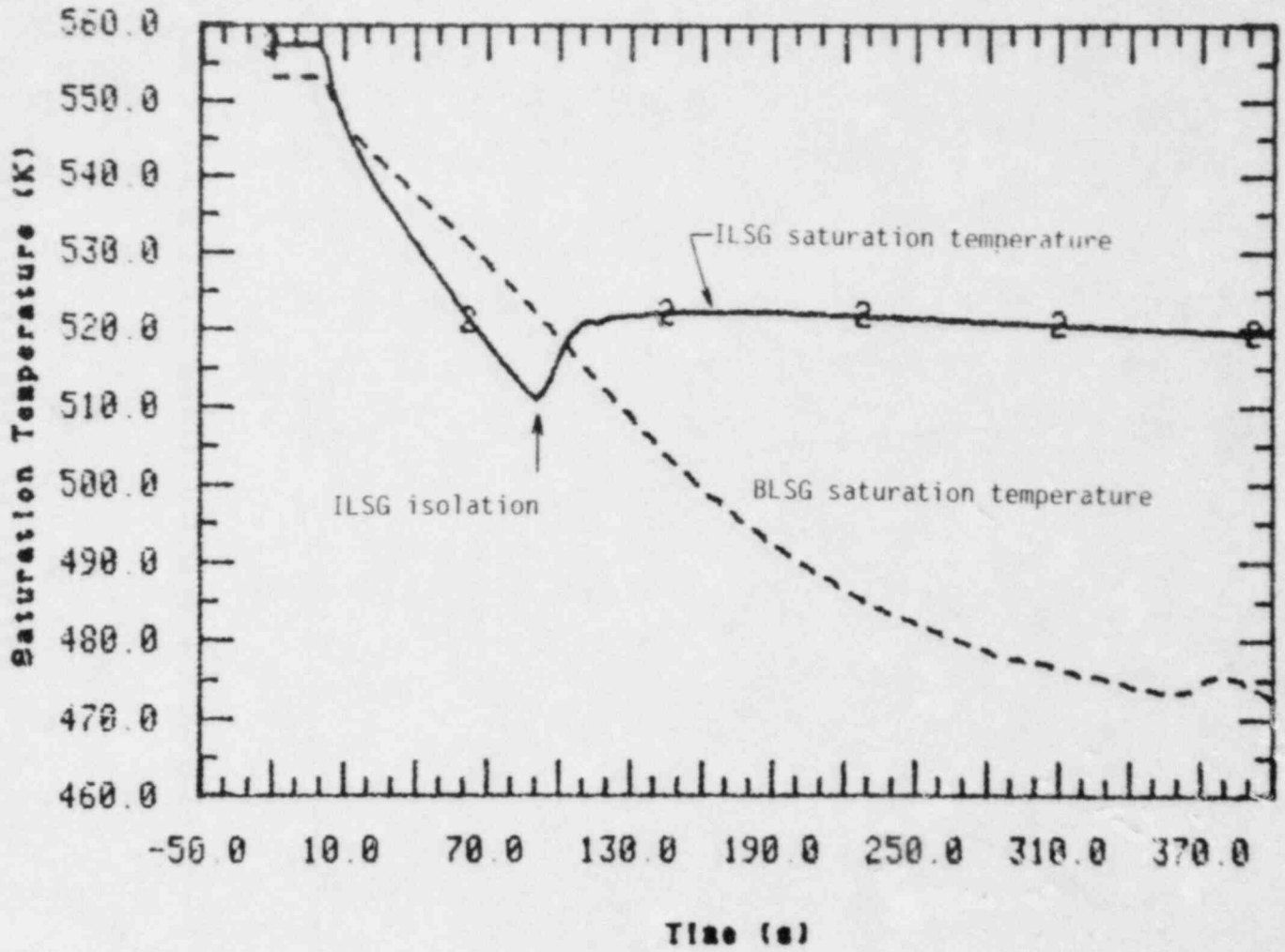

Figure 38. Secondary saturation temperatures for Test S-SI-5.

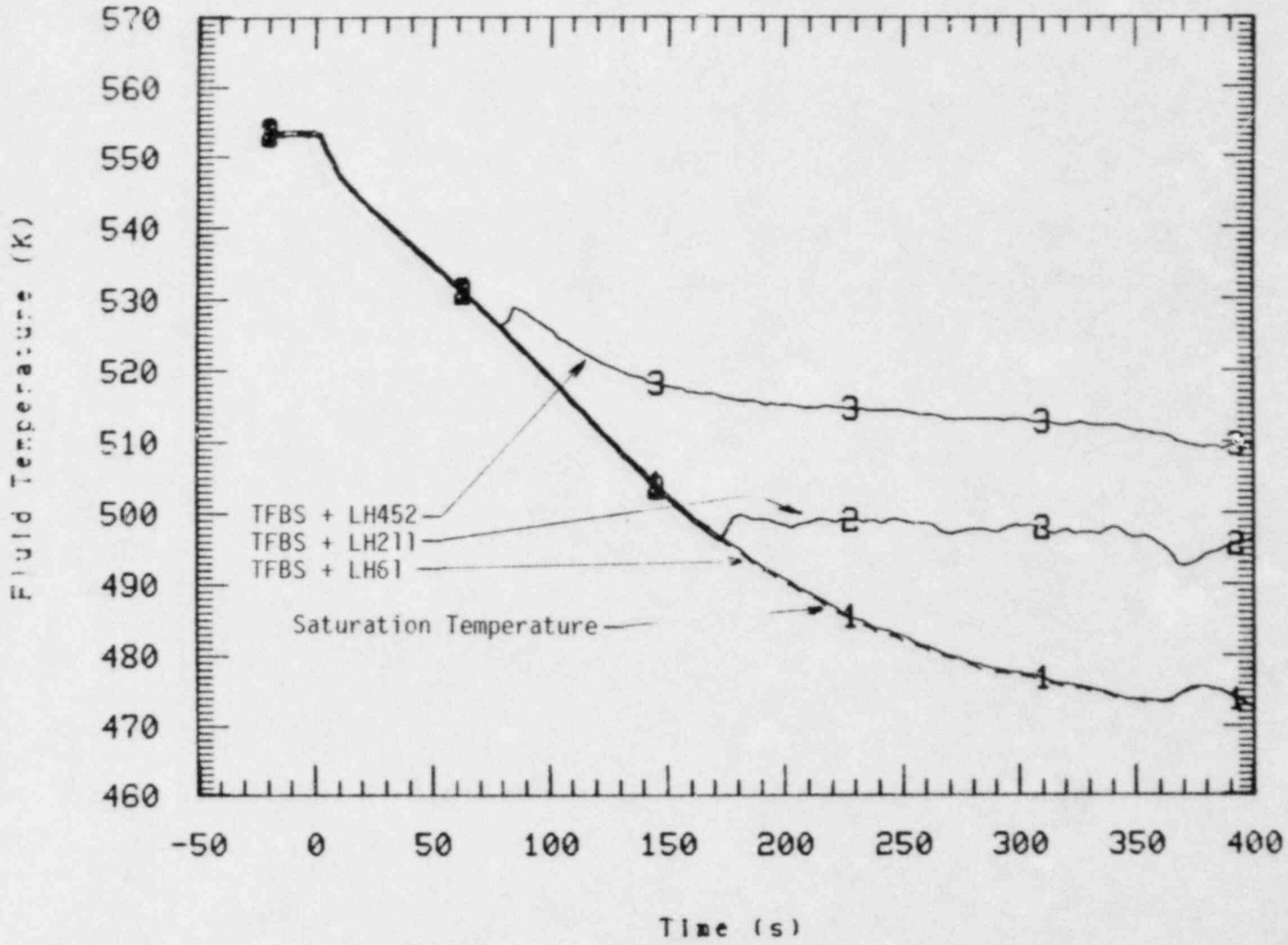

Figure 39. Selected broken loop secondary and saturation temperatures for Test S-SF-5.

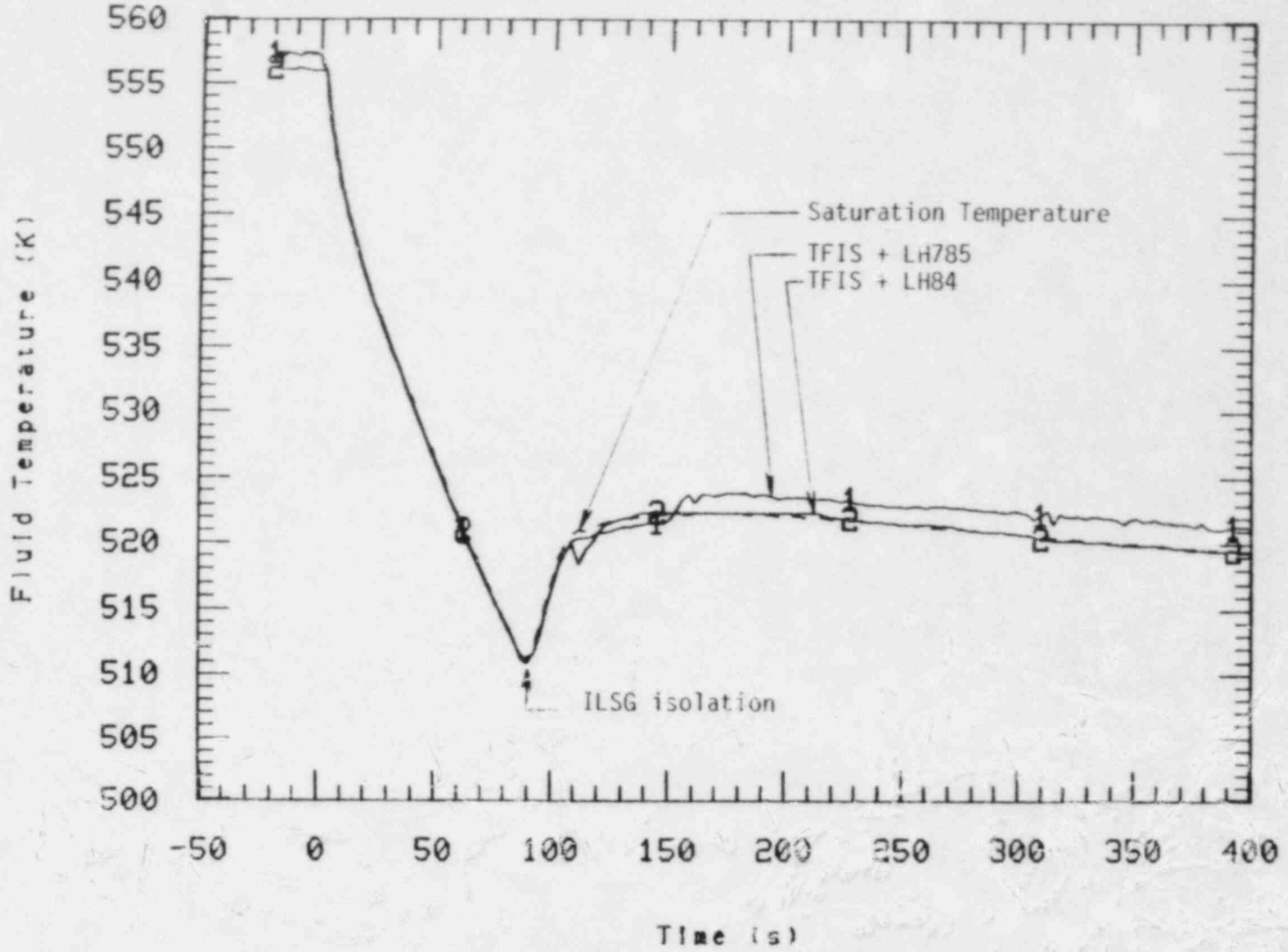

Figure 40. Selected intact loop secondary and saturation temperatures for Test S-SF-5.

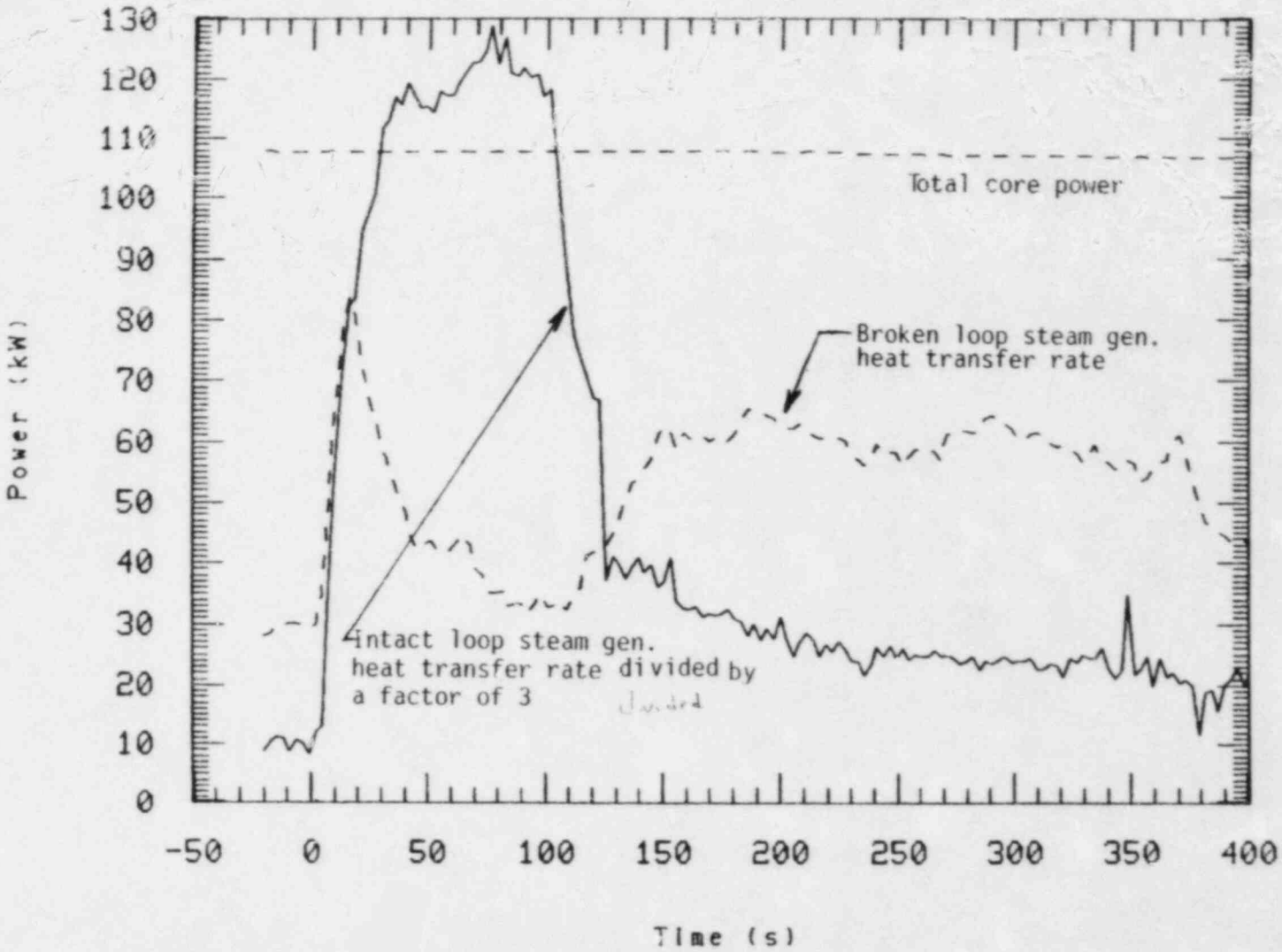

Figure 41. Core power and primary-to-secondary heat transfer rates for Test S-SF-5.

compared to the BLSG heat transfer. The ILSG heat transfer rate increased rapidly to a quasi-steady-state level then decreased rapidly after the ILSG steam valves closed thereby isolating the ILSG. The ILSG primary-to-secondary heat transfer then became a function of injection of auxiliary feedwater and secondary environmental heat loss.

3.2.3.1 Broken Loop Steam Generator Heat Transfer. The BLSG overall primary-to-secondary heat transfer responds much the same way it did in Test S-SF-4 without the effects due to changing core power. The heat transfer was initially enhanced, then decreased, then increased again due to auxiliary feedwater injection.

Figures 42 and 43 show local heat transfer rates in the BLSG at selected elevations for the upflow and downflow side of the U-tubes respectively. These curves show that heat transfer was initially enhanced throughout the entire generator at break initiation. This enhancement was short-lived for local heat transfer at the upper elevations. At elevations above 452 cm the local heat transfer rates peaked then decreased to their previous levels at near zero. This heat transfer behavior is due to an initial two-phase level swell followed by depletion of the secondary mass. The average primary-to-secondary temperature difference shown in Figure 44 is representative of local primary-to-secondary temperature differences throughout the generator. Figure 45 shows the local upflow side heat transfer rates compared to BLSG secondary mass inventory. Again 100% mass inventory on this curve represents the mass required to cover the U-tubes. As noted on this curve the initial BLSG inventory for this test was much less than that for Test S-SF-4. This may account for the differences in the behavior of local heat transfer at corresponding upper elevations between Test S-SF-5 and S-SF-4. In Test S-SF-5 the two-phase level swell developing at break initiation wetted the upper tube elevations only temporarily because of the low secondary level. Test S-SF-4 had a higher initial secondary level and the two-phase level swell wetted the upper tubes for a longer period of time.

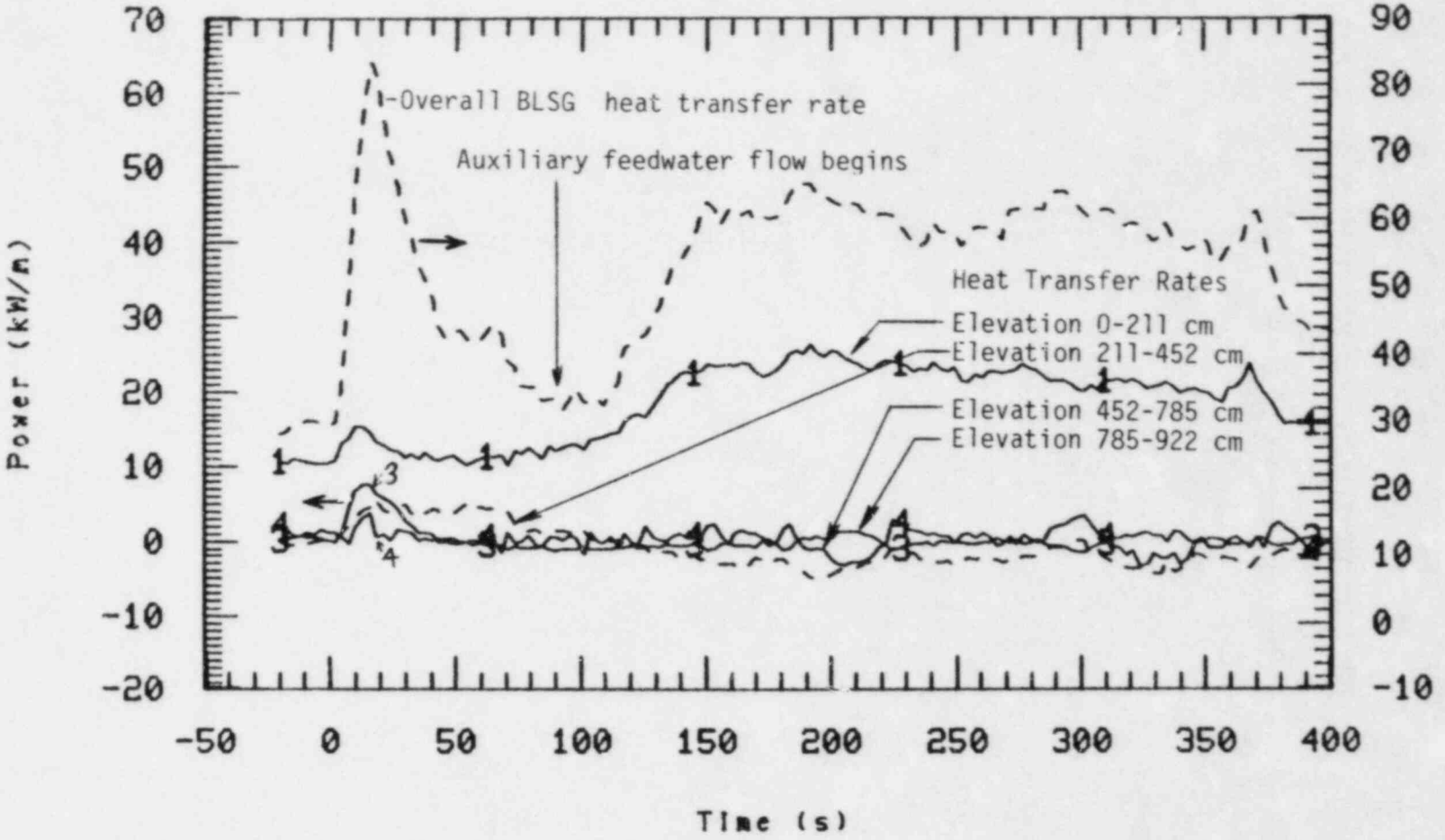

Figure 42. Selected BLSG local heat transfer rates in upflow side of U-tubes and overall heat transfer for Test S-SF-5.

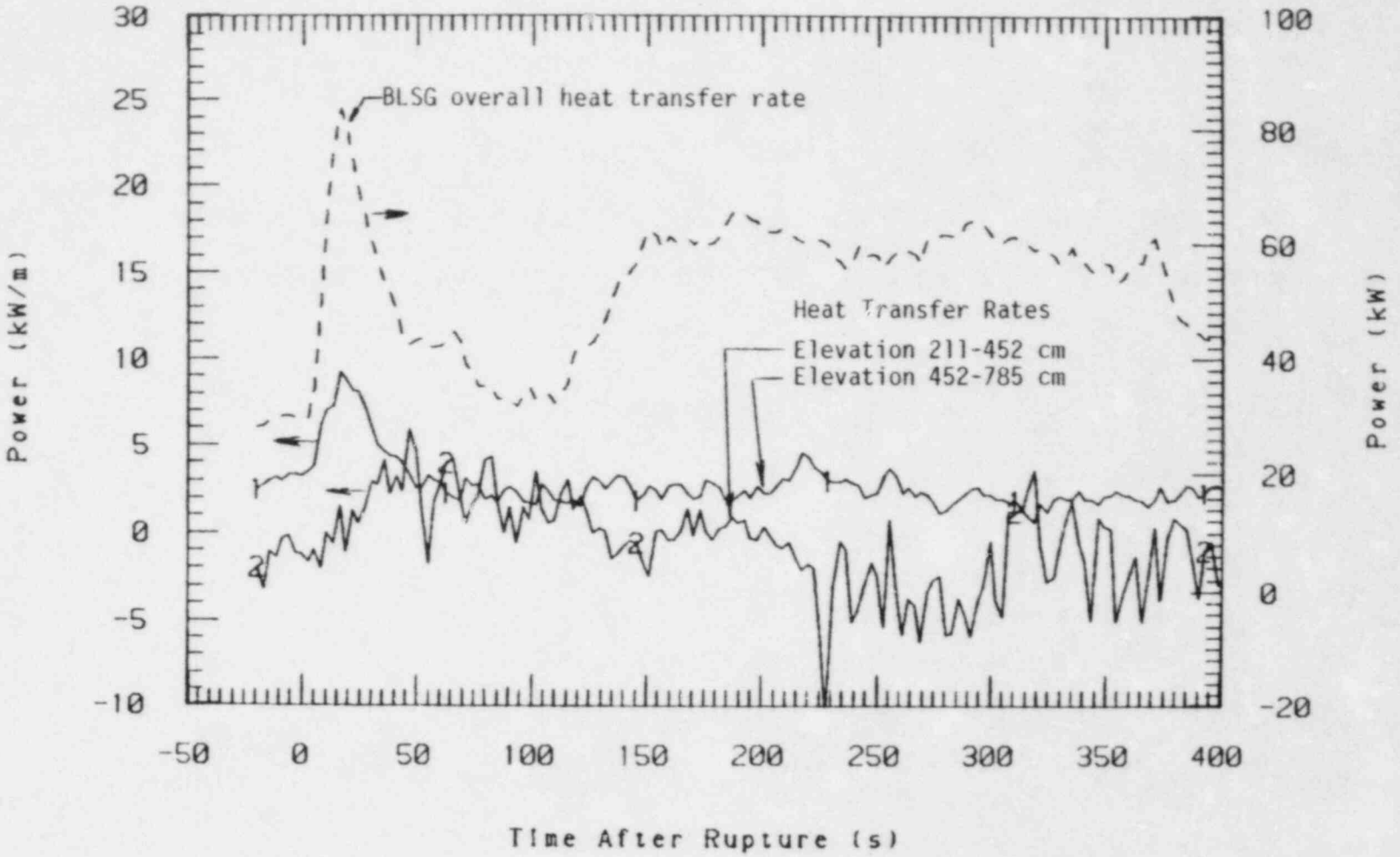

Figure 43. Selected BLSG local heat transfer rates in downflow side of U-tubes and overall heat transfer for Test S-SF-5.

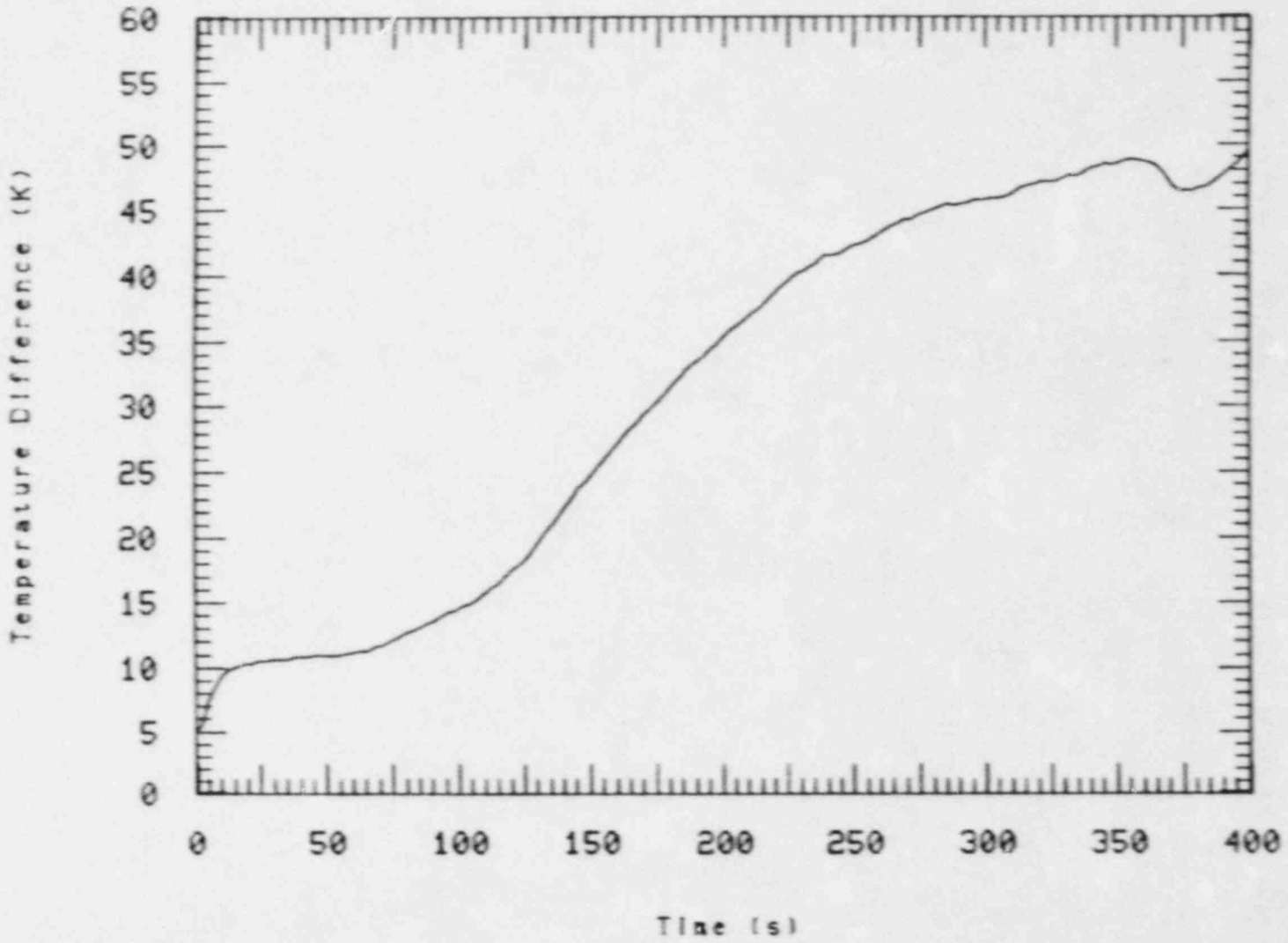

Figure 44. Broken loop primary-to-secondary temperature difference for Test S-SF-5.

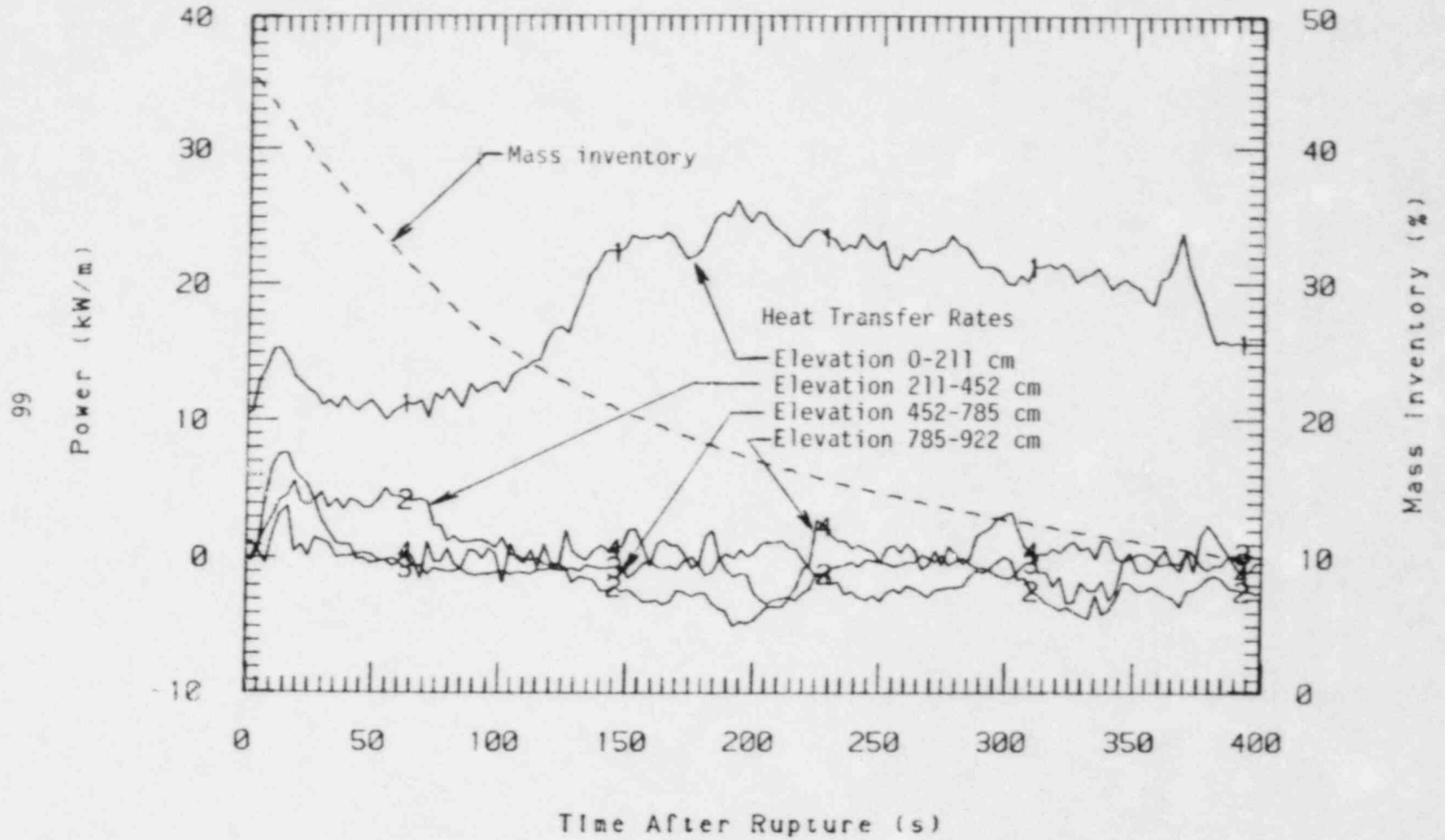

Figure 45. Selected BLSG local heat transfer rates in upflow side of U-tubes and secondary mass inventory for Test S-SF-5.

The local heat transfer rate below the 452 cm level responded similarly to S-SF-4. Again, as secondary mass was depleted the local heat transfer between 211 and 452 cm decreased. After 90 seconds the heat transfer at the bottom elevation increased due to the effects of relatively cool auxiliary feedwater entering the riser at this time. The overall and lower elevation heat transfer then remain relatively steady until the secondary mass depletion was sufficient to decrease the effective heat transfer area.

Figure 46 shows overall normalized BLSG heat transfer rate as a function of BLSG secondary mass. So that this information can be compared to similar data in S-SF-4, the BLSG primary-to-secondary heat transfer rate is normalized to the heat (power) produced by the core. 100% heat transfer then indicates that the BLSG heat transfer rate is equivalent to the core power. The inventory initially began at 42%. The break then initially enhanced heat transfer to a peak of 80% of core power. The heat transfer then decreased due to loss of inventory as previously discussed. The heat transfer then increased as a result of auxiliary feedwater injection. The heat transfer then remained relatively constant until about 10% inventory at which time the heat transfer decreased due to loss in secondary inventory.

3.2.3.2 Intact Loop Steam Generator Heat Transfer. Figures 47 and 48 show local heat transfer rates in the ILSG at selected elevations for the upflow and downflow side of U-tubes, respectively. The local heat transfer rates increased at break initiation and maintained a relatively constant level until isolation. Figure 49 shows the average primary-to secondary temperature difference in the intact loop steam generator which is representative of local primary-to-secondary temperature differences throughout the generator. Local heat transfer remained elevated until the ILSG was isolated from the break. At that time the local heat transfer rates decreased throughout the steam generator due to the collapse of the two-phase level swell which had developed at break initiation and from an increase in secondary temperature. Again, as in Test S-SF-4, the major portion of the primary-to-secondary heat transfer occurred at the bottom of the steam generator due to injection of auxiliary feedwater.

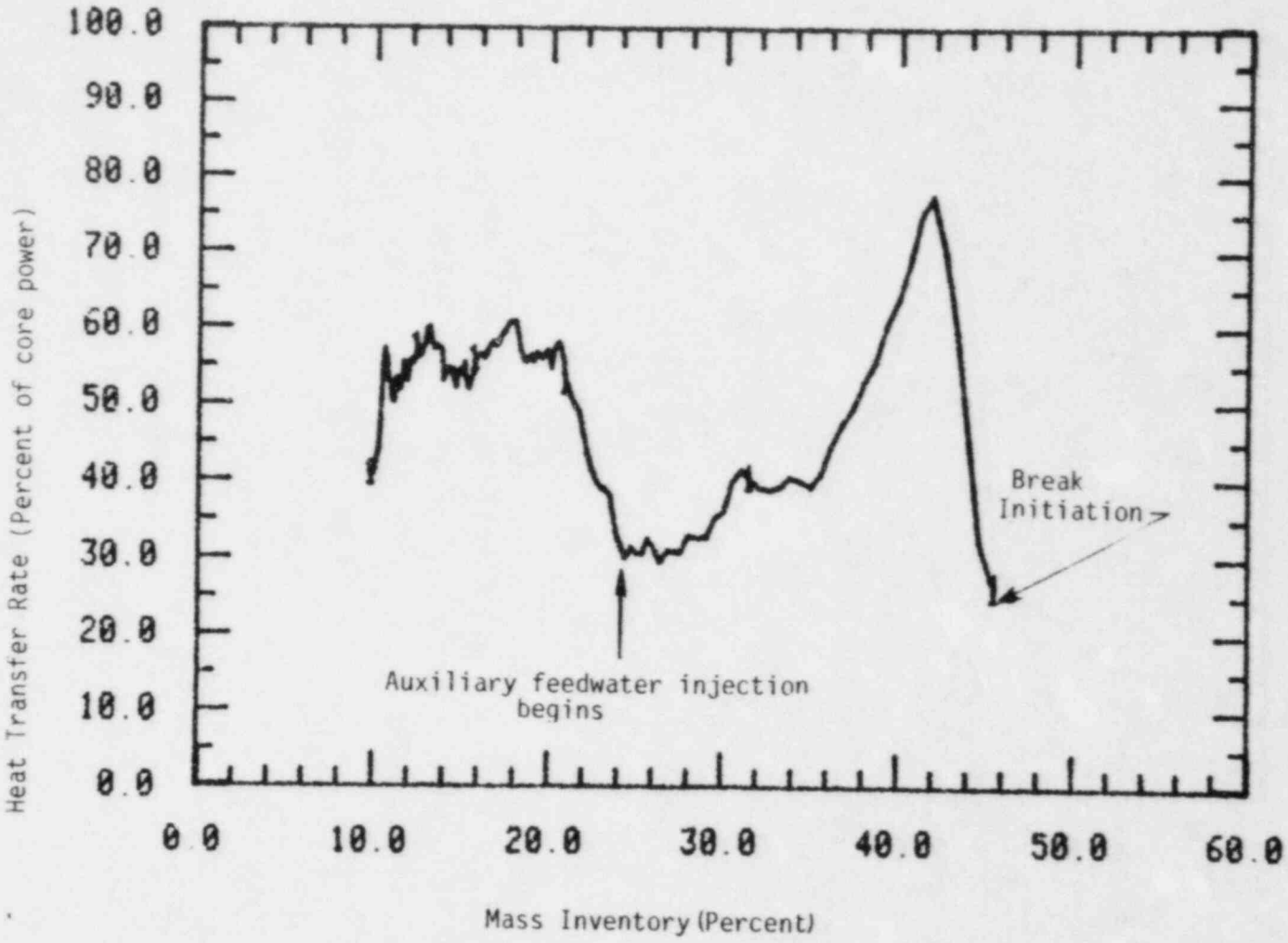

Figure 46. BLS6 normalized heat transfer rate vs. secondary mass inventory for Test S-SF-5.

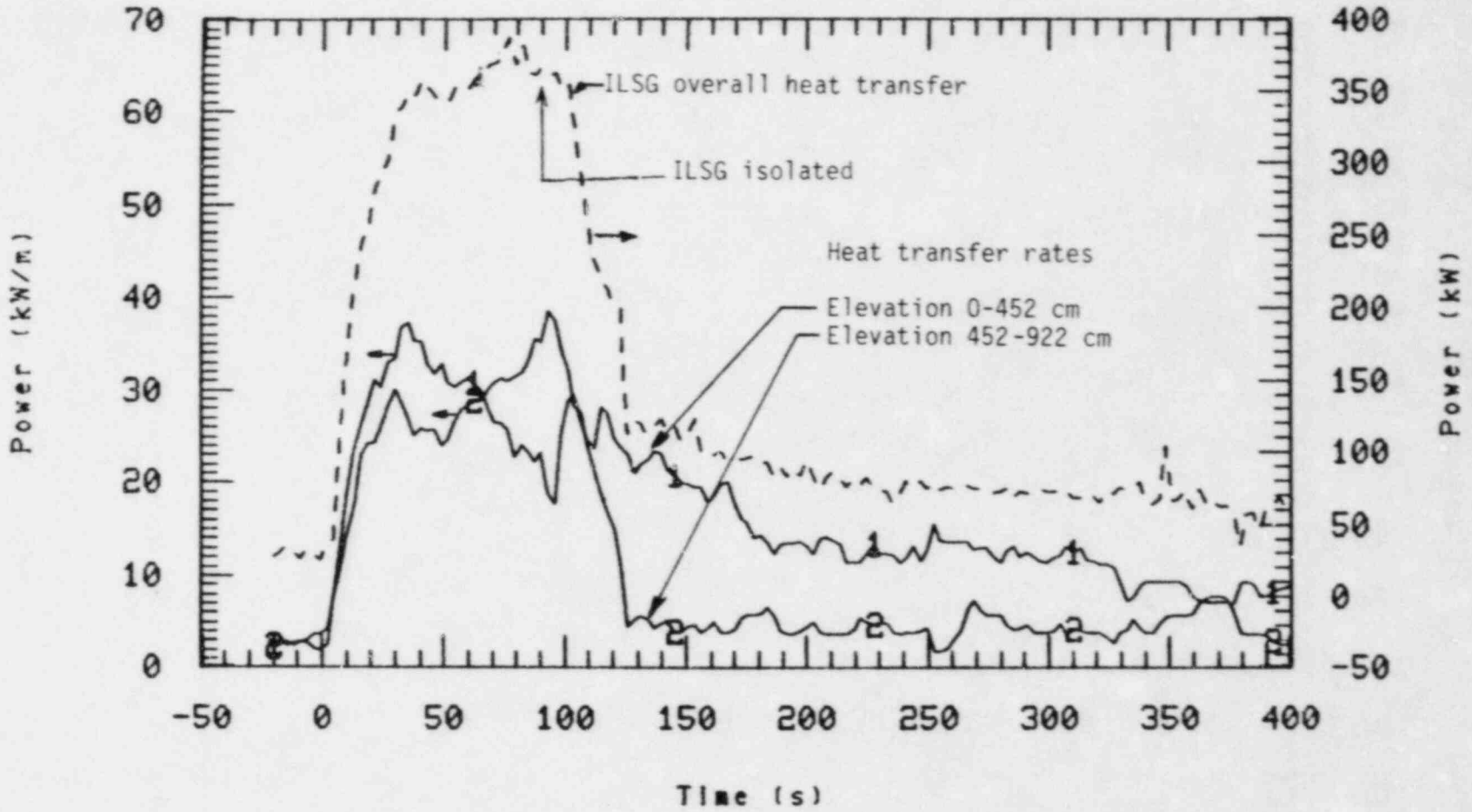

Figure 47. Selected ILSG local heat transfer rates in upflow side of U-tubes and overall heat transfer rate. Test S-SF-5

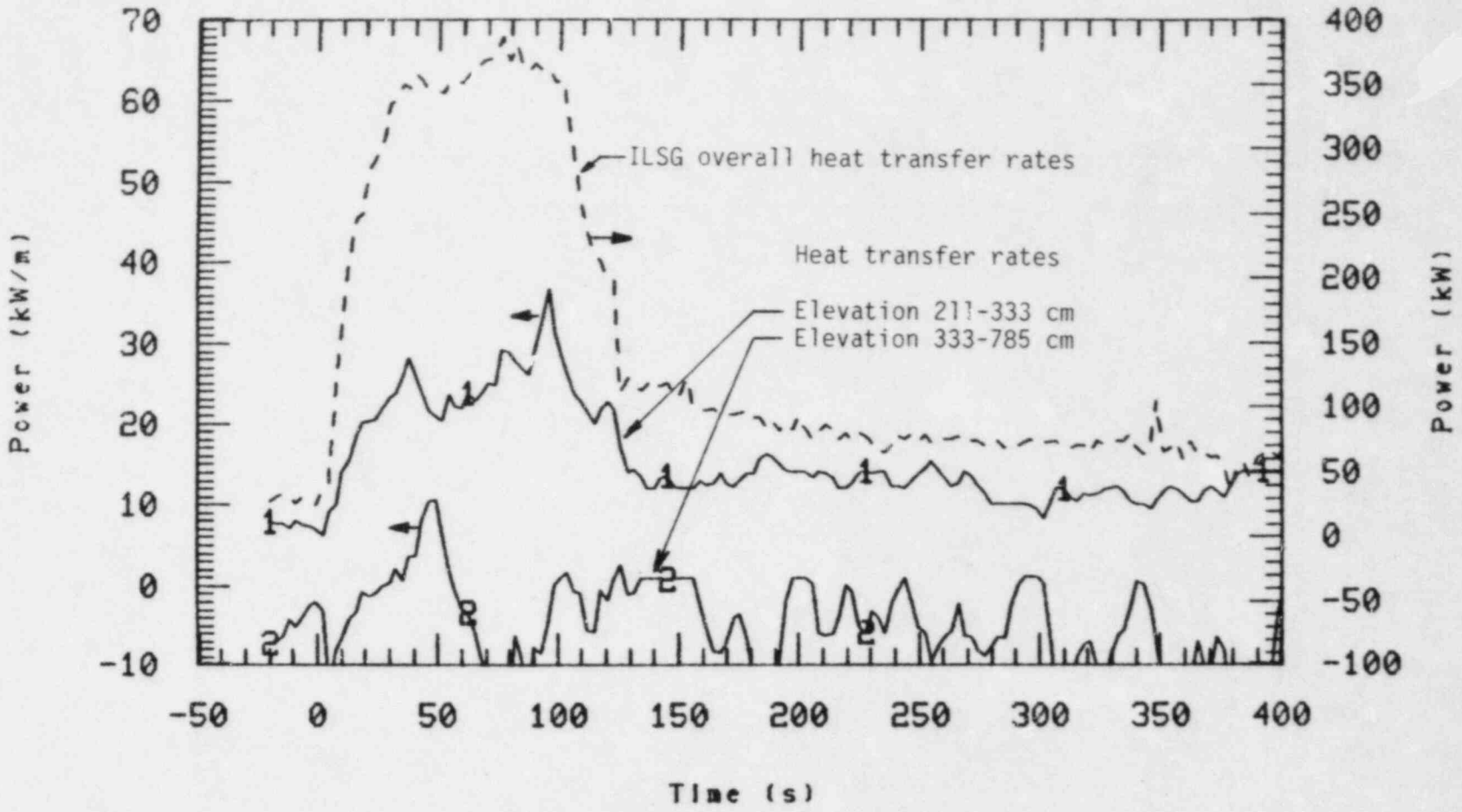

Figure 48. Selected ILSG local heat transfer rates in downflow side of U-tubes and overall ILSG heat transfer rate. Test S-SF-5

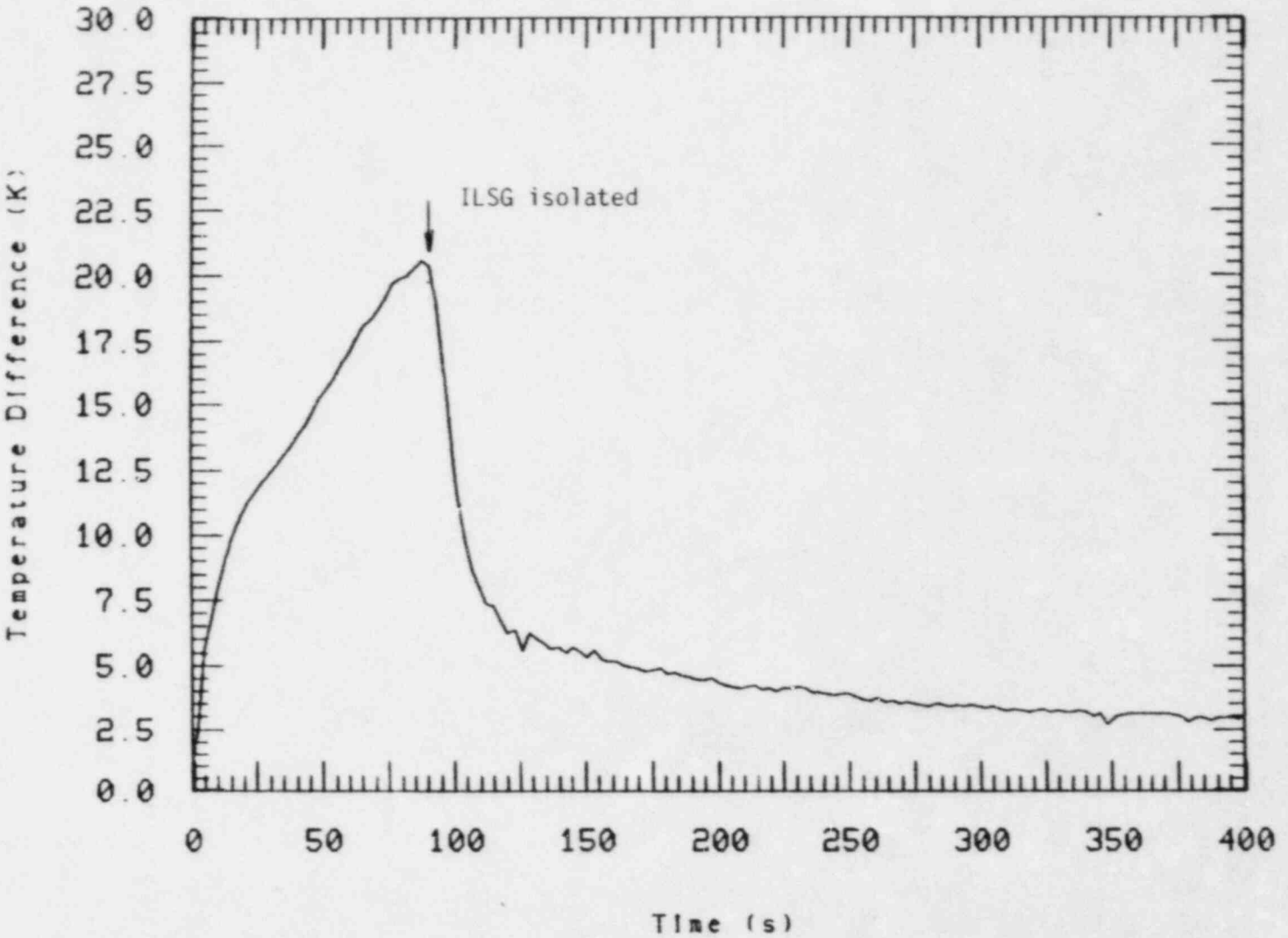

Figure 49. Intact loop primary-to-secondary temperature difference. Test S-SF-5.

Figure 50 shows local heat transfer rates in the upflow side of the ILSG U-tubes and the ILSG mass inventory. The initial mass was nearly enough to cover the U-tubes. The loss of secondary mass did not affect local heat transfer until the two-phase level swell collapsed at ILSG isolation (90 seconds).

Figure 51 shows normalized heat transfer rate in the ILSG (normalized to core power) as a function of secondary mass inventory. Again the overall heat transfer rate was not affected by the loss of secondary mass at the low core powers used in the test. As indicated earlier most of the primary-to-secondary heat transfer occurs at the bottom of the steam generator, and two-phase level swell and temperature decrease keeps the heat transfer high until ILSG isolation. The inventory began at 96% and at break initiation the overall heat transfer increased to a relatively steady value of 350% of core power. The heat transfer remained approximately at this level until the ILSG was isolated at which time the heat transfer rate decreased to 50%.

3.3 Comparison of S-SF-4 and S-SF-5 BLSG Behaviors

Figure 52 shows normalized BLSG heat transfer rate versus normalized BLSG secondary inventory for both tests. It should be noted that when initial secondary inventory was 80% the overall heat transfer stayed relatively high for a period of time (Test S-SF-4) regardless of secondary mass inventory loss. When the initial secondary inventory was lower (46%) the heat transfer rate peaked then rapidly dropped due to inventory loss (Test S-SF-5).

Figure 53 shows normalized ILSG heat transfer rate versus normalized ILSG secondary inventory for both tests. The initial inventories for the ILSG were high enough so that overall heat transfer rates stayed high until the ILSG was isolated from the break. The peak heat transfer rate for S-SF-5 is half that for S-SF-4 which was the same ratio as the break orifice areas.

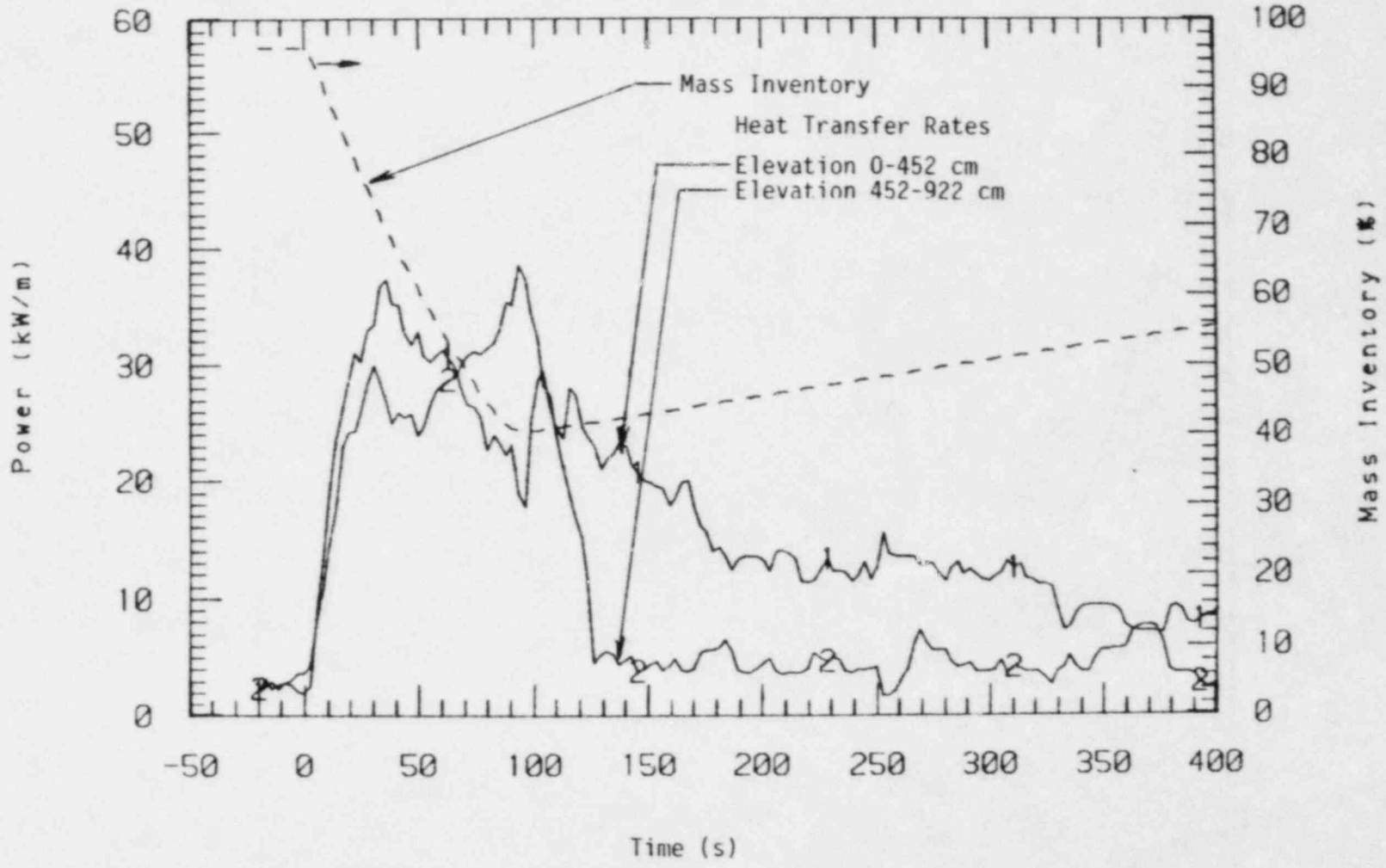

Figure 50. Local ILSG heat transfer rates in up-flow side of U-tubes and secondary mass inventory. Test S-SF-5.

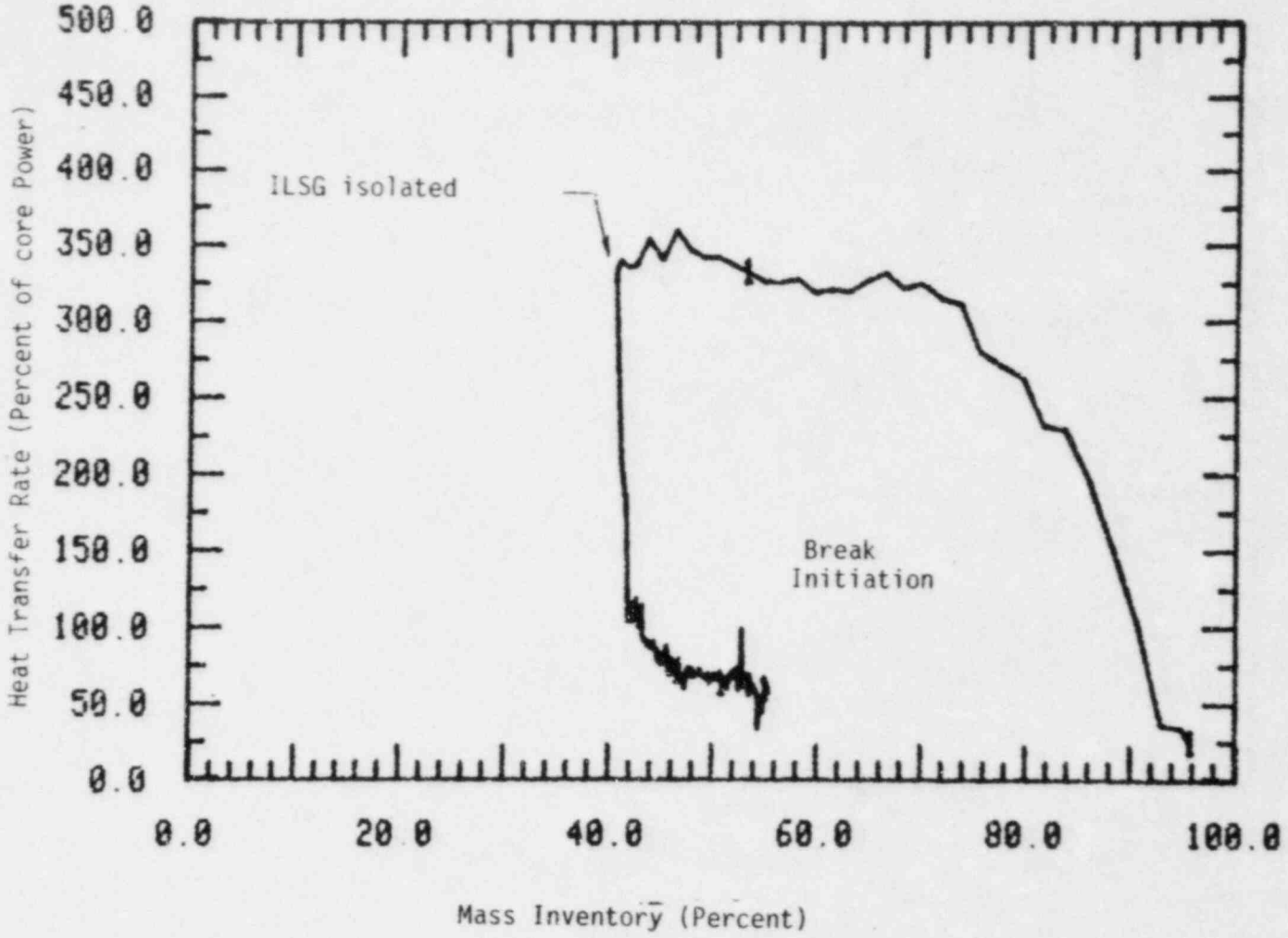

Figure 51. ILSG normalized heat transfer rate vs. secondary mass inventory for Test S-SF-5.

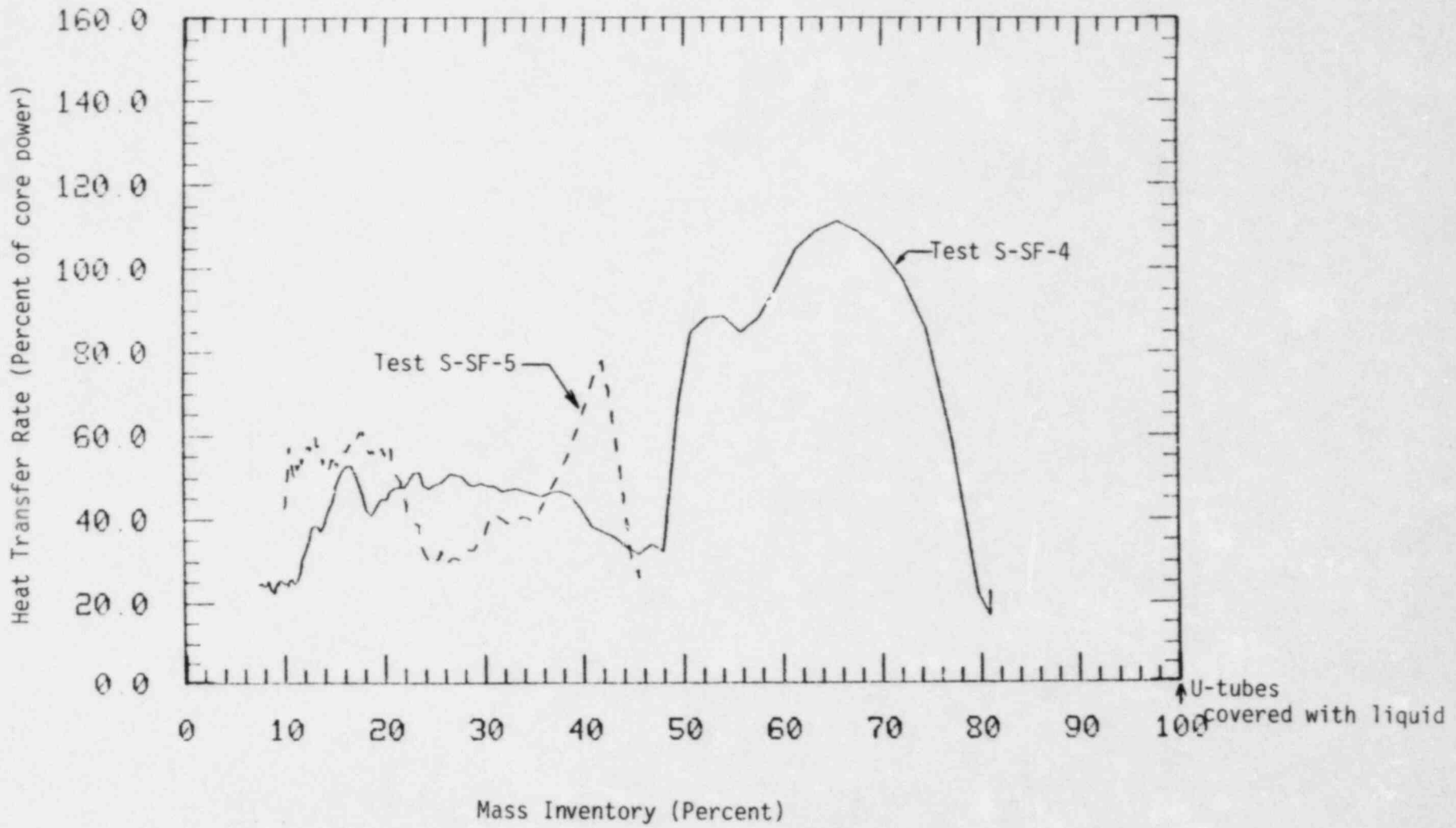

Figure 52. BLSG normalized heat transfer rates vs. secondary mass inventory for Tests S-SF-4 and 5.

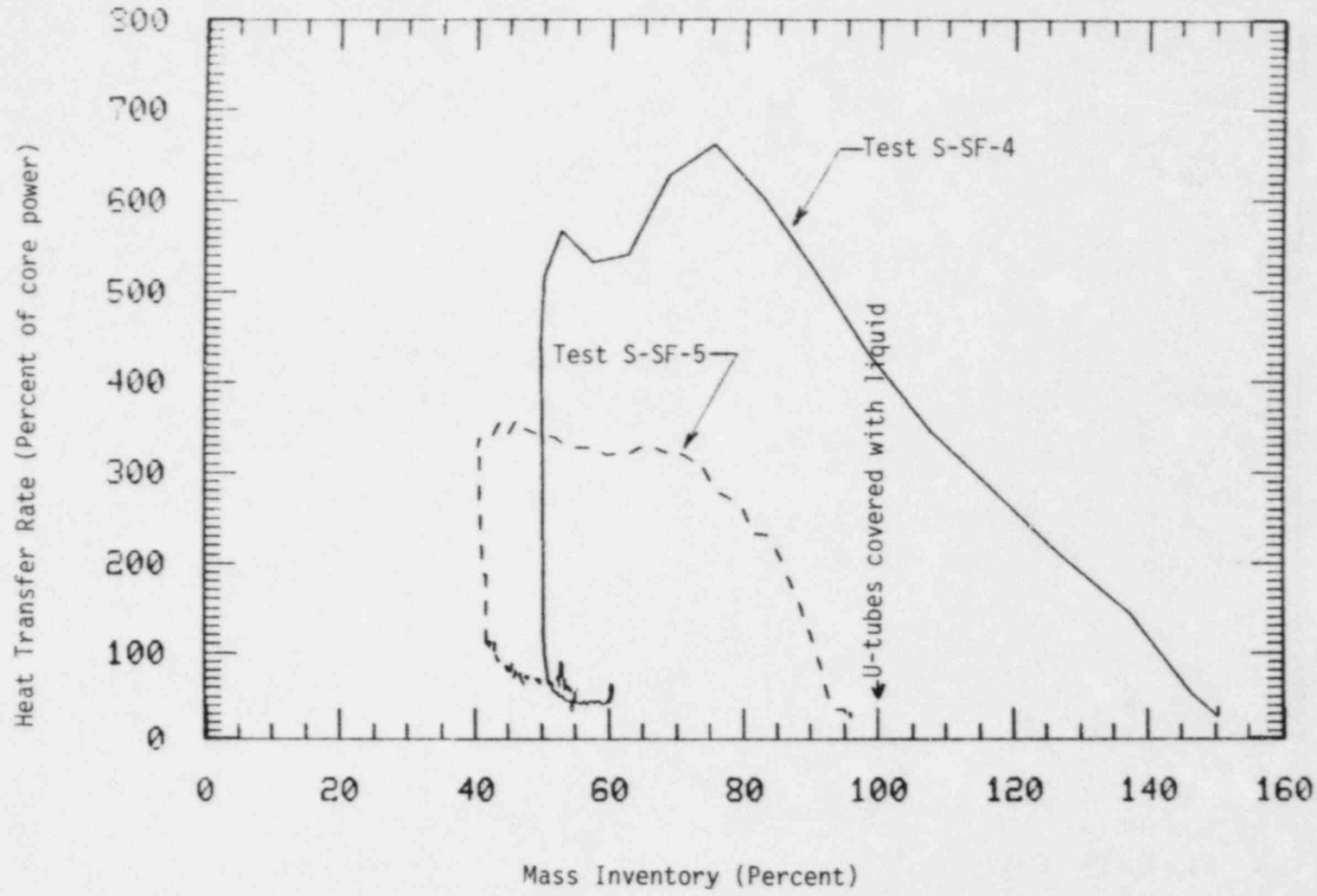

Figure 53. ILSG normalized heat transfer rate vs. secondary mass inventory for Tests S-SF-4 and 5.

4. SENSITIVITY STUDY

Prior to conducting the steamline break experiments, scoping calculations were performed with the RELAP5/MOD1[a] computer code. Several of the initial and boundary conditions used in the actual experiments varied significantly from those used in the calculations. However, the calculated results are valuable for examining the sensitivity of transient behavior to various parameters, and for identifying distortions introduced as a result of scale. A very brief review of the results is presented here. A more complete RELAP5 posttest analysis report is in preparation.

As mentioned earlier, in order for a MSLB transient to induce a significant primary depressurization the primary coolant volume shrinkage must be sufficient to empty the pressurizer; otherwise, flashing of the pressurizer fluid acts to hold up the system pressure and maintain subcooled conditions in the remainder of the primary. This is typical of results predicted in Reference 6 for example. While preserving other boundary and initial conditions, two parameters were varied relative to a base case calculation. These were pressurizer initial mass inventory, and primary structural heat transfer. Other calculations performed during the scoping studies showed little influence of break size over a range of 50% to 100% of the maximum break area. Important initial and boundary conditions are listed in Table 4. The secondary side initial mass inventories were comparable to those actually used in Test S-SF-5, while the break sizes were closer to those used in Test S-SF-4.

Figure 54 shows the primary system pressure response for the three different cases. The depressurization for the base case behaved similar to those observed in the experiments. Only a moderate depressurization occurred. The pressurizer, which started from a nominal half-full (7.8 kg) condition, did not empty, and significant subcooling was maintained in the

---

a. Calculations were performed with RELAP5/Mod1, Cycle 18, Configuration Control Number F00885. The Semiscale Mod-2A model was derived from information in Reference 7.

TABLE 4. CONDITIONS FOR RELAP5 STEAMLINE BREAK CALCULATIONS

Parameter	Value
ILSG Inventory	104 kg
BLSG Inventory	45 kg
Core Power	30 kW
Environmental Heat Loss	0
ILSG Break Size	1.70 cm ID
BLSG Break Size	1.27 cm ID
Pressurizer Mass	7.8 kg (Base case)
	7.8 kg (Adiabatic fluid boundary case)
	1.0 kg (Low pressurizer mass case)

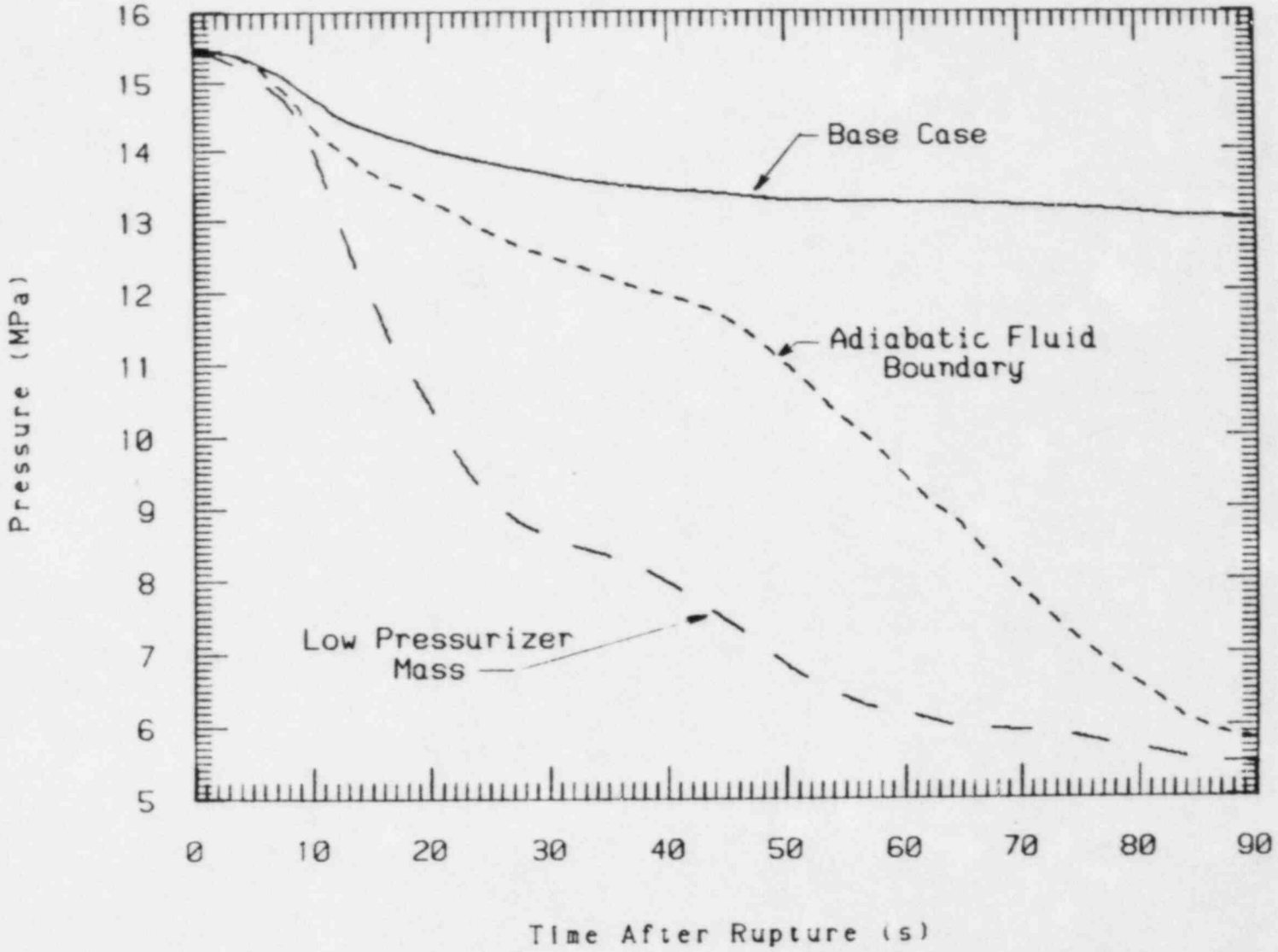

Figure 54. RELAP5 predicted primary system pressure response to a steam line break.

primary. For the calculation initiated with only 1 kg of water in the pressurizer, the pressurizer emptied very soon after the transient was initiated. As expected, a much more rapid and greater depressurization occurred.

Results from the adiabatic fluid boundary case are a reflection of distortions introduced as a result of using a small-scale facility. The ratio of pressure boundary surface area-to-fluid volume is not preserved between different size facilities (given similar geometry). Additionally, in the case of high pressure facilities the metal mass to fluid volume ratio is much larger in a small facility due to design constraints. Such are the distortions between a full-scale PWR and the Mod-2A facility. The net influence on system response to a MSLB induced cooldown transient would be expected to be a mitigation of depressurization and cooldown in the small-scale facility due to excess stored heat in the structure. This was indeed observed to be the case as shown in Figure 54. With the same initial pressurizer inventory as in the base case, by modeling an adiabatic inside pressure boundary (i.e. no stored heat in structures) the cooldown and resultant volume shrinkage was sufficient to empty the pressurizer. The point where the pressurizer empties is readily observable on the pressure curve as a sharp change in depressurization rate at about 45 s.

Results from this sensitivity study indicate that emphasis must be placed on the use of computer code calculations to extrapolate the integral small-scale system response of a MSLB to a full-scale system. The experiments performed in Semiscale offer valuable insight into associated thermal-hydraulic phenomena, especially primary-to-secondary heat transfer, when analyzed with a proper understanding of the limitations.

5. CONCLUSIONS

The Semiscale Mod-2A steamline break scoping experiments S-SF-4 and 5 accomplished their objectives of determining the behavior and characteristics of primary-to-secondary heat transfer rates during a steamline break and its dependence on secondary mass inventory. It provided data on the severity of primary cooldown as a function of secondary inventory and repressurization once secondary heat sinks were lost; provided a data base for assessment of water reactor safety codes; and is useful for planning future experiments.

No significant depressurization induced cooldowns were observed in either of the steamline break experiments. In neither of the experiments was the primary coolant volume shrinkage sufficient to empty the pressurizer, which is prerequisite to the occurrence of a rapid depressurization.

In Test S-SF-4 the depressurization was mitigated by a core power excursion resulting from the on-line nuclear point kinetics reactivity feedback to the core power controller. The resulting core heat generation was sufficient to prevent a severe cooldown in spite of the fact that the secondary coolant masses were far in excess of the properly scaled values.

In Test S-SF-5 core power was held constant, but the use of more closely scaled secondary inventories did not provide enough energy removal from the secondary side blowdowns to cause a severe primary cooldown.

The primary-to-secondary heat transfer behavior in both generators was generaliy characterized by an initial large increase along the entire axial length of the tubes. A top down degradation in heat transfer was then observed to occur, apparently corresponding to the reduction in two-phase froth level resulting from mass depletion due to the break flow. Further evidence for this phenomena was the dependency of the duration of enhanced heat transfer on the initial secondary side inventory.

The delivery of scaled, ambient temperature auxiliary feedwater flows to the secondaries upon receipt of a safety injection signal was found to be sufficient to maintain a substantial heat transfer rate in the lower elevations of the secondaries. Heat transfer to this fluid in both generators was sufficient so as to prevent any substantial repressurization of the primary system.

Sensitivity studies conducted with the RELAP5 computer code have shown the primary system pressure response to be sensitive to structural heat transfer. The large surface area-to-fluid volume, and metal mass-to-fluid mass ratios in the Mod-2A system acted to mitigate the depressurization by transferring stored heat to the fluid.

6. REFERENCES

1. Trojan Nuclear Plant-Final Safety Analysis Report, USAEC Docket No. 50-344 Portland General Electric Co., October 1973.

2. System Design Description for Mod-2A Semiscale System, Addendum I, "Mod-2A Phase I Addendum to Mod-3 System Design Description," December 1980.

3. James R. Venhuizen, Computerized Core Power Control Program Semiscale Experiment, EG&G-MC-5184, EG&G Idaho Inc. September 1980.

4. J. R. Venhuisen ltr to D. J. Shimeck, "Report on the Computerized Core Power Controller for Semiscale Test S-SF-4," JRV-2-82, June 22, 1982

5. D. J. Shimeck, Experiment Operating Specification for Semiscale Mod-2A Steam and Feedwater Line Break Scoping Experiment Series, EG&G-SEMI-583, EG&G Idaho Inc. March 1982 with revision incorporated per P. North ltr. to R. E. Tiller "Changes to Semiscale SF Series Experiments Operating Specification" PN-117-82, July 9, 1982.

6. Zion Station Final Safety Analysis Report, Commonwealth Edison Co., 1973.

7. M. T. Leonard, RELAP5 Standard Model Description for the Semiscale Mod-2A System, EGG-SEMI-5692, December 1981.

8. V. H. Ransom, et. al., RELAP5/MOD1 Code Manual, Volumes 1 and 2, NUREG/CR-1826, EGG-2070, March 1982.

9. Response to Round 1 Question 440.40 on the CESSAR FSAR ECCS Line Analysis and Plant Safety Analysis, Combustion Engineering Inc., January 1982.